Development of a sustainable composite crash structure for Formula Student vehicles

João Vítor Barbosa de Almeida

Thesis submitted to Universidade do Porto – Faculdade de Engenharia
in partial fulfilment of the requirements for the degree of
Master in Mechanical Engineering

Supervisors
Professor Albertino Arteiro
Dr. Denis Dalli

Mestrado em Engenharia Mecânica (M.EM)
Departamento de Engenharia Mecânica (DEMec)
Faculdade de Engenharia (FEUP)
Universidade do Porto (UP)

"I know of no better life purpose than to perish
in attempting the great and the impossible."

-Friedrich Nietzche

Aos meus pais,
à minha irmã,
à minha Daisy
e à FSFEUP.

Acknowledgments

Firstly, I would like to thank my supervisors, Prof. Albertino and Dr. Denis Dalli for accepting this thesis theme, for the knowledge transmitted, for the opportunity to integrate this project and for all the help, support, and availability throughout this work.

I would also like to express my gratitude to all the Formula Student FEUP members for filling my place whenever I was working on my thesis, and for all the knowledge shared that helped me complete this work.

There is a special group of people that would I like to thank for these amazing five years: the "018". They were there in the best and worst moments of my academic path, without their love and support in every second, this would not have been possible to achieve. They've made this walk one hundred times more beautiful and I cannot be grateful enough.

To Coletivo 4585, for never letting my artistic vein dry. For all the moments shared, all the songs and all the stages shared. These moments were essential to keep the balance in my life and endure these 5 years.

To all the professors at the university for the knowledge transmitted both for the completion of this course as well as the development of the first FSFEUP car.

Finally, and most importantly, I would like to thank my family for all the effort they had to go through to allow me to go to university and to have the opportunity that they unfortunately never had. For all the love, support, encouraging and especially for never doubting my capabilities even when myself didn't believe in them. To my sister, which was always there to remember me to aim to the sky and to never give up. To my dog, Daisy, for always putting a smile on my face, whenever I got home.

Abstract

In the past years, occupant safety in every kind of vehicle has been gaining more and more importance, resulting in the increase of the safety measures applied. Every modern vehicle is equipped with at least one crash structure, which absorbs energy in case of a collision to avoid reaching the occupants. In the case of motorsports, this kind of safety structures is mandatory, with the teams having to find clever ways to incorporate them in their vehicles without compromising their performance. Composites, due to their high specific mechanical properties have been used for these kinds of applications, especially carbon fibre reinforced polymers (CFRP), allowing the teams to have safe lightweight crush structures.

In the last few years, the European Union has been releasing new rules regarding carbon dioxide emissions, to achieve carbon neutrality by 2050. This led engineers to rethink their material options, since carbon fibre, besides being obtained from oil, also requires high processing temperatures in the carbonization process, which results in high embedded energy values.

An alternative to CFRP are natural flax fibres obtained from the stems of the flax plant. Despite the lower energy absorption, this material allows for a more sustainable option for these kinds of applications. Several studies have been conducted, through coupon testing to determine carbon fibre and flax crushing capabilities as well as hybrids between the two materials.

Formula Student is a worldwide competition that encourages students to design and manufacture their own formula type cars. These types of cars are also required by rules to have a frontal impact attenuator to absorb energy in case of a frontal impact. Most of the teams use foam or aluminium impact attenuators since they are standardized materials that do not require testing. On the other hand, the usage of composites for this application allows for the design of more complex lightweight structures reducing the overall weight of the car.

In this thesis, the possibility to design a sustainable hybrid or pure flax structure to serve as impact attenuator in a Formula Student car was explored. Several designs were compared in terms of cost, difficulty of manufacturing, and overall energy absorption performance. The preliminary chosen designs were tested using a finite element analysis through ABAQUS and its CZone plugin, to assess if they passed the Formula Student rules.

Several studies have shown that the energy absorption has a dependency on the radius of curvature of the specimen. To assert the influence of this dependency on the simulated structures initially they were simulated assigning the crash properties of flat coupons to the whole structure, and then the crash properties as a function of curvature. It was proved that the curvature dependence can introduce significant variations in the energy absorption capabilities of a certain crash structure.
Several structures were able to pass the acceleration and energy absorption requirements from carbon fibre and flax to hybrid structures. It was proven that it is possible to reduce both the weight and the carbon footprint of a rule compliant impact attenuator when compared with the most common used aluminium honeycomb impact attenuators. Besides that, it was found that hybridising a structure with carbon and flax fibres may reduce the carbon footprint of a structure in 25% in relation to the full CFRP structure with a slight mass increase of 6%.

Keywords: Composites, Crashworthiness, Finite elements analysis, Formula Student, Hybrids, Impact attenuator, Natural fibres, Simulation, Sustainability

Resumo

Nos últimos tempos, a segurança dos ocupantes de todo o tipo de veículos tem ganho cada vez mais importância, resultando no aumento das medidas de segurança aplicadas. Todos os veículos modernos são equipados com pelo menos uma estrutura de impacto, que absorve energia em caso de colisão evitando que esta chegue aos ocupantes. No caso dos desportos motorizados, estes tipos de estruturas de segurança são obrigatórios, obrigando as equipas a encontrar formas inteligentes de as incorporar nos seus veículos sem comprometerem o seu desempenho. Os compósitos, devido às suas elevadas propriedades mecânicas específicas, têm sido usados para este tipo de aplicações, especialmente os polímeros reforçados com fibras de carbono (CFRP), permitindo às equipas ter estruturas de impacto seguras e leves.

A União Europeia tem lançado novas regras respeitantes às emissões de dióxido de carbono, de modo a alcançar a neutralidade carbónica em 2050. Isto levou a que os engenheiros tivessem de repensar as suas opções de materiais, já que as fibras de carbono, para além de serem obtidas de petróleo, também requerem elevadas temperaturas de processamento no processo de carbonização, o que resulta numa elevada energia embebida.

Uma alternativa aos CFRP são as fibras naturais de linho obtidas do caule da planta do linho. Apesar de terem tensões de esmagamento mais baixas que os CFRP's, os resultados para a energia específica de absorção são bastante promissores. Vários estudos foram feitos através de testes de provetes para determinar as capacidades de absorção de energia de compósitos de fibra de carbono, de fibra de linho e de híbridos dos dois tipos de fibra.

A Formula Student é uma competição internacional que encoraja os estudantes a projetar e produzir o seu próprio carro do tipo Formula. Este tipo de carros, de acordo com as regras da competição, também deve ser equipado com um atenuador frontal de impacto para absorver energia no caso de uma colisão frontal. A maior parte das equipas utiliza uma espuma ou alumínio como atenuador de impacto já que estes são materiais considerados padrão para a competição e de tal modo não necessitam de testagem. Por outro lado, o uso de compósitos para este tipo de aplicações permite projetar estruturas complexas mais leves reduzindo o peso total do carro.

Nesta dissertação, a possibilidade de projetar uma estrutura híbrida ou totalmente em linho para servir como um atenuador de impacto num carro de Formula Student foi explorada. Várias estruturas foram comparadas em termos de custo e dificuldade de produção e do seu comportamento de absorção de energia. As estruturas escolhidas inicialmente foram testadas através de uma análise de elementos finitos usando o software ABAQUS e o seu plugin CZone, para saber se passavam as regras da Formula Student.

Vários estudos demostraram existir uma dependência entre energia absorvida e o raio de curvatura de um provete. De modo a perceber a influência desta dependência nas estruturas simuladas, estas inicialmente foram simuladas considerando o desempenho ao impacto de amostras planas em toda a estrutura, e posteriormente considerando o efeito da curvatura nesse desempenho. Foi provado que esta dependência da curvatura introduz variações significantes nas capacidades de absorção de energia de uma determinada estrutura de choque.

Diversas estruturas conseguiram passar os requisitos de aceleração e de absorção de energia desde as estruturas de fibra de carbono e linho até às estruturas híbridas. Foi provado que é possível reduzir

tanto o peso como a pegada carbónica de um atenuador de impacto capaz de passar as regras quando comparado com os atenuadores de impacto mais comuns feitos em favo de abelha de alumínio. Para além disso, percebeu-se que ao hibridizar uma estrutura com carbono e linho é possível reduzir a pegada carbónica de uma estrutura em 25% em relação a uma estrutura de fibra de carbono com um reduzido aumento de massa de 6%.

Palavras-Chave: Compósitos, Estruturas de choque, Análise de elementos finitos, Formula Student, Híbridos, Atenuador de impacto, Fibras naturais, Simulação, Sustentabilidade

Contents

List of Figures

List of Tables

Nomenclature

Abbreviations

AIP	Anti-intrusion plate
Al	Aluminium
ASTM	American Society for Testing and Materials
CFRP	Carbon fibre reinforced polymers
CPU	Central processing unit
CTE	Coefficient of thermal expansion
DCB	Double cantilever beam test
EA	Energy absorbed
EDM	Electric discharge machining
ENF	End notched flexure test
F1	Formula 1
FFRP	Flax fibre reinforced polymers
FIA	Federation Internationale de L'Automobile
FSAE	Formula Society of Automotive Engineers
FSFEUP	Formula Student FEUP
FSG	Formula Student Germany
GFRP	Glass fibre reinforced polymers
GWP	Global warming potential
IA	Impact attenuator
MDF	Medium density fibreboard
PBLT	Precision Board High Density Urethane
PTFE	Polytetrafluoroethylene
PVC	Polyvinyl chloride
RIMP	F1 Rear impact attenuator
RoC	Radius of curvature
SAE	Society of Automotive Engineers
SEA	Specific energy absorption
UD	Unidirectional
UK	United Kingdom

USA	United States of America
VUMAT	Vectorized User Material
WRM	Woven roving mat

Symbols

δ	Displacement $[m]$
$F(\delta)$	Load $[N]$ for a displacement δ
F_{max}	Maximum crush load $[N]$
F_{mean}	Average crush load $[N]$
m	Mass $[g]$
EA	Energy absorbed $[J]$
SEA	Specific energy absorbed $[J/g]$
η_{eff}	Crush Efficiency
σ	Crush stress $[MPa]$
U_{total}	Total energy absorbed $[J]$
U_{1c}	Mode-I fracture energy $[J]$
U_{2c}	Mode-II fracture energy $[J]$
U_{σ}	Frond bending energy $[J]$
U_{ff}	Fibre fracture energy $[J]$
U_{fr}	Friction related energy absorption $[J]$
U_{others}	Other energies $[J]$
G_{1c}	Mode-I Fracture toughness $[MPa * m^{1/2}]$
G_{IIc}	Mode-II fracture toughness $[MPa * m^{1/2}]$
A	Cross-sectional area $[mm^2]$
P	Perimeter $[mm]$
N	Number of plies
th	Ply thickness $[mm]$
F	Crushing load $[N]$
m_I	Impactor's mass $[g]$
ε	Strain
d	Damage variable

E	Elastic constant $[MPa]$
ν	Poisson's coefficient
$\sigma_{11}, \sigma_{22}, \sigma_{33}$	Stress $[MPa]$
α	Loading direction
$\tilde{\sigma}_{\alpha}$	Effective stress $[MPa]$
G_{12}	Shear modulus $[MPa]$
F_{α}	Activation fuction
ϕ_{α}	Stress based criterion
X_{α}	Material strength $[MPa]$
r_{α}	Damage threshold
τ	Time $[s]$
t	Time $[s]$
G_f^{α}	Intralaminar fracture toughness $[MPa * m^{1/2}]$
L_C	Characteristic length $[mm]$
g_0^{α}	Elastic energy density [MPa]
σ_{12}	Shear stress $[MPa]$
ε_{12}^{pl}	Plastic shear strain
C	Hardness coefficient
p	Hardness power term
S	Shear strength MPa
d_{12}^{max}	Maximum shear damage variable
β_{12}	Experimental material constant
ρ	Density $[Kg/m^3]$
Δt	Time increment [s]
$\hat{\lambda}$	Material constant
$\hat{\mu}$	Material constant
SA	Surface area m^2
a_{max}	Maximum acceleration [g]
$a_{\max Al.}$	Maximum acceleration allowed by the rules [g]
a_{avg}	Average acceleration [g]

$a_{avg\ Al.}$	Average acceleration allowed by the rules [g]
l_{cr}	Crushed length [mm]
l_t	Total length [mm]
$S_{a\ max}$	Maximum acceleration safety margin
$S_{a\ avg}$	Average acceleration safety margin
S_{length}	Length safety margin

1. Introduction

The human species is currently facing one of its most threatening problems: climate crisis. Due to this problem, the European parliament is constantly releasing new updates concerning the move to carbon neutrality, affecting several industry sectors like the automotive industry. Having the objective to reach climate neutrality by 2050, very strict regulations are being imposed regarding fuel consumption and greenhouse gas emissions [1]. This is where carbon fibre reinforced polymers (CFRP) take its place, having the capability to last for half a century with barely any maintenance, and to produce extremely strong and stiff structures with low weight, leading to less fuel-consumption in the transporting industry. Despite that, the carbon fibre production requires high levels of energy due to the oxidation and carbonisation processes, most of the higher strength and modulus carbon fibre come from oil and they are hard to recycle due to the thermoset matrices that cannot be melted to recover the fibres. This led companies into pursuing more sustainable composite materials like natural plant-based fibres to replace the oil-based synthetic fibres [2]. In this chapter, the background of this thesis will be presented focusing on crashworthiness of composite materials and its use in the motorsports industry. Then, the motivation for this work development will be presented and the objectives of the thesis clarified. Finally, the thesis structure will be summarized.

1.1. Background

Composites are materials that by combining two materials with very different properties can achieve requirements that none of the single materials can achieve [3]. Composites are generally composed of two materials, a reinforcement that carries the load and ensures high strength and stiffness of the composite, and a matrix that shapes the material , transfers the load to the reinforcement and protects it from the environment [4]. High specific stiffness and strength make this material more common in various industry areas since it results in low-weight and high-performance structures. Composites are generally composed of several stacked layers called plies, which can be oriented at different angles resulting in material anisotropy, which can be optimized for each specific structure, this is the main distinguishing point between metals and composite materials.

Composites have been present in humanity for a long time, straw-reinforced clay bricks were already used in the ancient Egypt. Masonry in the nineteenth century was reinforced with iron rods, that later evolved to the commonly used steel-reinforced concrete. In 1942 the first fibreglass boat was created. And in the 1960s boron and high-strength carbon fibres were introduced, which led to its application in aircraft components in 1968 [4].

The first carbon fibre Formula 1 car appeared in 1981: the McLaren MP4/1. The news were received with some scepticism due to the known fragility of this material. But after the 1981 Monza Grand Prix, the scepticism was crushed after John Watson, the pilot of the car, came unhurt after an accident where everyone thought he was dead. This led other F1 teams to follow McLaren's lead to start creating full carbon fibre monocoques for their cars [5]. Despite this, fatalities in the competition were still present which lead the FIA to create stricter rules regarding driver's safety [6].

Currently, F1 regulations [7] define several mandatory composite crash structures, namely: the front, side and rear impact structures. These structures ensure that through several crushing mechanisms the energy from impacts gets absorbed by them and not the driver. Composite materials increase the specific energy absorption when compared with the previously used metal structures, allowing the same energy absorption with lighter structures [8]. Still, this technology has some drawbacks related

to the crushing mechanisms of these type of materials that have not yet been studied as well as its previous metal predecessors.

According to FSG (Formula Student Germany) regulations [9], a Formula Student car needs to have a frontal impact attenuator which is a "deformable, energy absorbing device located forward of the front bulkhead". Since the regulations allow for the use of standard foam and aluminium honeycomb that don't require testing, most of the teams use these materials. Nevertheless, Formula Student is a competition that makes students push themselves into greater challenges, and as is going to be seen later several teams have tried to make the move into composite structures, namely carbon fibre structures, to reduce the overall weight of the car and increase performance.

To comply with CO2 regulations, the next bold move for formula student is also going to be the move for natural fibres.

1.2. Motivation

The first Formula SAE competition was created in 1981, in Texas, USA, to implement a student competition that encouraged the participants to create a formula type car to compete in four dynamic events: acceleration, manoeuvrability, endurance and fuel economy. Initially, it was not mandatory for the cars to have a suspension resulting in the cars being nothing more than large karts, later it became mandatory for the cars to have a four-wheel suspension. In 1985, static events were also included to assert the students' knowledge about their cars and their decisions on design and manufacturing [10].

Later in 1998, FSAE saw a new brand competition being created in Europe mimicking the American competition – Formula Student, held in the UK and organized with IMeche, that counted with the participation both European and American teams [10].

In 2005, Formula Student Germany was created, being considered nowadays to be the best Formula Student competition in the world [11].

The Formula Student vehicles are required by rules to have a frontal impact attenuator able to absorb the necessary energy to protect the driver in case of a frontal impact. Throughout the years, several different impact attenuators have been used by the teams, going from the most common foam and metal impact attenuators to the rarest composite structures. With the competition growing and teams getting faster and more competitive cars, the use of composites becomes essential, inclusively in the frontal impact attenuator, due to their superior specific properties when compared with metals. But the composite crush behaviour is still not well understood, and the modelling of composite crash structures is still extremely difficult due to the lack of knowledge in this topic.

Allied with the urge to reduce weight on the automotive and motorsports industry, due to both performance and fuel consumption, and with the increase in the safety levels of new vehicles, appears the need to use more sustainable materials. The task of balancing all of these factors has been proving very difficult to achieve. It is therefore necessary to study the behaviour of more sustainable composite materials as well as to improve its modelling techniques to better represent the experimental behaviour.

Formula 1 has been trying to make the move into the usage of plant-based fibre reinforced polymers, both for non-structural and structural parts. Among these composites are the flax fibre reinforced polymers, that have become an interest to the scientific community both for its sustainable origin as well as for the promising energy absorption capabilities. Despite performing worse than the most common used carbon fibres, there have been attempts to make hybrids between the two types of fibre to achieve a compromise between performance, safety, and sustainability. Therefore, testing

these new types of materials or their hybridisation with ones with superior mechanical capabilities, as well as using the experimental data to construct simulation models able to predict the correct behaviour of large structures and to achieve more sustainable crash structures is a must.

1.3. Thesis objectives

This thesis main objective is to find a compromise solution between performance, safety, and sustainability in the development of a frontal impact attenuator for a Formula Student vehicle.

It aims to introduce an innovative design both in Formula Student as well as in the automotive industry by simulating a more sustainable lightweight crash structure composed of flax fibre reinforced polymers or flax and carbon fibre hybrid composites, using experimental data. One of the milestones of this work is to assert how different geometries and layups affect the overall performance of the structure.

It will add on to the university effort to understand and characterize composite crash behaviour and to bridge the gap between their characterization through dynamic and static coupon testing and the modelling of composite crash structures. Following upon the carbon fibre and flax coupon testing it aims to design a structure that is able to comply with the formula student rules, to reduce the carbon footprint and to be lighter in relation to the most common aluminium impact attenuators, within what are the constraints and context of the FSFEUP team.

The reader should have in mind that geometry optimization is not the main objective of this thesis and therefore no algorithms will be developed to find the structure design that results in the best energy absorption.

1.4. Thesis outline

The themes referred in the thesis will be now described in the same order described in the previous section.

In chapter 2 a literature review will be presented, describing the concept of crashworthiness as well as it's relevant parameters. Then, the evolution of the materials used for crush applications will be described with a focus on the description of composite fracture mechanisms and failure modes at the crush front. Then the geometric influence in the structures energy absorption capability will be explored. And finally, several methods of crashworthiness simulation will be described as well as different techniques to manufacture large composite crush structures.

In chapter 3 a description of the coupon testing will be presented, from the manufacturing of the coupons to its testing. The crushing parameters will then be obtained and explored so they can be used later in the design and simulation of the crash structure.

Chapter 4 explores the design selection through multiple criteria like cost, manufacturability, and performance parameters through the usage of several decision matrices. Using simulation and data gathered from bibliography a few designs will be chosen to be simulated and compared in the following chapter.

Chapter 5 will be focused on the previously selected structure's simulation through finite element analysis that will result in the final definition of a single structure able to achieve a compromise between the defined criteria. Several structures will be simulated with different designs and material configurations going from carbon and flax structures to hybrids.

Chapter 6 presents the conclusions of this work as well as the remaining gaps that should be addressed in future works.

2. State-of-art and literature review

In this chapter, a brief introduction to formula student and the impact attenuators used in this competition is presented. After that, a theoretical approach to the energy absorption parameters used in crashworthiness will be explored as well as a brief introduction to the materials generally used for the crash structure of these vehicles. An introduction to novel materials yet to be explored and its advantages and disadvantages will also be presented.

Later an extensive database collection of the designs found in the literature for crush structures was constructed, resulting in a collection of more than 30 articles.

The fracture mechanisms and composite failure modes at the crush front were later described, as well as the geometry influence on the energy absorption capabilities of certain structures.

Finally, a brief review of the crashworthiness models used for simulation was conducted, and several different types of moulds and manufacturing processes for composites were studied.

2.1. Introduction

A formula student vehicle is an open-wheeled vehicle with a single seat and open cockpit (formula style body) with four wheels that are not in a straight line. The vehicle must have fully operational front and rear suspension systems including shock absorbers and a predefined wheel travel. And most importantly for the scope of this thesis, it needs to have a frontal impact attenuator [9].

The first ever prototype from the FSFEUP team can be seen in Figure 1.

Figure 1 - FSFEUP 2022/2023 EV prototype

According to the FSG rules an impact attenuator is defined as "a deformable, energy absorbing device located forward of the front bulkhead" [9]. This goes in accordance with the definition of crashworthiness which is the capability of a certain material to absorb energy through controlled failure mechanisms and modes [12]. For any vehicle that has occupants impact attenuators are mandatory and crashworthiness ensures that, during a crash event, through energy absorption the energy that is able to reach the occupants compartment is not enough to breach it and that at the same time, this energy absorption does not generate decelerations that cannot be supported by the passengers inside [13].

In formula 1, for example, as can be seen in Figure 3 the cars have three mandatory impact structures: the front, side and rear impact structures, made out of CFRP that absorb impact energy in case of a

collision [14]. The most common absorbing structures found in, for example, modern passenger cars are made out of steel or aluminium that through folding and hinging, with extensive local plastic deformation, absorb the required energy [15].

This can also be the case for formula student impact attenuators since most of the times the investment to make these structures out of composites does not compensate for the weight loss. Therefore, most of the impact attenuators for FS cars are made out of aluminium or foam (See Figure 2).

Despite this, the motorsports industry constantly thrives for weight reduction to increase its performance on track, and the general automotive industry, due to the environmental issues and the need to reduce fuel consumption is making engineers trade the old heavy metal impact absorbing solutions by thin-walled composites [16].

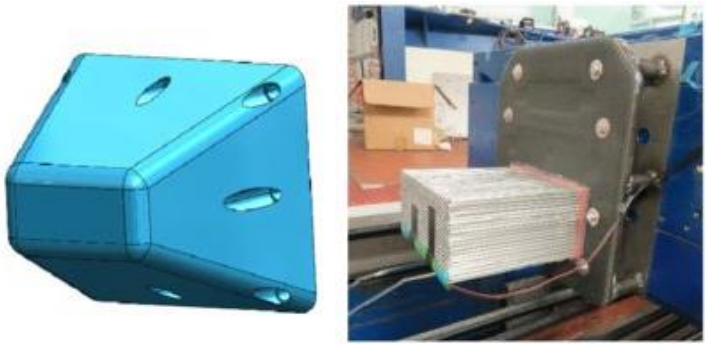

Figure 2 - Foam and aluminium FS car impact attenuators, respectively [17]

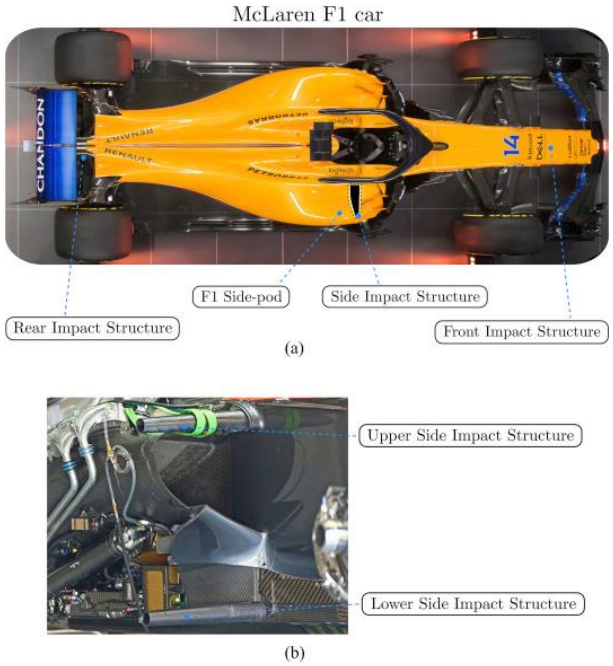

Figure 3 - Formula 1 impact structures [14]

2.2. Crashworthiness parameters

To understand and to qualify different structures according to its energy absorption capacity, a few parameters need to be defined. This subchapter describes those parameters.

2.2.1. Peak force

The peak force, or peak load, F_{max}, is defined as the maximum force that is applied on the crash structure. High peak loads can lead to injuries to the passenger due to the high decelerations induced and can also lead to unstable crushing behaviour that would lead the overall buckling supressing more stable mechanisms that are able to absorb more energy. To avoid great peak forces large structures should have an increasing number of layers from the beginning to the end of the structure. In the case of smaller structures, the introduction of a trigger in the beginning of the structure can induce the same effect.

If $F(\delta)$ is the force at each displacement then,

$$F_{max} = \max\left(F(\delta)\right) \tag{2.1}$$

Where δ goes from 0 to the length of the structure.

2.2.2. Average crush load

The average crush load, F_{mean}, is the average force during progressive crushing. This force should be measured after the initial crushing zone of the structure. In the case of composite structures this is going to be a highly serrated zone due to microfracture mechanisms [18].

This force can be determined by,

$$F_{mean} = \frac{\int_{\delta_1}^{\delta_2} F(\delta)\, d\delta}{\delta_2 - \delta_1} \tag{2.2}$$

Where δ_1 and δ_2 represent the beginning and the end of the progressive crushing zone, respectively.

2.2.3. Energy absorbed

The energy absorbed, EA, is the area below the force-displacement curve, corresponding to the crushed part of the structure. It can be calculated by

$$EA = \int_{\delta_1}^{\delta_2} F(\delta)\, d\delta \tag{2.3}$$

This energy is not only a material property characteristic but also a geometric property and layup dependent.

2.2.4. Specific energy absorbed

The specific energy absorbed is one of the most used parameters to characterize and compare different structures' crushing performance since it gives the energy absorbed per unit of mass. Since the main reason for the move to composite structures is weight reduction, this parameter is of essential use.

SEA can be calculated through equation (2.4).

$$SEA = \frac{\int_{\delta_1}^{\delta_2} F(\delta)\, d\delta}{m} \tag{2.4}$$

Where m is the structures mass.

2.2.5. Crush efficiency

This parameter relates the peak force with the average crush force, being therefore a measure of the crushing stability of the structure, if this value is not close to 100% than the structure is more prone to buckle than to crush in a progressive manner.

Its value is given by,

$$\eta_{eff} = \frac{F_{mean}}{F_{max}} * 100 \tag{2.5}$$

2.2.6. Crush stress

Crush stress is the most important comparison factor between different structures. It is material and geometry dependent and can be used for simulation purposes [19]. The average crush stress can be calculated through:

$$\sigma = \frac{F_{mean}}{Area} \tag{2.6}$$

Figure 4 can help understand all of the parameters mentioned before.

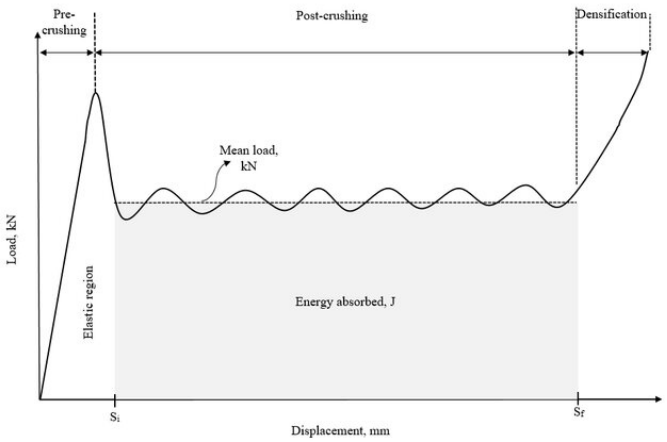

Figure 4 - Load-displacement for structure crushing [20]

2.3. Materials and designs for crush applications

This section makes a brief description of the most common used materials for crashworthiness purposes as well as a summary of the crush structure's designs that have been explored in the literature.

2.3.1. Metals

Metallic structures are often used as impact absorbers, due to their low cost, ease of manufacturing and good recyclability. As stated by S. Boria et al [21] aluminium absorbers collapse in three different modes: axisymmetric concertina folding, diamond fold mechanism and mixed mode. These modes absorb energy through plastic deformation and fracture or tearing [22].

Aluminium tubes can reach values of specific energy absorption of 20-60 kJ/kg. As it will be seen later these values are lower than the values obtained for carbon fibre structures.

Aluminium honeycomb is still the most used material for formula student impact attenuators, this is mainly to the fact that it is a standardized IA that does not require further testing (See Figure 5).

Santos [23] compared an aluminium honeycomb impact attenuator with carbon fibre impact attenuators through experimental and numerical results. Both the numerical and experimental results had into consideration the whole impact attenuator assembly including the anti-intrusion plate and the front bulkhead. The structures were simulated using Hypermesh® and Hypercrash® to define the mesh and the loads and boundary conditions, respectively and Radioss® to achieve a numerical solution. Despite the numerical solutions showing promising results for the composite structures with weight reductions of almost 50%, the experiments proved that none of the structures tested was able to fulfil the requirements due to catastrophic failures caused by buckling that were not predicted in the simulation model. This study has shown the main reason why aluminium honeycomb impact attenuators are still preferred to composite impact attenuators: the numerical simulations still cannot predict accurately the composite structures behaviour, and the money that is spent on manufacturing and testing this kind of structures may not compensate.

T3.17.7 A team may use one of the "standard" FSAE IAs, in order to avoid testing, provided that:

- if the front bulkhead width is larger than 400 mm and/or its height is larger than 350 mm a diagonal or X-bracing that is a front bulkhead support tube or an approved equivalent per T3.2, must be included in the front bulkhead. Or equivalent for mono-coque bulkheads.
- must use a 1.5 mm solid steel AIP that is welded along its full perimeter to a steel bulkhead or use a 4 mm solid aluminium AIP that is bolted to any bulkhead with a minimum of eight 8 mm metric grade 8.8 bolts
- if the "standard" honeycomb IA is used, the IA must be of pre-crushed type

T3.17.8 If the standard IA is used, but does not comply with the requirements of T3.17.7 physical testing must be carried out to prove that the AIP does not permanently deflect more than 25 mm.

Figure 5 - FSG rules 2023 regarding standard IA [9]

2.3.2. Foams

Foams are another Formula Student or FSAE standard impact attenuator material. To be considered as standard the impact attenuator must be made out of Impax 700 foam, and it doesn't require any additional testing as already referred in Figure 5. They are able to absorb energy through plastic deformation, more specifically at the cellular scale through cell wall bending and stretching, followed by wall buckling and tearing [24].

Due to the fact of being a standardized material, there are only a handful of works about formula student impact attenuators made out of foam, and the ones that effectively exist lack important information.

Tittu Paul [25] studied 3 different types of foam for a standard FSAE impact attenuator design: Impaxx 700, Rohacell-51WF and High density PU. The author simulated all of the materials using a

plasticity Von-Mises model in a drop test feature included in SolidWorks®. The stress-strain curves for each material were used to define the material properties. For all the materials, only the IMPAXX 700 foam was able to comply with the requirements with the other two materials exceeding the maximum average deceleration. Nevertheless, the benefits of using any of the other materials is not mentioned throughout the work, neither is the specific energy absorption determined.

J.M.J. Schormans [26] simulated a foam impact attenuator with two different types of foam: Rohacell 51 WF and Rohacell 110IG. The author used Abaqus with an elastic-plastic model with volumetric hardening which was calibrated using an experimental compression test. Despite both structures passing the requirements the author does not mention a final choice or the specific energy absorption of each structure.

Finally, Shaaban et al. [27] studied different polyurethane foams numerically and experimentally for a formula student impact attenuator. Initially, the authors found a solution with an $80\ kg/m^3$ polyurethane foam that was able to pass the requirements with a mass of 1.138 kg, that was later optimized by hollowing out the impact attenuator, being able to achieve a 13.4% mass reduction and still complying with the rules.

Nevertheless, the mass of this impact attenuator is still high compared with what can be achieved with other materials. This was the main reason for the progressive change to aluminium honeycomb impact attenuators.

Nevertheless, foams never stopped being used in crashworthiness applications. They are still applied to fill other structures and increase their specific energy absorption. Goyal et al. [28] experimentally tested star-shaped polygon thin-walled aluminium tubes filled with different types of foams, for a constant speed of 1000 mm/s and it was found that the incorporation of foam almost doubled the specific energy absorption reaching a value of 36.03 kJ/kg and increased the crushing stability of the tubes.

2.3.3. Carbon fibre reinforced composites

Inside the composites category, carbon fibre reinforced polymers (CFRP), are the most used, especially because of their excellent specific properties like high specific strength and stiffness. Generally, CFRP come in unidirectional (UD) or weave types of configurations. While UD configurations can have excellent performance in specific cases, the fact that they have poor out of plane properties can cause them to delaminate. Weave or woven fabric composites can mitigate this problem. Their balanced mechanical properties, easy handling and impact resistance make them suitable for multiple applications, one of them being on crash structures [29].

Regarding the specific energy absorption as can be seen in Table 1, CFRP can have more than double the SEA of conventional metals like aluminium and steel. This makes them desirable for the automotive industry since it results in lighter structures that will result in increased performance and lower fuel consumption.

But while conventional metals fail by well-known mechanisms like plastic deformation, that doesn't apply to composites which fail by more complex mechanisms like splaying with axial splitting and fragmentation with debris [21]. These intricate mechanisms can be influenced by several parameters like fibre and matrix type, fibre volume fraction [30], stacking sequence of the plies [19], and geometry [31, 32].

Besides this, when talking about the energy consumption to produce CFRP, this value amounts to 5 times the amount of energy needed to produce flax-based bio composites (1100 MJ/kg vs 202 MJ/kg)

and also 4.5 times more global warming potential (GWP), ~54 $kgCO_2Eq.$ against 12 $kgCO_2Eq.$ [33]. These values keep pushing the move towards natural fibre composites.

Table 1 - Specific energy absorption for aluminium and CFRP for different geometries [21]

Geometry	SEA [kJ/kg]	
	Al	CFRP
External diameter: 80 mm Thickness: 2.5 mm	47.2	65.5
External diameter: 80 mm Thickness: 2 mm	36.5	60.3
External diameter: 80 mm Thickness: 1.5 mm	22.1	54.5
External diameter: 50 mm Thickness: 2.5 mm	58.5	72.2
External diameter: 50 mm Thickness: 2 mm	40.2	54.4
External diameter: 50 mm Thickness: 1.5 mm	37.1	48.5

2.3.4. Natural fibre reinforced composites – Flax

As referred before natural fibre reinforced composites can be a more sustainable alternative to the more common synthetic fibre composites, namely CFRP. In terms of energy for the production, a flax-based bio composite accounts for 202 MJ/kg of energy while for CFRP it accounts for 1100 MJ/kg. There are several natural fibres that have been studied for crashworthiness purposes namely Bamboo, Ramie, Kenaf, Hemp, Flax, Jute, etc. As it can be seen in Table 2 and Table 3 flax stands out for being one of these natural fibres with the greatest mechanical properties and SEA. Besides that it also has lower density than the most common fibres like glass or carbon [34].

Flax (*Linum usitatissimum)* was one of the first fibres to be extracted, spun and woven into textiles, which were already found in Egyptian graves dating back to 5000 BC, and some recent studies may indicate that they were already in use 30000 years ago [35]. Flax fibres are produced in the stems of flax plant. It is a cellulose polymer with a crystalline structure and roughly 12–16 μm in diameter.

Despite what was stated before, Flax fibres have a major problem which is related to its hydrophilic properties, making their adhesion to hydrophobic matrices so poor that the composite properties may be inferior to the properties of its individual components on their own. This problem can be solved by applying treatments to reduce the moisture absorption, but in turn the processing energy of this fibres is going to rise and make them less sustainable [35].

Another drawback has to do with the high variability on the flax properties which is induced by the variety of the plant, agricultural variables, and weathering conditions. This variability does not exist in synthetic fibres where the processing of the fibres is more controlled [35].

Generally, crushing can occur in composite laminates through 3 different types of fracture: elastic and inelastic buckling, failure initiation away from the crush front, and normal progressive crushing. The last type of fracture it's the most desirable since it can absorb more energy in a stable way. This type of fracture is mainly dependent on the material compressive strength and buckling, which makes flax fibres more prone to buckle instead of progressively crushing while CFRP are more prone to progressively crush.

All of these problems can be mitigated by the introduction of hybrid composites which will be explained in the next subchapter.

Table 2 - Reinforcement properties [34]

Fibre/Reinforcement	Density (kg/m^3)	Strength (MPa)	Elastic modulus (GPa)	Elongation (%)
Synthetic fibres				
Carbon/Graphite	1610-2200	4900	230	2.1
Glass	2500	2000-3000	70	2.5
Kevlar	1440	2920	70.5	3.6
Graphene	1800	130000		
Carbon nanotube	1300-1400	13000-53000	1000	16
Natural Fibres				
Jute	1300-1460	269-800	10-30	1.5-8
Flax	1400-1500	345-1500	27.6	2.7-3.2
Ramie	1500-1550	147-938	44-128	2.0-3.8
Kenaf	1450	930	53	1.6
Hemp	1480	550-900	70	1.6
Silk	1320	500-1300	5.22	15.3
Abaca	1500	400-760	12	3-10
Banana	1350	444-600	12	5.9
Bamboo	600-1400	140-800	11-33.87	1.4
Coconut	1150	500	2.5	20

Table 3 - Crashworthiness studies and material properties [34]

Composite	SEA (kJ/kg)
Synthetic fibres	
Carbon/Polyamide 6	120.8
Carbon/Aramid/Epoxy	95.7
Carbon/Epoxy	19.1-78
Carbon/Vinyl ester	71.0
Glass/Epoxy	17.42-82
Glass/Carbon/Epoxy	50.25-66.0
Glass/Polyester	52
Glass/Polypropylene	39.1
Glass/Polyamide	11
Glass/Graphite/Epoxy	1.1
Natural fibres	
Jute/Flax/Hemp/Epoxy	64.46
Flax/Epoxy	41
Flax/Polyurethane	37.9
Jute/Epoxy	33.2
Kenaf/Epoxy	9.2-38.9
Basalt/Epoxy	30.68
Ramie/Bio-Epoxy	15.8
Silk/Epoxy	12.0

2.3.5. Hybrids

Composite hybridisation consists of embedding two or more types of fibres in a single polymer matrix [36]. In the case of impact structures, the most common type of hybridisation is laminated hybridisation where layers of different materials are stacked upon each other. This kind of hybridisation allows for the natural, more sustainable flax fibres to be combined with stiffer and with higher compressive strength fibres like carbon fibre.

Strohrmann et al. [37] studied the crushing behaviour in quasi-static and dynamic procedures, 4 different layups: $[C]_8$, $[C_2/F_2]_S$, $[F_2/C_2]_S$ and $[F]_8$. The $[C_2/F_2]_S$ specimens revealed only 13% lower SEA than the pure carbon specimens with 24% bio-based material, reaching 53 J/g, showing that the hybridisation percentage does not have a linear relationship with the SEA, since the SEA for a 50% hybrid was higher than the arithmetic mean of the pure carbon and flax specimens. The exterior carbon fibre layers increased the overall structure stiffness and compressive strength inducing a fragmentation crushing mode. The specimens with flax on the outside revealed slightly less specific energy absorption.

As is evident from the study referred before, despite the promising results, hybridisation adds to the complexity of the structure, since SEA besides material type, ply orientation and geometry is also going to depend on the hybridisation ratio and stacking sequence. Therefore, extensive testing needs to be done to obtain a database to support hybrid structures simulation.

Despite Flax being described until now as a sustainable material, most of the flax prepregs used for crush applications have a thermoset resin which is makes the overall composite very difficult to recycle. Schrank et al.[38] states that thermoplastic composites should have even better SEA than thermosets and also that they are much easier to recycle since they can be melted and the fibres recovered, but the reason why these kinds of composites are not widely used has to do with its difficult processing which generally leads to voids and delaminations in the final structure.

2.3.6. Designs found in the literature

Several designs have been studied for self-made Formula Student impact attenuators and crash structures in general throughout the years using mainly foams, aluminium honeycomb and CFRP structures. Figure 6 shows some of these designs found in the literature.

From all the designs presented in this figure none explores composite hybridisation or the use of pure natural fibre structures. Up until now, only articles conducting small coupon testing were found on the subject.

2.4. Fracture mechanisms in composite materials

Composites energy absorption relies on complex fracture and damage mechanisms, this fact makes them harder to understand than the most common metals that absorb energy through plastic deformation.

Figure 7 shows several fracture mechanisms that generally occur in composite failure through compression: Fibre fracture, interlaminar crack growth and shear forces between the plies, friction between the bended fronds and the crush plate, matrix cracking, delamination, etc.

The total energy absorbed by a composite when subjected to crushing loads can be obtained by the sum of the energy dissipated by each of these mechanisms, and can be determined by [39]:

$$U_{total} = U_{1c} + U_{2c} + U_{\sigma} + U_{ff} + U_{fr} + U_{others} \quad (2.7)$$

Where U_{1c} represents de Mode-I fracture energy, U_{2c} the Mode-II fracture energy, U_{σ} the energy absorbed on frond bending, U_{ff} the fibre fracture, U_{fr} the friction related energy absorption and U_{others} other energies including the Mode-III effects.

This section will briefly describe some of these mechanisms, so that composite crushing can be better understood.

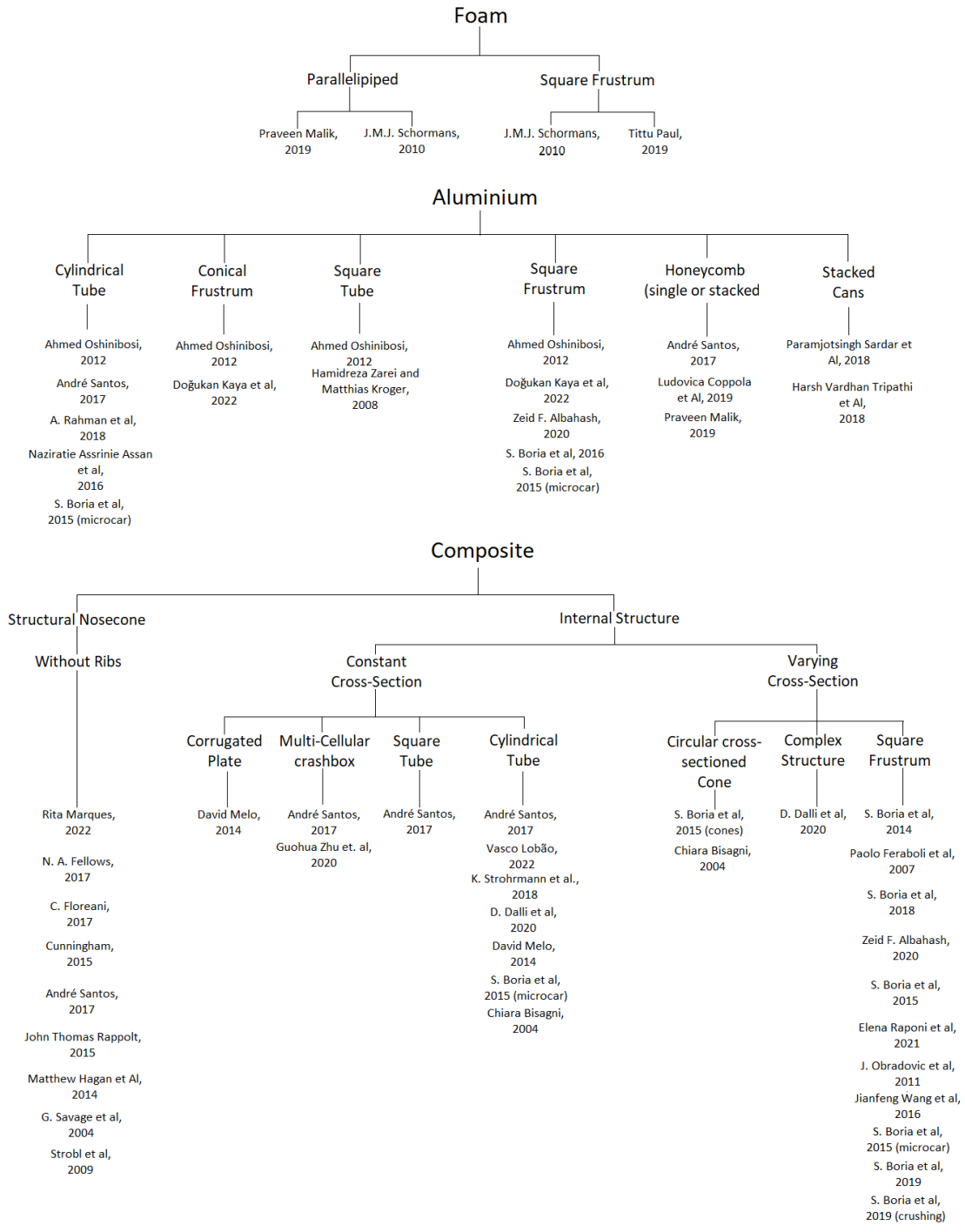

Figure 6 - Impact attenuator designs found in the literature [8, 14, 21, 23, 25, 26, 37, 39-68]

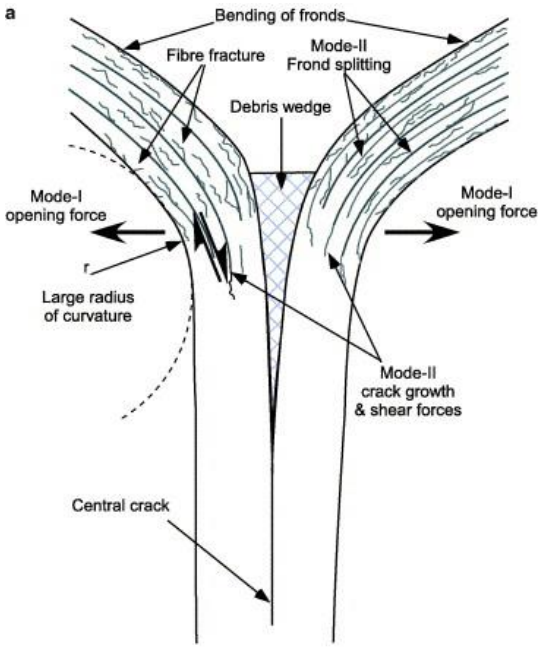

Figure 7 - Composite fracture mechanisms [69]

2.4.1. Matrix cracking

Matrix cracking as the name indicates is the formation of cracks in the composite matrix. This type of damage reduces the mechanical properties of the material and, despite being a non-catastrophic type of damage, can induce fatal types of failure like delamination. These cracks can be preceded by matrix debonding that form visible voids that can later propagate and are formed under static loading or fatigue [70].

2.4.2. Fibre breakage

Fibre breakage or failure occurs when the individual fibres break. This type of failure is generally the one that defines the final composite failure, which justifies the fact that in fibre bundle theory the final tensile failure of the composite occurs when a certain number of fibre failures occur [71]. In the case of compressive loads, the fibres can fail by fibre kinking, this type of failure results in small fibre misalignments that when loaded in compression increase the misalignment angle generating matrix and later fibre failure [72].

2.4.3. Delamination

Delamination is the bonding failure between the plies of the composite. It can be caused by matrix cracking, bending cracks and shear cracks. This type of failure affects the composite compressive strength resulting in composite failure by buckling, which for an energy absorption structure is unacceptable [71].

There are three modes of interlaminar cracking that result in delamination with some having more importance in crashworthiness. These will therefore be explained in this section.

2.4.3.1. Mode-I interlaminar fracture toughness

Mode-I interlaminar fracture toughness corresponds to fracture of a composite by applying a tensile load normal to the plane of the crack in both sides of the laminate. The double cantilever beam test (DCB) (ASTM D5528) is the most common method to measure the fracture toughness (critical value

of delamination growth for an opening load P), G_{1c}, for this failure mode under static or dynamic conditions. The test works by inserting a crack in one of the sides of the laminate using a non-adhesive film between the plies for a certain length and then loading the specimen in the normal direction of the crack (See Figure 8) [73].

Both Hussein [74] et al. and Mamalis et Al.[75] determined the importance of this failure mode to predict the energy absorption capability of a certain structure due to the phenomena that occurs at the crush front and will be explained in another section.

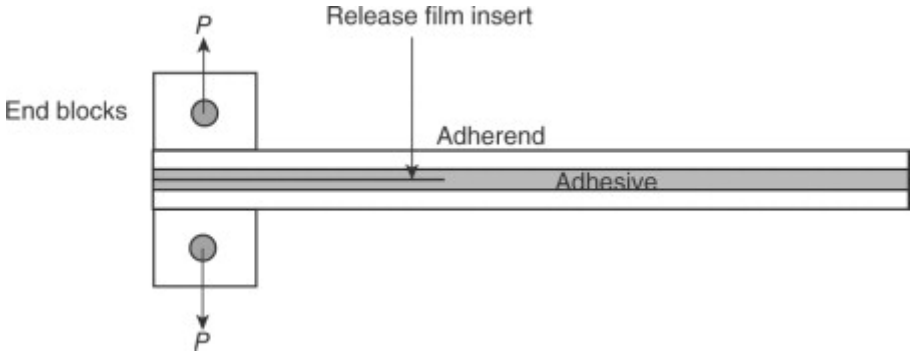

Figure 8 - Double cantilever beam test [73]

2.4.3.2. Mode-II interlaminar fracture toughness

Shear stresses acting parallelly to the crack plane and perpendicular to the crack front result in composite delamination that can be characterized by the Mode-II fracture toughness. One of the tests to determine this fracture toughness, G_{IIc}, is the end-notched flexure test (ENF) described by the ASTM D 7905 standard or the similar four-point bending configuration of the same test (4-ENF) (See Figure 9). This test works by introducing a crack in one side of the specimens similarly to what is done in the DCB test, but this time loading the specimen in bending, through 3 or 4 contacting points, the crack is then going to propagate, and the crack length measured for a certain load applied.

Savona et al. [69] concluded that this type of failure has a strong correlation with the specimens crush stress, where high values of Mode-II fracture toughness relate with high crush stresses.

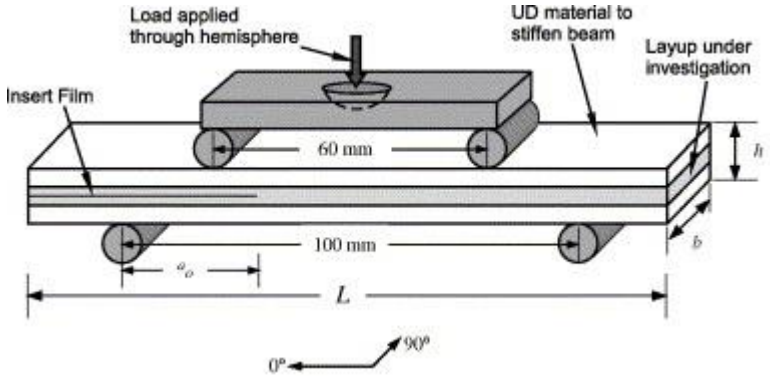

Figure 9 - 4 point bending ENF test [69]

2.5. Composite failure modes at crush front

Hull [19] defined the two failure modes at the crush front of composite tubes: splaying and fragmentation. To describe both modes, experiments were conducted on $[0/90]_S$ glass fibre-polyester resin tubes and glass cloth-epoxy tubes, respectively. These modes are based on the fracture mechanisms described before and are going to be presented in this section.

2.5.1. Splaying mode

In a $[0/90]_S$ composite tube, two kinds of fibres can be defined: axial and hoop fibres, corresponding to the 90º and 0º degrees respectively, in Hull's [19] notation. The axial fibres are responsible for carrying most of the compressive load while the inner and outer hoop layers are responsible for supporting the axial layers and minimizing buckling [19].

When a squared ended tube is compressed, since there is no fracture trigger, the tube tends to resist more load before starting to crush, resulting in a higher peak force and higher tendency to buckle. To avoid this, generally triggers are added in the crushing front, like for example chamfers that allow for damage initiation [19].

This damage trigger will allow for the beginning of the splaying mode. This failure mode consists in the splaying of the axial fibres in a series of frond to the outside and the inside of the tube (See Figure 10). Due to the crushing of fibres and resins, a debris wedge is going to form in the middle of the splayed fronds increasing the tendency to splay. This splaying is only resisted by the hoop fibres until the external hoop fibres break due to tension and the internal hoop fibres break due to buckling and kink and intralaminar shear normal to the fibres [19].

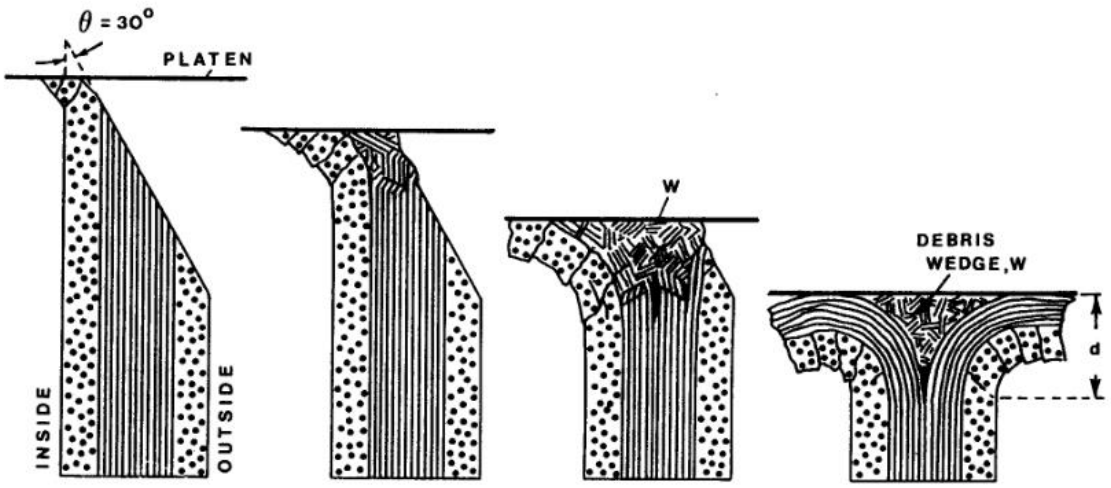

Figure 10 - Splaying fracture mode [19]

This failure mode is induced by several different forces including compressive forces between the crushing plate and the specimen, friction between the plate and the sliding fronds, friction between the debris wedge and the fronds, friction between adjacent laminae in the fronds and hoop constraints [19].

2.5.2. Fragmentation mode

Fragmentation mode is the formation of fragments in the crush zone that are pushed to the inside and the outside of the tube before being separated from the tube walls (See Figure 11). This failure mode is a mixture of several types of failure like fibre fracture, buckling and interlaminar-type failure, and its mainly generated by high shear forces [19].

Hull [19] found evidence that there is a competition between these two failure modes, whenever splaying does not occur, the stress accumulates in the crush zone until the critical value for shear fracture is reached and fragmentation occurs. The tendency to each one of these types of failure is going to be dependent in several factors like laminae configuration, elastic properties, and failure strengths of the individual laminae failure mechanisms.

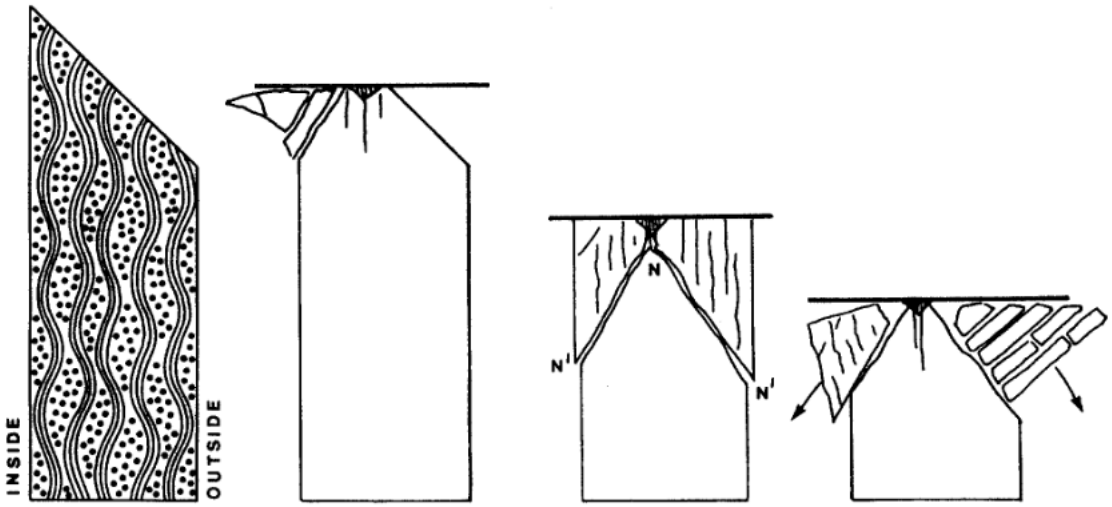

Figure 11 - Fragmentation failure mode [19]

Solaimurogan et al.[76] produced tubes with different stacking sequences and percentages of hoop and axial fibres. The author used woven roving (WRM) glass fibre mats of density 610 g/m^2, unidirectional glass fibre of density 750g/m^2 and isophthalic polyester resin to produce planar and cylindrical specimens by hand lay-up. The woven roving mats were oriented so that the fibres were aligned with the axial and hoop directions. The specimens were made with a D/t ratio between 15 and 25 mm to avoid global buckling and catastrophic failure and a chamfer trigger was included, and were tested quasi-statically at 2 mm/min.

The author concluded that increased circumferential fibre content supresses splaying and the SEA increases proportionally with the increase in the number of axial fibres until a percentage of 68% from which the splaying mechanism is supressed, and the SEA starts to decrease.

As it can be seen these two mechanisms govern the crushing of composites and can influence SEA and crush stress values.

2.6. Geometry influence

Crush stress is not a material parameter, it is dependent on both the material used, geometry, lay-up, and other parameters. To obtain a structure capable of absorbing the necessary energy, the engineer needs to dominate these several aspects.

Paolo Feraboli [15] studied the influence of the trigger in the coupon energy absorption efficiency between a saw-tooth and a steeple trigger. The later led to lower SEA measurements even though the same failure loads were obtained. Generally, saw-tooth triggers lead to a more progressive crushing. Khan et al. [77] studied the influence of trigger mechanisms on glass epoxy/PVC composite tubes, between specimens with no trigger, a chamfer trigger and a double-step trigger. It was concluded that the inclusion of a trigger in the coupons resulted in an increase on SEA of the tubes, due to the decrease in the initial peak force and the increase in the mean crushing force. This induced an uniform and progressive failure mode in the tubes through fibre splaying and progressive folding while in the specimens without trigger the failure was catastrophic with transverse shear and interpenetration. The authors also studied the influence of the chamfer angle and the second step height on the chamfer trigger and double-step trigger, respectively. Increasing the chamfer angle and the second step height resulted in lower initial peak values but the influence on mean crushing force was not clear. Generally, double-step triggers resulted in better energy absorption properties. Palanivelu et al. [78] studied the difference between tulip and chamfer triggers and concluded that the first result in lower initial peak

forces, higher crushing efficiency and SEA. With this we can conclude that despite the trigger being only a way to initiate the crushing it can have a great influence in the energy absorption capability of the specimens.

Besides trigger influence, another parameter was found to influence the energy absorption capabilities of a certain structure: the inclination of the laminate with respect to the impacting body. S. Boria et al. [65] studied the influence of this effect, the thickness and the minor diameter in the axial crushing behaviour of truncated cones both statically and dynamically. It was found that the increase in slope reduced the specific energy absorption and crush stress, mainly due to the reduction of the bending energy and for higher slopes due to the inhibition of the debris wedge formation, while the increase in thickness increased the average crushing stress and SEA but also the initial peak force. Finally, the reduction in the minor diameter increased the SEA but not the average crush stress. Despite this decrease in SEA for greater inclinations, the use of a small 5-degree angle allows for the initiation of a more stable crushing. Figure 12 shows the dependencies that were referred before.

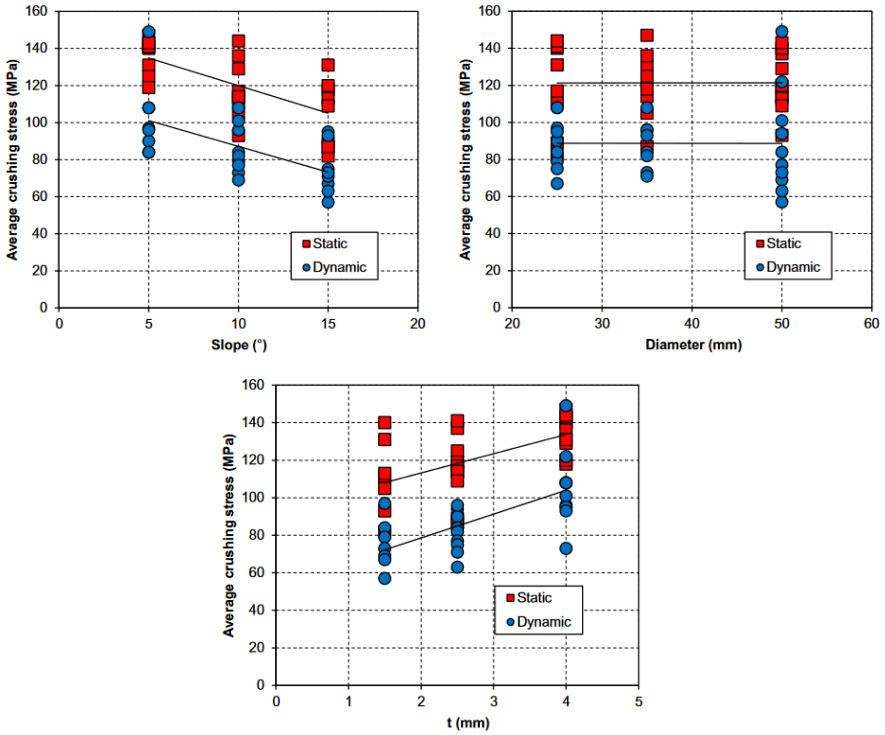

Figure 12 - Average crush stress dependency on slope, minor diameter and thickness [65]

Vasco Lobão [39] found that increasing the radius of curvature in tubular coupons leads to a decrease in both crush stress and SEA by testing several CFRP, Flax and Hybrid flat and tubular coupons quasi-statically (See Figure 13). The author also concluded that open section coupons tend to fail catastrophically contrarily to what happens with closed section coupons.

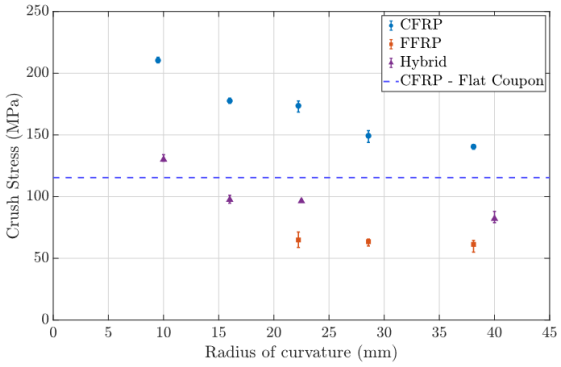

Figure 13 - Crush stress dependency on the radius of curvature [39]

2.7. Crashworthiness simulation

For the purpose of this thesis, several crashworthiness simulations had to be run. In this section a brief literature review on different types of simulation models will be described.

2.7.1. Macro vs meso-scale modelling

There are several methods that can be used to study or simulate composite behaviour: micro-scale, where reinforcement and matrix are considered separately; meso-scale, where, through the reinforcement and matrix properties, the ply properties are calculated and the composite is considered as a stack of plies; and macro-scale, where the laminate properties are calculated using the ply properties, orientation, stacking sequence, etc.

Meso-scale and macro-scale models are the most commonly used in crashworthiness simulations. Several authors simulated in meso-scale by using solid elements for the plies whilst using cohesive surfaces to capture interlaminar failure [79-81], or in macro-scale by using shell elements to represent the whole laminate [82, 83].

Solid elements are used whenever out of plane stresses are significant while shell elements are used to represent the behaviour of thin structures with significantly low computational time [56].

Solid elements can be composed of a single material, or several layers of different materials like in the case of simulating solid composite structures where each ply is considered as a different material. When these elements are not distorted, they are the most accurate, since they can represent both in-plane as out-of-plane stresses and strains, especially in the case of isoparametric quadrilateral and hexahedral elements, which are more cost-effective and allow for smooth stress transitions between the elements (see Figure 14). These types of elements can be used for several different applications from linear analysis to complex non-linear analysis involving contact, plasticity, and large deformations [84, 85].

This type of elements comes in different geometric shapes. In the case of explicit simulations, they can be triangular and quadrilateral in two-dimension simulations and tetrahedral, triangular prism, and hexahedral elements in the case of three-dimensional simulations. All of these elements have nodes at their vertexes with the triangles and tetrahedra having the option to have additional nodes at the middle points of the edges (First- and second-order elements respective). First-order elements are recommended for simulations where large strains exist.

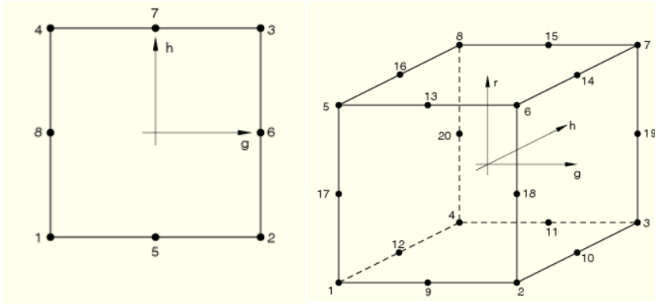

Figure 14 – Solid quadrilateral and hexahedral second-order elements [86]

Shell elements on the other hand are used whenever the thickness of an object is significantly smaller than the other dimensions. The element, in its conventional variant, than uses a reference surface to define the geometry of the body and discretize it [87].

Both solid and shell elements can used full or reduced integration to calculate the outputs at the elements. In the case of the reduced integration a lower-order integration forms the element stiffness reducing the CPU time due to the lower number of points. In the case of the existence of bending or large distortions first-order elements with reduced integration are recommended, which is the case of crashworthiness simulations. Nevertheless, the use of this kind of elements may result in the hourglass effect that can affect the simulation accuracy and that will be described in a later section [87].

In the case of the shell elements, the whole composite laminae is simulated as a single structure while with solid elements it is possible to include interlaminar failure representing fracture mechanisms that are responsible for a great amount of energy absorption and therefore representing a closer behaviour to the one that is shown in real specimens.

S. Boria et al. [56] studied the influence and accuracy of solid and shell modelling in an impact attenuator for formula student applications. The structure with a geometry similar to square frustum was initially simulated using the LS-Dyna software, then it was manufactured with CFRP plain weave prepregs and tested in a drop tower. Double cantilever bending and four-point end notch flexure tests were conducted to determine mode-I and mode-II fracture toughness.

In the case of the shell model after all of the plies of an element failed the nodes would be erased while in the solid model cohesive elements were included between bundles of a certain number of plies to capture interlaminar failure.

The authors concluded that both the solid and shell simulations were able to accurately predict the structure failure in terms of quantitative values when compared to the experimental results, but the solid simulation had a CPU time 60 times higher than the shell simulation.

Denis Dalli [88] compared a meso-model with experimental results for quasi-static testing of flat and tubular coupons as well as meso and a macro-models with experimental results of quasi-static crushing for a Formula 1 side impact structure. The meso-model uses one reduced integration hexahedral element through thickness for the plies and built-in Abaqus® cohesive behaviour to simulate the interlaminar properties for a total of 619000 elements, whilst the macro-model uses 4 and 3 node shell elements for a total of 59000 elements.

For the coupons the meso-model was not able to represent neither qualitatively or quantitatively the behaviour of flat and tubular coupons, with the curvature of the splayed coupons not being consistent with the experimental results. Qualitatively, the same happened in the side impact structure which folded in the simulations like a metallic structure, while quantitatively the load results, despite

following the same trend as the experimental results, underestimated the forces generated in the crushing of the structure. Besides that, the simulation took 7 days in 20 CPUs.

In the case of the macro model, it was able to predict with good agreement the load-displacement results with a slight overestimation being more cost effective and taking only 20 hours in 1 CPU.

The meso-model, due to its low cost-effectiveness, limited the amount of elements in the through thickness direction reducing the accuracy on the prediction of bending behaviour and increasing the probability of the occurrence of hourglassing and high distortions [88].

Despite the possibility for representation of intralaminar and interlaminar mechanisms and better representation of through thickness stress distribution, the meso-models require well-adjusted material models and a mesh alignment strategy to correctly represent these mechanisms, as well as large computation times which may not be interesting in the industry [88].

On the other hand, macro-scale models, allow for the determination of force-displacement curves in close agreement with the experimental results, as long as the model is fed with good crushing properties obtained from coupon testing. Nevertheless, if the model is not giving accurate results at first, due to the much lower computational times it is possible to adjust the model until it matches the experimental results without massive delays on the structure designs.

2.7.1.1. Stacked shell

Another option, that can offer a compromise between the meso-model using solid elements and cohesive surfaces and the macro-model using shell elements, is a meso-model approach using stacked shell elements (See Figure 15). This approach allows for the representation of interlaminar failure without the computational cost of a solid model.

Joosten et al. [89] compared a stacked shell model against experimental results for crushing of a hat-shaped open section composite structure. The authors used stacked plies modelled with 4-node shell elements with a decohesion fracture model to control the initiation and propagation of the delamination between the plies. Each shell was assigned with 4 through-thickness elements to ensure an accurate bending response. Each layer had a self-impacting contact applied to avoid them to penetrate each other and themselves.

The initial simulations showed significant lower crushing loads than the experiment results and a behaviour which wouldn't match the reality. By eliminating the friction coefficient between the plate and the structure from 0.2 to 0, the simulation was able to qualitatively represent the crushing behaviour of the real specimens, although this change increased the quantitatively error of the simulated loads even more. The problem was solved by manually increasing the Mode I and II energy release rates to have a better correlation with the experimental results [89].

The model was able to predict the steady state crushing load within 1.5% and the SEA within 0.2%, although deviating from the peak crushing load in 11%. Nevertheless, this simple simulation still took 6 hours in one CPU [89].

Waimer et al. [90] used a stacked shell approach with cohesive elements to simulate the dynamic crushing of CFRP components. The study conducted both numerical and experimental tests at two different velocities axially and also with off axis loading in aircraft fuselage crush structures.

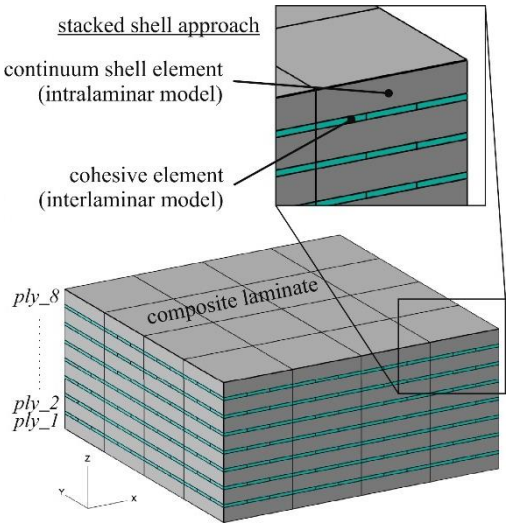

Figure 15 - Stacked shell modelling. Adapted from [90]

The authors used continuum shell elements with reduced integration for the intralaminar modelling in detriment of 4-node conventional shells to obtain a precise representation of the laminate stacking [90]. These types of elements are more accurate for contact modelling than conventional shells since they account for two-sided contact and thickness changes. Nevertheless, they perform worse in capturing the bending behaviour [91].

While the intralaminar properties needed for the simulation were determined via experimental tests, for the interlaminar behaviour represented by cohesive finite elements, due to the impracticality to determine the necessary parameters via experimental tests, these values had to be calibrated through several simulations.

In the initial simulations, the simulation results did not match the experimental results, so the authors had to readjust the cohesive parameters manually to improve the results. It was also found that the continuum shell elements were affecting the cohesive elements behaviour.

After some readjustment the simulation was able to capture the relevant effects and to obtain force-displacement results in accordance with the experimental results despite the underestimation of the steady state crush force. Nevertheless, the simplest simulations in this study took between 29 and 33 hours with 4 processors for 159000 elements [90].

Both studies demonstrate that despite being able to represent the correct crushing behaviour with force-displacement values close to the ones found experimentally, there is the need to calibrate the models by running several simulations. Considering the high computational time of each one of these simulations, this kind of modelling is expensive in terms of CPU time, which might not be acceptable in the industry, especially formula 1 and motorsports, where fast results are crucial.

2.7.2. Softwares and material models

Several material damage models have been used throughout the literature to describe damage initiation and propagation in crashing simulations. Most of these models are specific to the software that is being used to simulate the structures.

For the LS-Dyna®, the most used material models are MAT54 [60, 82, 83, 92], MAT55 [56, 59, 60, 93] and MAT58 [94, 95], with the first being suitable for unidirectional composites and the last one for woven fabric composites. With PAM-Crush® the most used material model is the Ply type 7 model [89, 96]. Finally, Abaqus® software has a built-in composite model for woven materials that

can be called using the material name ABQ_PLY_FABRIC [88, 90] and that is also of common utilization in crash simulations. Besides this model, there is still an in-built model for damage of unidirectional composites based on Hashin's criteria [97] and models developed by the science community like a phase-field fracture model developed by Konica et al. [98].

Fellows [51] used MAT58 within LS-Dyna® to simulate the behaviour of a structural nosecone to serve as a formula student impact attenuator for the Oxford Brooks team in 2017, with a varying layup in 2/2 twill weave carbon fibre prepreg from 3 to 11 plies. The simulation was based on a macro-modelling approach using a single shell element through the thickness of each ply. The structure was also manufactured and dynamically tested with a sled impactor using the parameters defined by the competition rules.

The author studied the influence of varying the different parameters of the damage model to determine the parameters that resulted in the most similar results with the experiments, being able to reach a close agreement between them, after several runs.

Boria et al. [59] used MAT55 within LS-Dyna® to study the behaviour of an impact attenuator for a FSAE vehicle for both solid and shell elements. The material damage model was fed with properties obtained on material characterisation and crush tests. The simulation results were compared with the experimental results obtained through the usage of a drop tower and revealed a close agreement for both simulation methods.

Raponi et al. [60] used optimization strategies to determine the best suitable parameters in MAT54/MAT55 material damage model, to simulate a thermoplastic composite structure composed of polypropylene matrix and reinforcement. This structure was designed to serve as a FSAE impact attenuator. The element deletion occurred via maximum strain in the longitudinal and transverse directions via compression or tension.

This material damage model has a soft parameter that degrades the elements after the crush front to reduce instabilities due to element deletion which was one of the parameters that went through the optimization. This optimization was carried out trying to minimize the mean squared residual error between the force values of the experimental and numerical load-displacement curves.

The authors found that the final results had a high sensitivity response to the variation of the parameters, and after the optimization problem the simulation was able to have similar results to the experiments.

Dalli [88] used ABQ_PLY_FABRIC within Abaqus® in conjunction with the CZone® plugin to simulate in a macro-model the crushing behaviour of a Formula 1 side impact structure. The author determined the necessary parameters for the material damage model through material characterization tests and the parameters to input on CZone® through crush tests. The numerical results were compared with experimental results and were in close agreement.

From the studies presented, LS-Dyna® material damage models seem to require more parameter optimization to have a good agreement between numerical and experimental results than the conjunction of for example ABQ_PLY_FABRIC and the CZone® plugin. Nevertheless, this last approach requires a large number of experiments to determine the necessary crushing parameters to input in CZone® that are dependent on ply orientation, coupon geometry and crushing velocity.

2.8. Manufacturing of composite structures

There are several composite manufacturing processes that are best suited for each specific application. In this case, since we are working with a technology that requires high manufacturing quality and we have prepregs of both carbon fibre and flax available at our university, prepreg hand layup is going to be the process used.

Therefore, what remains to be chosen are the material moulds. Multiple solutions have been found for the manufacturing of CFRP parts, both in industrial and formula student context.

L. Hamilton et Al. [99] and Alexander Carline [100] both manufactured CFRP monocoques using female GFRP moulds made by hand-layup on a high density foam male mould. Yusuf M. Binderwala and Karl N. Karbhari [101] used CFRP prepreg hand-layup on plain exterior MDF to produce a non-structural nose cone.

Boria, S. et Al [58] produced a CFRP impact attenuator with a square frustum geometry using prepreg hand-layup on an mould machined from an epoxy block. In the same article the author also produces a thermoplastic carbon fibre reinforced impact attenuator with the same shape using a machined aluminium mould, material previously used on another of his crashworthiness works where truncated cones were studied [65], and a CFRP countermould.

Folded and welded aluminium plates were used by Leon S. and Kieran R. [102] to manufacture a CFRP monocoque using prepreg hand-layup. Cunningham et Al [53] manufactured a structural nose cone using a high density urethane (PBLT) machined board as a mould, with an extended curing cycle at low temperature due to the temperature restrictions of this material.

C. Floreani [52] and the Oxford Brookes Racing team [103] manufactured a structural nose cone and a monocoque, respectively, using a female CFRP mould made using a machined epoxy block. Paolo Feraboli [57] also used a CFRP mould to make a RIMP for a formula 1 car (included in the structural nosecone design class due to the complex shape). The same author had also used an epoxy/graphite mould to produce body panels for a Lamborghini Murcièlago in an article from 2004 [104].

To finalize, Matthew Hagan [54] used a plaster/hemp mould to produce a CFRP monocoque.

Later in this work the several materials found above are going to be compared to make a final choice for the mould material to be used.

2.9. Concluding remarks

After a search into the current state-of-art of the design of crash structures and the materials used for this kind of applications it became clear that the design of large composite structures is still underdeveloped, especially concerning more sustainable structures. It is necessary to increase the amount and quality of the data that is fed into the material models as well as to understand the geometric effect on the structure's energy absorption capability. Therefore, three major problems were identified regarding the design and simulation of large composite impact attenuators. Firstly, the numerical analysis of this type of structures is still underdeveloped with simulations failing to predict stress-displacement results in agreement with experimental results. The geometric influence on the energy absorption capabilities is still not well understood and generally its effect is not accounted for in the simulations. Therefore, it is necessary to study this influence through coupon testing and to use this data to feed the numerical simulations of large structures.

Secondly, the simulation and testing of composite impact attenuators within formula student is scarce, with the majority of the teams still relying on the heavier metallic solutions made out of aluminium honeycomb, due to their simplicity and cost effectiveness. Nevertheless, due to the growing competition, lightweight design was never as important as it is at the moment, pushing the teams to increase the percentage of composite materials on their cars. Therefore, there is the need to start to understand the behaviour of this structures and how to simulate them properly.

Finally, the modern-day CFRP structures contain high levels of embodied energy and carbon footprint due to their production method, which involves high temperatures, and to their oil-based origins. It is therefore necessary to find alternative solutions to these composites like the natural fibre reinforced polymers namely the ones using flax fibres or a hybrid solution that is able to reach a compromise between weight saving and sustainability. Nevertheless, the energy absorption capabilities of these materials are still not well understood, so there is the need to obtain experimental data, to incorporate it in numerical models to simulate the effects of the presence of these materials on large impact structures, as well as to understand its environmental impact and to verify its applicability in a formula student impact attenuator able to comply with the competition rules.

3. Coupon testing

Simulating with composite crash structures requires a large amount of data, since, as it was mentioned in the literature review, there are many variables that influence the crush stress and, therefore, only with a very large database it is possible to obtain simulation results with predictions close to the reality.

To obtain the necessary database for the simulations that are going to be later presented in this work, initially coupon manufacturing and testing was performed, both for carbon and flax fibre pure specimens in the form of round and square tubes with different sizes. The aim of this section is to briefly describe the manufacturing process and testing of some of these tubes. Since this is not the main focus of this thesis, a more extensive manufacturing and testing was done in a parallel master thesis [105] from which the remaining data for the simulations will be acquired.

3.1. Materials selection

The materials chosen for this study are the CFRP E745 prepreg from Toray® and the FFRP APX 300T IMP503Z-HT BC 44 prepreg, whose properties will be presented later in the simulation chapter. These materials are used in the crash structures of formula 1 vehicles and are, therefore, in accordance with the cutting-edge technology.

Besides that, for the CFRP and flax material there exists already sufficient data for modelling, including data that accounts for the geometry influence, that can be found in the works of Dalli et al. [14] and Lobão [39].

3.2. Manufacturing

The manufacturing of composite structures through hand-layup of prepregs is a very time-consuming process due to the care that needs to be taken when laying up the plies and the multiple processes that need to be made during the process to ensure the maximum final product quality.

Since the main objective of this testing was to determine the influence of curvature in crush stress, several tube diameters were tested, including square tubes whose results showed tend to the flat coupon results as the crush stress versus radius of curvature hits a plateau.

The process starts by applying PTFE tape to the aluminium mandrels, this is going to help remove the tubes from the mandrels when cured. After this, a non-perforated peel-ply should be wrapped around the mandrel, which is going to ensure that no resin flows from the composite plies to the metallic mandrel, therefore no gaps should be left, otherwise the tubes are going to be permanently stuck to the metal. A large overlapping should also be avoided, since this is going to cause wrinkles on the tube, which increase the stiffness of the tubes and may generate incorrect results. The film should be tapped at the ends with PTFE tape. This specific kind of tape needs to be used since all of these components are cured in an autoclave at high temperature and pressure and therefore every component in the assembly should endure these conditions. Figure 16 shows the mandrels after these initial steps.

Figure 16 - Mandrels covered with PTFE tape and non-perforated peel-ply

Since prepregs come in large rolls, the necessary amount of fibre should be calculated, and the respective plies cut. The carbon fibre that is going to be used is the E745 prepreg from Toray and the ply configuration is $[45/0/45/0]_S$, while the flax that is going to be used is APX 300T IMP503Z-HT BC 44 prepreg and the ply configuration is $[0]_8$.

Since we are working with composites that have specific orientations, care should be taken to cut the rectangular plies correctly oriented. During the process of cutting the plies, a marker was used to write on each rectangular ply what was the orientation of the fibres and for which tube should that ply be, which minimized human error. Despite all the plies in the stack being oriented at 0 degrees the plies were stacked back-to-back and front to front, since due to the weaving process the properties might not be exactly the same, and this ensures the composite to be symmetric. The cut plies can be seen in Figure 17.

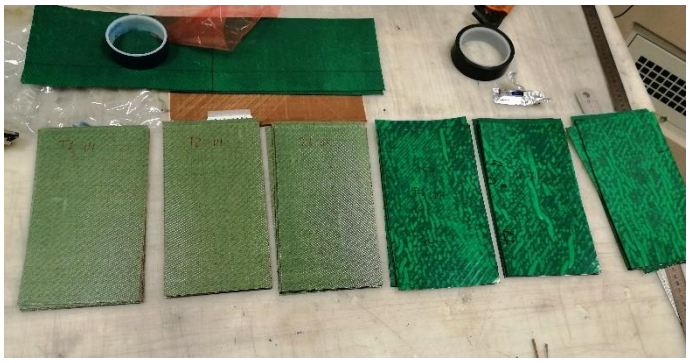

Figure 17 - Cut carbon fibre and flax plies

After this step the plies can be stacked. A tight wrapping of the plies around the mandrel should be ensured, because otherwise during the debulking and curing processes due to the pressure applied the plies are going to be compressed and form wrinkles. Since flax fibre plies are easier to stretch than carbon fibre plies, their laying up process is going to be harder, since they can more easily form defects. Figure 18 shows the mandrel after two plies have been laid up on the tube.

Figure 18 - Flax fibres wrapped around the mandrel

After one ply has been wrapped on the tube, everything is wrapped with perforated peel-ply and breather and is inserted in a vacuum bag properly sealed with sealing tape (See Figure 19). The tube

is going to be under vacuum, in a process called debulking, until all of the tubes from the set have that ply applied, then the second ply is applied, and the process is repeated. Each ply is applied with an offset to ensure that the tubes are not weakened due to consecutive overlapping of joints. After a complete set has 2 plies, all of the mandrels are wrapped with perforated film and breather and undergo a debulking in the autoclave where a temperature of 70 degrees will be applied while the tubes are under vacuum. The cycle is composed by 25 min heating process where the temperature goes from room temperature to 70 degrees, then it stays at 70 degrees for 30 minutes, and its then brought back to room temperature in a ramp down that takes 25 minutes. Then all the steps are repeated until 8 plies are laid up.

At the end of the laying up process the tubes are going to be cured in an autoclave at a pressure of 6 bar and temperature of 135 ºC (See Figure 20). The tubes are then removed from the mandrels.

Figure 19 - Debulking at room temperature

Figure 20 - Tube cure in the autoclave

3.3. Testing

Several sets of tubes were manufactured both for quasi-static and dynamic testing. In the case of this initial set of tubes, it is going to be tested in a quasi-static manner using an Instron testing machine. Since we are talking about closed section coupons and this test is performed at low velocities, these do not need any base support. The loads applied on the tube are then going to be recorded and analysed to calculate the respective crush stress.

An example of a round and square tube after quasi-static testing is shown in Figure 21. As it can be seen, in the round tube, the crushing occurred in a progressive manner forming fronds. Splaying and fracturing failure modes can be easily identified.

Figure 21 - Round and square tubes after crushing

Besides the quasi-static testing, and with more importance for the scope of this thesis, several sets of coupons were tested dynamically in a drop tower. Due to dynamic behaviour, tubes can no longer be self-supported and therefore there was the need to develop a fixture to hold them. This fixture was developed in a thesis occurring parallel to this work that was responsible for the manufacturing of the tubes to be tested dynamically. This device is shown in Figure 22.

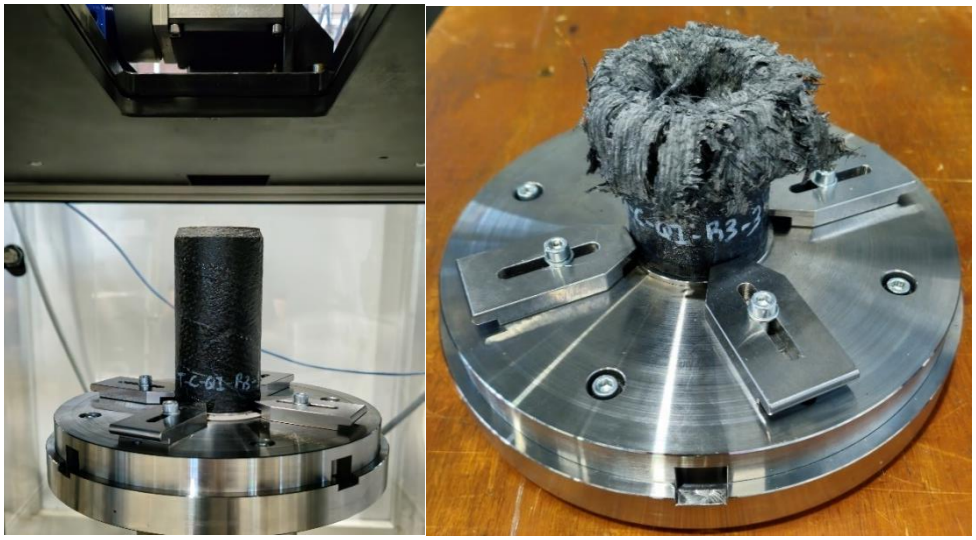

Figure 22 - Dynamic testing setup and fixture, respectively

A total of 30 tubular coupons were tested dynamically, 15 from carbon and 15 from flax. The tubes had 5 different targeted radii of curvature ranging from 11 to 40 mm, that due to the manufacturing process resulted in tubes with small variations on these values. This variation was mitigated by averaging the results of the 3 tubes with the same theoretical radius of curvature.

As it was explained before, the crush stress is determined by averaging the crush stress in a zone posterior to the pre-crush zone where the values remain stable, as it can be seen by Figure 23, by the zone delimited by red dotted lines. Nevertheless, since the specimens increase in area with the increase of the radius of curvature, the energy absorption is algo going to increase. Therefore, to maintain a roughly similar length of analysis for the crush stress the mass and the velocity of the tests was increased with the increase of tube diameter. This resulted in velocities ranging from 8.3 to 8.9 m/s and to masses changing between 30 to 50 kg for the carbon coupons and 17 kg and 50 kg for the flax coupons. This allowed a relatively constant value of 50 mm of crushing for the majority of the coupons leaving 25 mm for the analysis. Nevertheless, 6 specimens did not crush to 50 mm due to the drop tower limitations of maximum 1800 J, which reduced the length of analysis to 13 mm for the 40 mm radius carbon coupons and 21 mm for the 30 mm carbon coupons. This length variation can be seen in Figure 23.

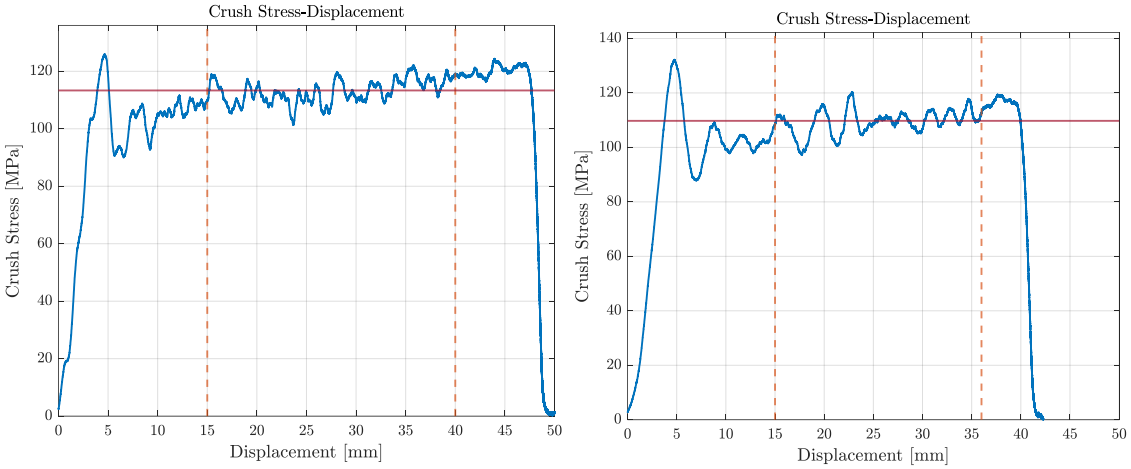

Figure 23 - Crush stress determination for tubular coupons dynamic testing

The raw data, containing the time and forces for a sampling frequency of 1 MHz was retrieved from a load cell, which results in a force value for each 0.001 ms. With the impactor's mass the acceleration can be retrieved and the respective velocity and displacement through integration. The crush stress is calculated through the average force in the analysed zone divided by the cross-sectional area.

These tests resulted in the discretized data represented in Table 4. For each set of 3 coupons with the same theoretical external diameter, the diameters and crush stresses were averaged resulting in a crush stress for each radius of curvature.

Table 4 - Average crush stress for the average radius of the tested coupons

Carbon Fibre		Flax	
RoC (mm)	**Crush Stress (MPa)**	**RoC (mm)**	**Crush Stress (MPa)**
10.98	136.59	11.44	58.14
17.35	125.81	17.80	54.71
23.88	115.88	24.30	51.74
29.87	108.63	30.28	48.71
39.12	102.48	39.52	43.60

Using the discretized data of crush stresses for each radius of curvature, a curve was fitted to determine a progressive crush stress variation with curvature, until the stress would achieve the values obtained for the flat coupons from where the crush stress would remain the same. Then, this curve was used to distribute the crush stress for several bands of radius of curvature. These bands were defined according to the desired sensitivity to curvature change, for example, a new band can be created whenever the crush stress drops 10%, 5% or 1%, which will generate sets of data with less or more bands (see Figure 24 and Figure 25).

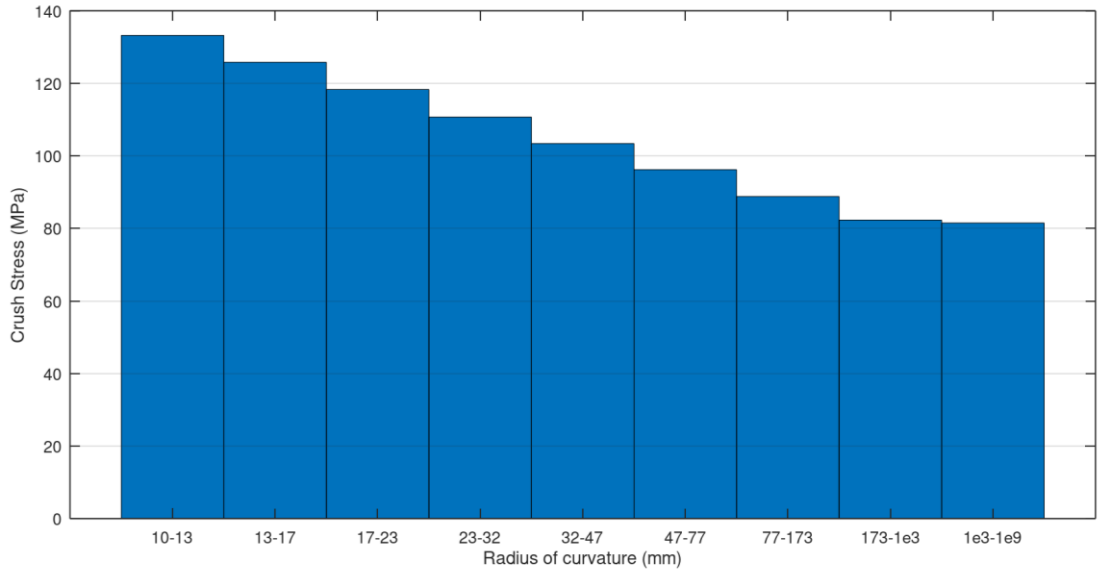

Figure 24 – CFRP crush stress curvature dependence for 5% sensitivity

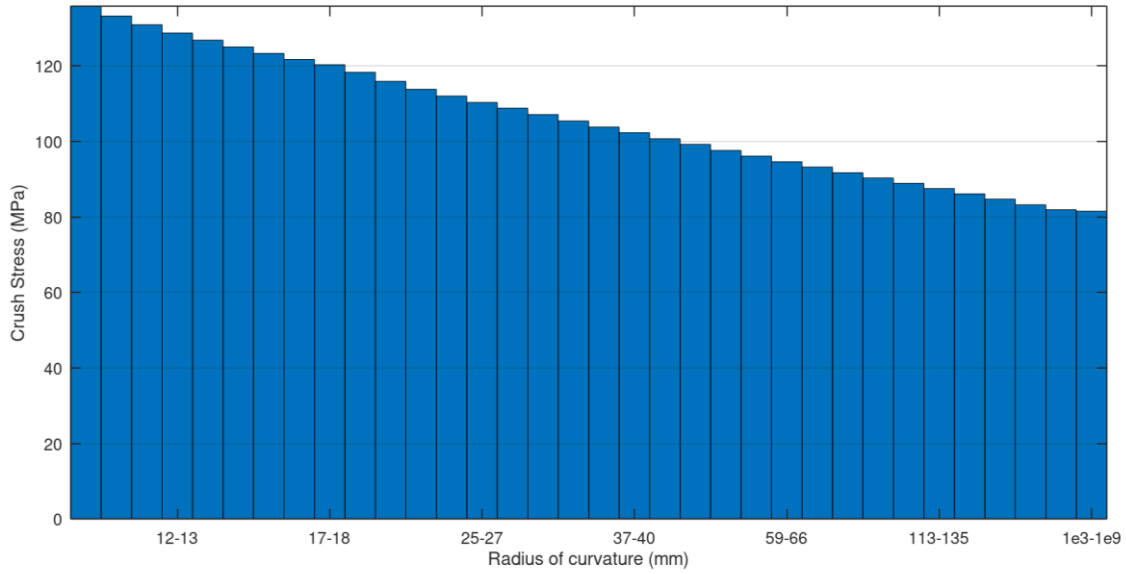

Figure 25 – CFRP crush stress curvature dependence for 1% sensitivity

4. Design selection

To define the final geometry of the impact attenuator several designs were studied both from the literature review as well as some new innovative designs. Initially, to reduce the number of choices available for the final design, three different categories were compared through a decision-matrix. Then, from the selected category several designs were compared with a second decision matrix.

According to the FSG rules 2023 [9], specifically rule T 3.17.2: "The IA must be:

- Installed forward of the front bulkhead.
- At least 100 mm high and 200 mm wide for a minimum distance of 200 mm forward of the front bulkhead.
- The 100 ×200 ×200 mm3 volume of the IA cannot be positioned more than 350 mm above the ground.
- Not able to penetrate the front bulkhead in the event of an impact.
- Attached securely and directly to the AIP.
- Not part of the non-structural bodywork.
- Designed with a closed front section.
- Cannot be wider or higher than the AIP"

In addition, "T 3.19.3 Teams using IAs (typically structural noses) directly attached to the front bulkhead, which shortcut the load path through the bulk of the AIP, must conduct an additional test. This test must prove that the AIP can withstand a load of 120 kN (300 kg multiplied by 40 g), where the load applicator matches the minimum IA dimensions." Which is the only rule that refers structural nosecones.

This limits the initial selection to three categories: structural nosecones, directly attached to the bulkhead of the car, with or without internal reinforcements, and internal structures inside the nosecone attached to the anti-intrusion plate (AIP).

4.1. Decision matrix criteria weighting

Regarding the criteria used for both decision matrices, several criteria were chosen, which were then ranked based on importance which allowed for the attribution of different weights from 1, corresponding to very low relevance to 5, corresponding to very high relevance.

4.1.1. Cost

The cost criterion is related to the mould material cost and the structures material cost. In the case of a Formula 1 car, this criterion, despite the cost cap rules added in 2021, comparing to performance criteria is almost irrelevant with teams spending huge budgets to acquire the best performance to weight ratio. In the case of Formula Student cars, different constraints are applied. Generally, FS teams rely on sponsors as the only source of income and therefore have very limited budgets. This implicates that money should be spared in every step of the design and manufacturing of a certain part. This applies especially for new teams like ours, which do not have many sponsors and access to free materials, therefore, this criterion will receive a weight of 4 out of 5.

4.1.2. Manufacturability

The manufacturability criterion refers to the ease to manufacture the respective structure. This includes the ease to manufacture the mould and the structure, the relative accessibility to the necessary means to fabricate each of these components and how time consuming would it be. Having in mind

the time constraints that this project has and also the context of FSFEUP team with limited knowledge in composite manufacture, any drawbacks caused by excessive complexity of the structure or by the complicated logistics to manufacture it could be extremely penalizing. Therefore, this criterion will receive the same importance as the cost parameter: 4 out of 5 points.

4.1.3. Oblique crushing stability

In terms of performance parameters, oblique crushing stability is one of the criteria chosen to make the design selection. It ranks the structures according to its capability to absorb out-of-axis impacts. Despite the Formula Student impact attenuator being mainly designed for frontal impacts, this is not always the case, in the event of an oblique impact, designs with lower angle inclinations will result in premature failure and may result in serious damage to the pilot. Despite the rules not referring anything related to this parameter it is still considered a relevant parameter since it is a matter of the pilots' safety. Nevertheless, since the Formula Student tracks are far away from walls, with no wheel-to-wheel race, this kind of events should be rare, and therefore this parameter will receive a weight of 3 out of 5.

Since this criterion is related with specific geometry of the designs it will only be used in the second decision matrix.

4.1.4. Overall structure stiffness

Overall structure stiffness defines the structure resistance to non-frontal loads and can be asserted by determining the structures lateral stiffness. The stiffer the structure is laterally, the higher the tendency it has to crush in a stable manner. This criterion is therefore extremely important, since a structure without good overall structure stiffness may not be able to meet the rule requirements and be therefore completely obsolete. Having this in mind this criterion will receive a weight of 5 out of 5 points.

4.1.5. Geometry optimization

This criterion will be specifically used on the first decision matrix, since in this table only categories of designs will be judged and not specific geometries. It judges the capability of a certain design category to be further optimized in terms of geometry. Geometry optimization allows fine-tuning of a specific design to increase its energy absorbing capabilities and can be used to further improve designs that are rule compliant or to allow for structures that are close to be rule compliant to meet the necessary requirements. Considering all that was stated before this criterion will receive a weight of 3 out of 5.

4.1.6. Weight

This criterion includes the final structure weight.

Formula 1 is well-known for its lightweight composite structures, achieving very high power-to-weight ratios that allow the car to be as fast as possible. These structures generally come associated with increased costs and designs with lower safety factors. In Formula Student as referred before, the budgets are limited and increased costs for weight reduction are not always possible. Besides that, being a team that is at the moment manufacturing its first car, the main objective is to have a rule compliant and reliable car and therefore reduced safety factors for weight decrease is not an option. Having all of this in mind, weight is not an extremely relevant criterion and will be classified with 1 out of 5 points.

4.1.7. Energy absorption efficiency

Finally, energy absorption efficiency, is again a criterion that is only going to be used in the second decision matrix since it is dependent on the geometry of the structure. It is mainly influenced by the curvature influence on crush stress and tendency to induce a progressive crushing, that was already described in the literature review. It is a parameter that can greatly influence the structure energy absorption, separating compliant and non-compliant designs. For these reasons it will receive a weight of 5 out of 5 points.

4.2. First decision matrix

Table 5 represents the results of the first decision matrix. All the categories were classified for every criterion using a system of points from 1 to 5 (worst to best).

Table 5 - Initial matrix decision

	Weights	Structural Nosecone W/ Ribs	Structural Nosecone Without Ribs	Internal structure
Cost	4	2	3	4
Manufacturability	4	1	2	4
Overall Structure stiffness	5	2	1	4
Geometry optimization	3	1	1	4
Weight	1	2	3	4
Sum	_	8	10	20
Weighted sum	_	27	31	68

Starting by the cost criterion, because internal structures need to be contained in the nosecone volume, their volume is naturally going to be lower, as well as the mould volume used to produce them, this allows for the use of heavier materials like aluminium, but that are significantly less expensive than the epoxy blocks generally used for big and complex structures. Besides that, since the nosecone's main purpose is aerodynamics, its manufacturing should be taken with more care resulting in the usage of more expensive materials that for example avoid distortion of the final part. The added benefits of this structure does not compensate for the increased price of the epoxy tooling blocks. This discussion will be further addressed in the following sections. The addition of internal reinforcements may require in some cases the addition of internal moulds and extra material which results in an increased cost.

Regarding manufacturability, having in mind all the impact attenuator designs that were found in literature, internal impact attenuators have considerably simpler forms than structural nosecones, since nosecones are designed based on aerodynamic purposes and needs the presence of mounts to be directly attached to the car front bulkhead, generally reinforced to allow the attachment and load transfer to the chassis. This affects the manufacturability of the latter in relation to the former. The introduction of internal reinforcements requires the addition of additional internal moulds which again affects the manufacturability.

In terms of overall structure stiffness, the clear worst option will be the structural nosecone without internal reinforcements since this structure was not designed for crash purposes. It generally contains steep angled surfaces that are prone to buckle and large flat sections that, as discussed in the literature review, decrease the structure energy absorption capability. The addition of internal reinforcements may contribute to mitigate this problem but not solve it completely. The internal structure will be specifically designed for energy absorption upon crushing and therefore will be stiffer than both structures described before.

As referred before, the geometry of the nosecone is defined based on aerodynamic purposes and therefore has a non-optimizable geometry. On the other hand, internal structures, besides its basic shape, can be optimized by controlling curvature and angles, which as referred in the literature review increase the structures energy absorption capability.

Regarding the weight, as it will be seen later, generally internal structures, since they are smaller, result in lower weight, and therefore the structural nosecone is going to be worse classified than the internal structures. The addition of internal reinforcements also contributes to weight increase and therefore the nosecone with internal reinforcements was classified with lower points than the structural nosecone without internal reinforcements.

Looking through the final results of the initial decision matrix, internal structures clearly come on top. Despite this fact, the nosecone without internal reinforcements will still be simulated for comparison purposes, despite being discarded for the final manufacturing.

4.3. Second decision matrix

Then, from the composite internal structures' designs found in the literature and some other designs proposed, only a few were chosen to be simulated. The initial selection consisted of the following designs: corrugated plate, square multi-cellular crashbox, square and round tubes, circular cross-sectioned cone, and square frustum.

From the formula student rules, stated above, we can immediately eliminate any kind of plate since it doesn't have a front closed section. To surpass this problem for the case of the corrugated plate, it was transformed into a corrugated tube. On the other hand, it limits the tube dimensions to a minimum diameter of 200 mm to the circular tubes, 200x200 mm section to the square tubes or 200x100 to rectangular tubes. Despite the rules not prohibiting the enclosure of smaller structures inside an external box of the required dimensions (For example a smaller tube without the required dimensions inside a 200x100x200 box), this option was discarded since it would probably not be approved during scrutineering. Nevertheless, a solution was included where multiple smaller tubes are enclosed in an external CFRP layer but in this case the result is a single structure which will function as a multi-cellular crashbox.

Secondly, as referred in the literature review presented before, the presence of curvature in crash structures greatly increases their energy absorption capability. Thus, a few solutions can immediately be eliminated. Figure 26 represents the designs eliminated on the left and the designs that can replace the ones that were discarded. From top to bottom the nomenclature that is going to be used is the following: round tube, multi-cellular crashbox, corrugated frustum, corrugated tube, and cone.

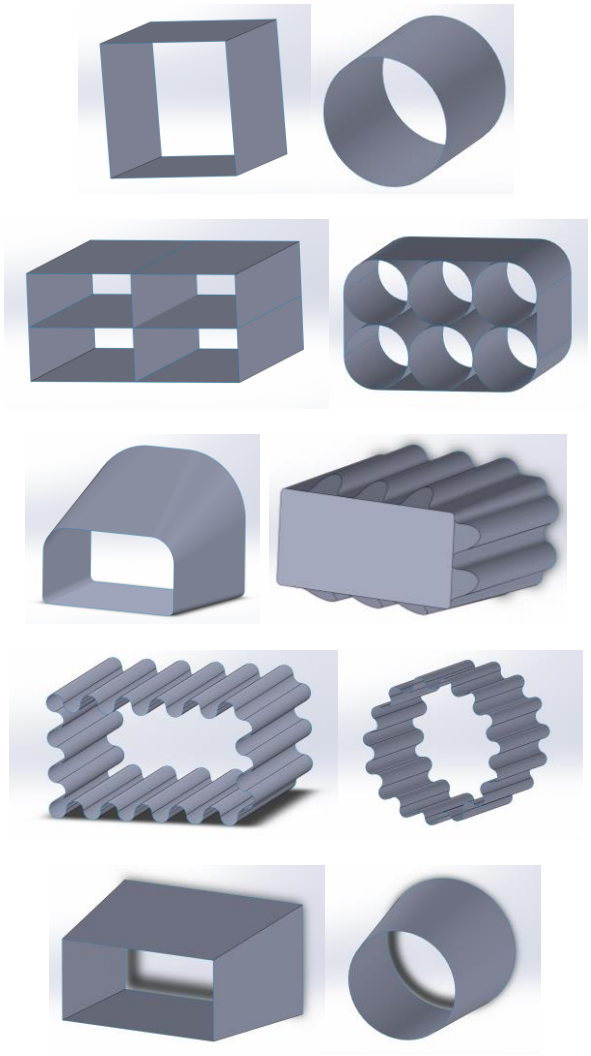

Figure 26 - Design elimination due to curvature. On the right from top to bottom: round tube, multi-cellular crashbox, corrugated frustum, corrugated tube, and cone.

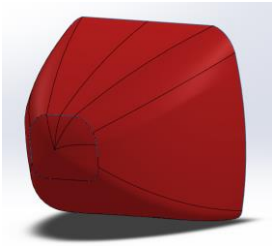

Figure 27 – Structural nosecone design

To do the final decision regarding the designs to be simulated, a decision matrix was done, whose results can be seen in Table 6. This decision matrix followed the same classification methodology with a scoring from 1 to 5 (Worst to best).

Table 6 - Design decision-matrix

	Weights	Round tube	Corrugated tube	Corrugated frustum	Multi-cellular crashbox	Cone
Cost	4	5	1	2	5	5
Manufacturability	4	5	3	1	4	4
Oblique crushing stability	3	1	1	4	1	5
Overall Structure stiffness	5	4	1	2	1	5
Weight	1	1	4	2	1	1
Energy absorption efficiency	5	3	4	2	4	3
Sum		19	14	13	16	23
Weighted Sum		79	48	46	65	92

The following subsections describe in detail the process of value attribution to each design studied for each criterion. Despite the structural nosecone being already discarded from the final production and decision matrix, since the manufacturing of the nosecone is still necessary even if it is not a structural one, it will still be compared in the following sections, to be used as the baseline.

4.3.1. Cost

The cost scoring will be defined according to the following categories:

- 5 points: 100 to 230 euros
- 4 points: 230 to 360 euros
- 3 points: 360 to 490 euros
- 2 points: 490 to 620 euros
- 1 point: 620 to 750 euros

To define the cost scoring for all the structures defined in the decision matrix, firstly the manufacturing process and material need to be defined. The manufacturing process that will be used is prepreg hand-layup since the material to produce the structure that is available is a pre-impregnated roll. The process is going to be similar to the one used in the coupon testing section. Only the mould material needs to be chosen.

Table 7 contains a summary of the properties of the materials used in the articles mentioned in section 2.3, as well as steel since this is a material which can be easily obtained and worked. The several structure designs were designated by letters in the "Structure built" line, to have a more compact table, according to the following nomenclature: a) Monocoque; b) Structural Nosecone; c) Non-structural nosecone; d) Square frustum; e) Cone; f) Body panels. These structures are presented in the same order as the articles where they were used that are shown in the table in the line above.

Table 7 - Material selection, Value References: [54, 101, 104, 106-112]; Structure definition: a) Monocoque; b) Structural Nosecone; c) Non-structural nosecone; d) Square frustum; e) Cone; f) Body panels;

	GFRP	MDF	Epoxy Blocks	PBLT blocks	Steel	Al	CFRP	Epoxy/ Graphite	Epoxy /GFR Ppaste	Plaster/ Hemp
Max Working Temperature(ºC)	210	180	130 - 145	93	400	200	135-210	130-180	125	120
Articles where it was used	[99, 100]	[101]	[52, 58]	[53]	-	[58, 65, 102]	[52, 57, 58, 103]	[104]	-	[54]
Structure built	a)	c)	b); d)	b)	-	b); e); a);	b); b); d); a)	f)	-	a)
Need for a buck	x						x	x	x	
Cure temperature	50-75	-	-	-	-	-	65-135	45	Room temp	Room temp
Post-Cure	x						x	x	x	

For the maximum service temperature of Steel, 400 ºC is a value that is recommended to be used for plain carbon steels for a service life of 20 years [113]. Despite, for our application the life of the component being much lower than 20 years, we still considered a maximum temperature of 400 ºC since this should not be a limiting factor for the prepregs we are going to use.

A few materials were immediately discarded for every design: Plaster due to its brittleness at high temperatures that may lead to high temperature cracking during the impact attenuator cure and cause problems; Steel due to its low conductivity relative to a big mass that would cause high temperature gradients between the side of the composite which is directly in touch with the mould and the other side, generating residual tensions on the final part and Epoxy/Graphite due to the difficulty of finding providers on the market.

Between the remaining materials and considering that we are using for the final part E745 CFRP prepreg from Toray, that is going to be cured at 135 ºC and 6 bar, we can also discard the epoxy moulding paste and the PBLT tooling board as direct moulds due to temperature constraints. PBLT can still be used as a buck to produce a composite mould. MDF was also discarded for a direct mould because of the maximum working temperature. Despite Karl N. Karbhari and Yusuf M. Bhinderwala [101] affirming that this material can be used up to 180 ºC, this is not specified by the provider and additional tests would have to be conducted to confirm it. It was also discarded as a buck for a composite mould due to the increased difficulty in removing the buck from the interior of female mould, as stated by Matthew Hagan et Al [54], in comparison with other buck materials like for example foams. The GFRP mould was also discarded due to the different CTE of this material in relation to the part material which could cause distortion on the final structure.

Therefore, the remaining options are to use moulds of carbon fibre tooling which can be obtained by laying the fibres or prepregs in a mould that can be made from epoxy or PBLT tooling block, to directly use an epoxy tooling block that can sustain high temperatures or aluminium by machining blocks or welding plates. According to one of the providers of the tooling prepreg the PBLT tooling blocks are not recommended to be used as a buck for CFRP tooling prepregs due to the inhibition of the epoxy curing (Chemical incompatibility). Therefore, only the epoxy tooling blocks, CFRP tooling and aluminium remain, the final decision will depend on each design, since the cost and manufacturability are going to change.

4.3.1.1. Structural Nosecone, corrugated frustum, and corrugated tube

For the cost section, structural nosecones, square frustums, and the corrugated tube were included in the same category since they correspond to big structures with complex shapes that would require complex machining.

For the structural nosecone, the moulds were chosen to be female moulds since the exterior face of the final part needs to have the best surface finish due to aerodynamic purposes, and laying the fibres against the machined surface of the mould is the best way to ensure this. In the case of the other designs, male or female moulds can be used since surface finishing is not important, but male moulds were considered since they are easier to produce.

Table 8 represents the prices and weights for each mould material, considering the structural nosecone design. Despite some of these materials being already discarded in the last selection, the prices were also included for reference.

Table 8 - Prices and weights for the initial list of mould materials

	GFRP	MDF	Epoxy Blocks	PBLT blocks	Steel	Al (Block)	CFRP	Epoxy /GFRP Paste
Max Working Temperature (°C)	210	180	130 - 145	93	Max 723	200	135-210	125
Price (€/m^3)	318.92+ Buck	95	400	214.15	498.4	399	393.64 + Buck	336.15 + Buck
Mould weight before machining (kg)	3.7	29.79	49	16.8	553	135	0.47	11.91
Mould weight (kg)	3.7	1.21	2	0.68	22.54	7.79	0.47	11.91
Provider/Price info	[112]	[114]	[115]	[116]	[112]	[112]	[110, 117]	[111]
Need for a buck	x						x	x
Cure temperature	50-75	-	-	-	-	-	65-135	Room temp
Post-Cure	x						x	x

From this table we can also see that steel would also be discarded for this design due to the weight of the resultant mould.

For the price calculation the composite moulds were considered to have 6 plies (2 surface plies and 4 backing plies applied in a symmetric layup), roughly 6 mm thick in total (Due to manufacturer indication [106], except for the Epoxy moulding paste which was considered to be 15 mm for the same reason[111]) and to have the surface area of two times the surface area of the FSFEUP 2023 car nosecone, whilst the bulk materials, with the exception of the PBLT and Epoxy Molds, were considered to have the volume of a parallelepiped that contains the entire nose cone with at least 10 mm of clearance. For the calculation of the stock for the PBLT and Epoxy moulds, 3D cad models were made to obtain the blocks needed and then proceeded by a nesting of these blocks within the dimensions provided by the manufacturers (See Figure 28). This allowed to obtain the number of blocks needed, the respective dimensions and prices. With these considerations, for the materials for which prices could be found, the prices were obtained considering the sizes that the manufacturer could provide and trying to minimize the waste. The prices obtained consider everything except for transportation.

These prices for the epoxy, PBLT and MDF blocks do not include the prices of the necessary products for the surface preparation. For example, for the epoxy moulds, Table 9 contains the necessary material and respective prices.

Table 9 - Necessary material for the production of the epoxy moulds besides the epoxy blocks

Description	Provider	Quantity	Price (€)
800 grit sanding paper	[118]	10 sheets	7.5
S120 Advanced Board & Mould Sealer	[119]	250 mL	61.55
Spray Nozzle for 50ml and 250ml Bottle	[120]	1	1.1
CR1 Easy-Lease Chemical Release Agent	[121]	500 mL	19.2
EA700 Epoxy Tooling Board Adhesive 495g Kit	[122]	1 kit	30.25
Total			**119.6**

For the remaining materials the prices were obtained with a simple calculation of the price for the volume of material needed, using the values of price per unit of volume provided by GRANTA EduPack [112]. The mould weight (Before machining) was calculated using the density of the material provided by the manufacturer or, when this value was missing, through the value indicated by GRANTA EduPack.

The weights of the moulds for the composite moulds were calculated using the surface area of the FSFEUP 2023 car nosecone, the thickness indicated by the manufacturer and the density indicated in the datasheets. For the Epoxy/GFRP paste the weight was calculated using the volume calculated before for the price and for the bulk materials the volume used for the weight calculation was the volume of material bought minus the volume of the nosecone.

To ensure higher manufacturing quality, the best option would be to use the epoxy tooling blocks as a buck and CFRP tooling prepregs for the final mould, despite the considerably higher price for this option. In this way the cure of the CFRP mould can be executed at low temperatures avoiding excessive expansion of both the mould and the buck and the distortion caused by the different CTE of both components. Then the mould can be post-cured ensuring resistance at high temperatures and pressures in the autoclave. The use of prepregs instead of resin infusion allows for lower space for errors during manufacturing ensuring a correct impregnation and lower number of voids.

This decision was also considered for the other two structures, since it is easier and faster to machine epoxy than aluminium (See Table 10), and these are complex structures that otherwise would take a lot of time to machine. Nevertheless, the price and weight comparison for the materials of the other structures is presented in Table 11.

Table 10 - Cutting parameters for aluminium and epoxy tooling boards with tungsten carbide tools [123, 124]

Parameters for roughing	Aluminium	Epoxy board
Feed per tooth (mm)	0.1-0.30	0.35
Cutting velocity (m/min)	99-175	100 to 400

Table 11 - Mould cost, weight, and maximum work temperature (The cost for the squared structures was also considered and is stated in appendix 9.1)

	Corrugated Frustum			Corrugated tube		
Mould material	Epoxy Blocks	Aluminium 6082	Tooling prepreg	Epoxy Blocks	Aluminium 6082	Tooling prepreg
Cost (€)	268.02	41.79	230.77	419	96	301
Mould Weight (kg)	3.43	13.39	0.25	2.43	9.5	0.3
Maximum mould temperature (°C)	120	200	135	120	200	135

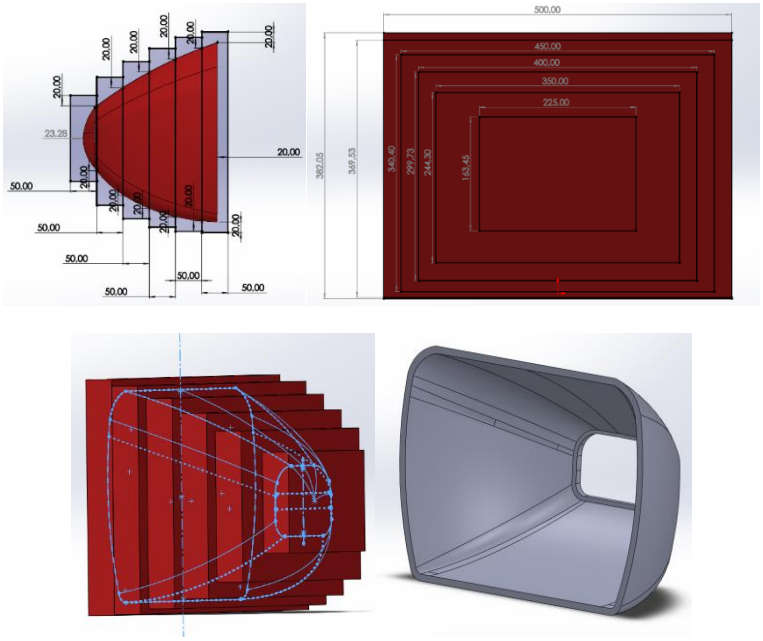

Figure 28 - Stock definition (In red the epoxy plates before machining, and in grey a final machined mould)

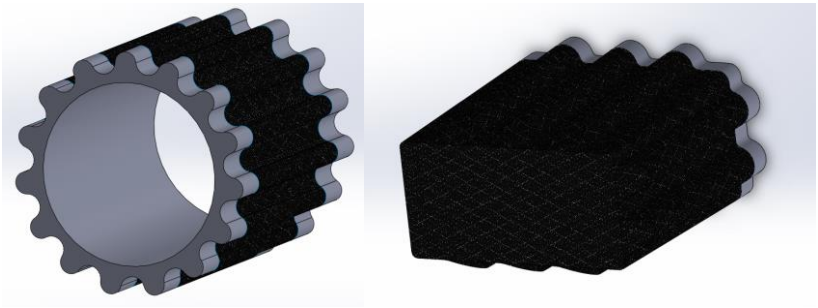

Figure 29 - Corrugated tube and corrugated frustum mould (Structure in black, mould in grey)

4.3.1.2. Remaining structures

For the remaining structures the manufacturing would not require complex machining since the basic shapes are very simple (Cylinders, parallelepipeds, and circular cross-sectioned cones).

Starting with the circular and the circular cross-sectioned cones, the moulds would simply consist of a male shape of the pretended final tubes. For the multi-cellular crashboxes the same type of male mould would be used. In this case the male moulds would be used to produce single cells and then

joint together, and some layers would wrap the exterior of all of the tubes forming the whole structure (See Figure 30).

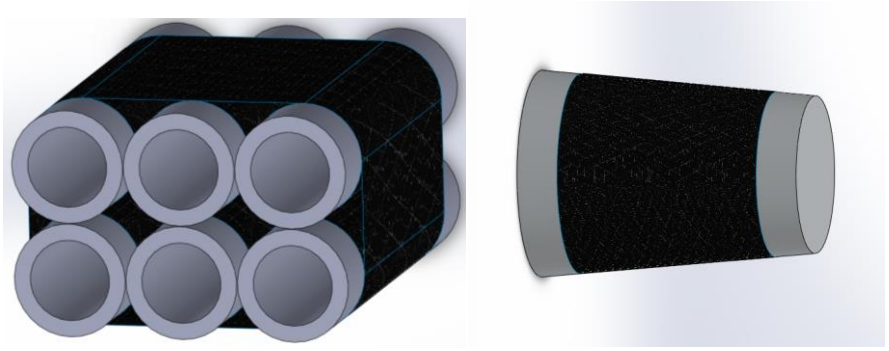

Figure 30 - Crashbox and cone moulds

The moulds were considered to be 40 mm longer on each side to allow for room to apply the plastic films that are required in the manufacturing. For the bought volume the moulds were considered full, and the round stock considered to have 40 mm to be able to be hold on the lathe to be cut to the final dimensions.

For this case carbon fibre tooling was not considered due to its high price. Table 12 represents the cost, weights, and temperature capabilities of each mould for each of the remaining designs.

Table 12 - Prices and weights for different mould materials

	Round tube		Cone		Multi-cellular crashbox	
	Epoxy Blocks	**Aluminium 6082**	**Epoxy Blocks**	**Aluminium 6082**	**Epoxy Blocks**	**Aluminium 6082**
Cost (€)	455.91	58.45	455.91	58.45	455.91	44.56
Mould Weight (kg)	1.17	4.56	3.09	12.04	2.53	9.88
Maximum mould temperature (°C)	120	200	120	200	120	200

Looking at the table above aluminium is going to be the material chosen since its around 400 euros cheaper than the epoxy blocks (the price shown includes all the necessary manufacturing items). Even if the machining costs 200 euros per design, it's still a 200-euro difference. Besides that, the epoxy blocks can only reach 120 degrees Celsius due to the epoxy adhesive that joins the multiple blocks. Since we pretend to perform the cure at 135 degrees, this material is not suitable, or it would force us to do a cure at lower temperatures which is not ideal.

To the mould material prices, the material price for the structure was added. It was estimated by multiplying the surface area, by the number of plies and the price for carbon fibre, of around 150 euros per square meter. The number of plies was determined by using a preliminary ply calculation that will be explained in a later section.

Table 13 - Final prices for the different structures

	Round tube	Corrugated tube	Corrugated Frustum	Multi-cellular crashbox	Cone	Structural Nosecone
Material price (€)	115.05	749.89	540.42	103.38	120.23	1747.81
Mould price (€)	58.5	720	298.9	44.6	58.5	1653.6
Total price (€)	**115.05**	**749.89**	**540.42**	**103.38**	**120.23**	**1747.81**

Having in mind the choices made in these two sections, the cost scoring goes as follows:

- 5 points: round tube, multi-cellular crashbox and circular cross-sectioned cone
- 2 points: Corrugated frustum
- 1 point: Corrugated tube

4.3.2. Manufacturability

The manufacturability scoring will be done according to the following:

- 1 point: Requires difficult manufacturing processes like EDM or 5-axis machining, the laying process is complex due to sharp corners and need for inserts, the ply cutting process is difficult due to complex shapes that need to be divided in patterns that need to be flattened and planned to not compromise the structural integrity of the structure
- 5 points: Easy access to the necessary manufacturing processes, easy layup process and easy cutting process

Regarding manufacturability, one of the designs clearly stands in relation to the other in terms of simplicity: the round tube. Recalling the manufacturing process already described fabricating a round tube is fairly simple both in calculating and cutting the necessary material, laying it up and manufacturing the mould that simple needs turning in a lathe, it was therefore given 5 points on the decision-matrix.

Then, with 4 points: the curved multi-cellular crashbox that follows the same process of the cylindrical tubes, repeated multiple times with the addition of external layers that should be fairly simple to layup; the circular-cross sectioned cone that increases the difficulty both in cutting the material and laying it up since due to the material cut the layup orientation is going to slightly change which changes the way that the prepreg stretches.

With 3 points the corrugated tube that is fairly difficult to layup and to machine the mould but has a relatively easy cutting process since it is going to be a rectangular ply.

Finally, the corrugated frustum that reveals difficulty, in cutting the material since besides having inclination also has corrugations, in laying up due to the complex shape and in machining since it would probably require 5 axis machining, being therefore classified with 1 point.

4.3.3. Oblique crushing stability

Scoring methodology:

- 1 point: Constant cross-section and large flat sections
- 5 points: Varying cross-section and curved sections

In terms of the oblique crushing capability, the cone is going to score better, due to its angle which can improve the performance of these structures in the event of an off-axis impact as already state in the literature review, it will therefore receive 5 points.

The corrugated frustum, despite also having inclination, has large flat areas which can affect stability. It will be scored with 4 points.

On the other hand, the round tube, corrugated tube and curved multi-cellular crashbox have constant cross-sections, which in the event of an oblique crushing will result in premature buckling instead of a progressive crushing reducing greatly the structure energy absorption being therefore classified with 1 point.

4.3.4. Overall structure stiffness

To calculate the overall structure stiffness, all the structures were tested in bending with the application of the same force applied at the same point to calculate the respective displacements. To make the results fair for all the different designs, firstly, the number of plies necessary for each of them to absorb the impact within the same length needs to be calculated. For that, a MATLAB script was developed, and it will be explained in the next section.

4.3.4.1. Preliminary ply number calculation

According to the FSG rules [9] the impact attenuator must be able to withstand an impact of 300 kg at an initial velocity of 7 m/s, without exceeding a maximum acceleration of 40 g and an average acceleration of 20 g. It also needs to absorb at least 7350 J. These will be the guidelines for the preliminary number of plies calculation.

To do this, a MATLAB script was used. In the following paragraphs the calculation procedure will be explained based on the structural nosecone, it will then be applied in the same way to the remaining structures.

Firstly, the structure was divided in 9 sections, evenly spaced out with a 30 mm distance, with the exception of the front of the cone to simplify the partition process in the simulation software (See Figure 31). For each of these sections the perimeter of the shell was calculated. Then the resistant area was calculated to be

$$A = P * N * th \qquad (4.1)$$

Where P is the perimeter of each section, N the number of plies and th the thickness of each ply. The thickness was considered to be 0.3 mm, which is a common value for carbon fibre prepregs.

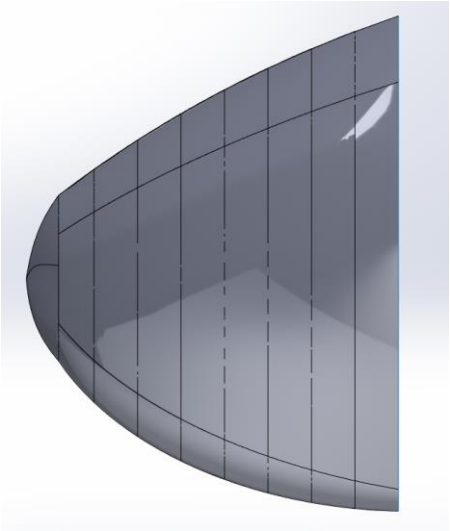

Figure 31 - Nosecone section division

Having the area for each section calculated we can determine the force that is applied in each section. Considering a crush stress, σ, of 91 MPa that is the value of stress obtained on the flat coupons test by Dalli et al. [14] and this structure is mainly composed of large quasi-flat sections, the force comes as,

$$F = \sigma * A \qquad (4.2)$$

Finally, considering, as stated in the rules, an impactor with a weight, m_I , of 300 kg, the acceleration can be calculated as:

$$a = \frac{F}{m_I} \qquad (4.3)$$

This acceleration cannot be larger than 40 g, but at the same time needs to stop the impact before reaching the end of the structure, so the maximum crushing distance was considered to be 20 mm less than the whole structure length. It should be noted that using this formula, the acceleration is never going to drop to zero since the area also doesn't go to zero, despite the velocity being zero. This is not accurate, but it serves for the purpose of doing a preliminary ply calculation.

To assess if the impactor is stopped before this distance, the velocity of the impactor was also calculated using,

$$v = \sqrt{v_0^2 - 2ax} \qquad (4.4)$$

Where v_0 is the initial velocity and x the distance travelled by the impactor.

Lastly, to calculate the absorbed energy, the values of force were integrated for the displacement travelled by the impactor before stop.

$$EA = \int_{\delta_1}^{\delta_2} F \, d\delta \qquad (4.5)$$

For 2 plies the results are presented in Figure 32.

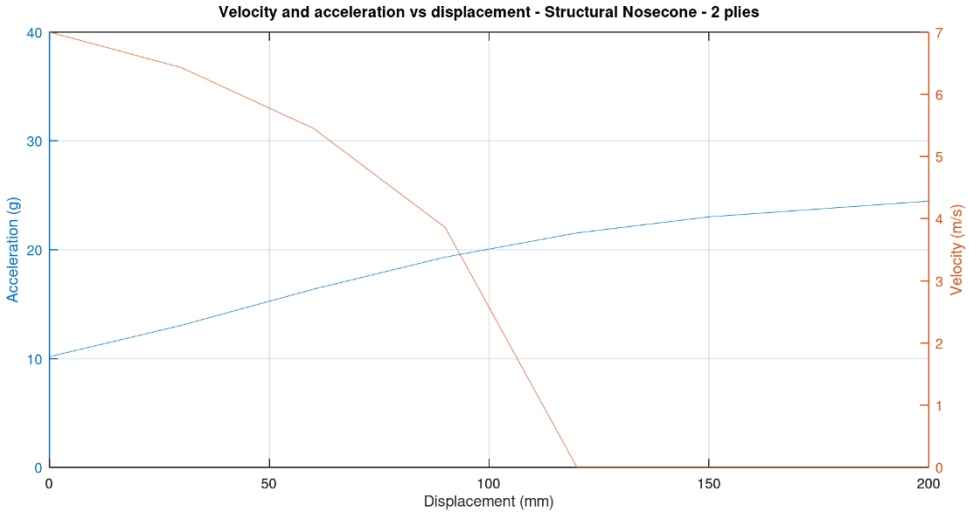

Figure 32 - Deceleration and velocity over displacement for 2 plies

The energy absorbed was $7350\ J$.

These results indicate that 2 plies are enough for the structural nosecone to absorb the necessary energy and fulfil the requirements, as it will be seen later this is not the case.

For the remaining designs, initially, only 1 ply was considered, if the design complies with the requirements for this number of plies than this is going to be the simulated number of plies, if it doesn´t the number of plies was increased by 1, and the script was run again until the design complies with the specification.

An example of this process is present in Figure 33: despite the structure reaching a null velocity right at the end of the structure, an increase of the number of plies would violate the average deceleration rule, as can be seen in Figure 34. The remaining graphics are in appendix B.

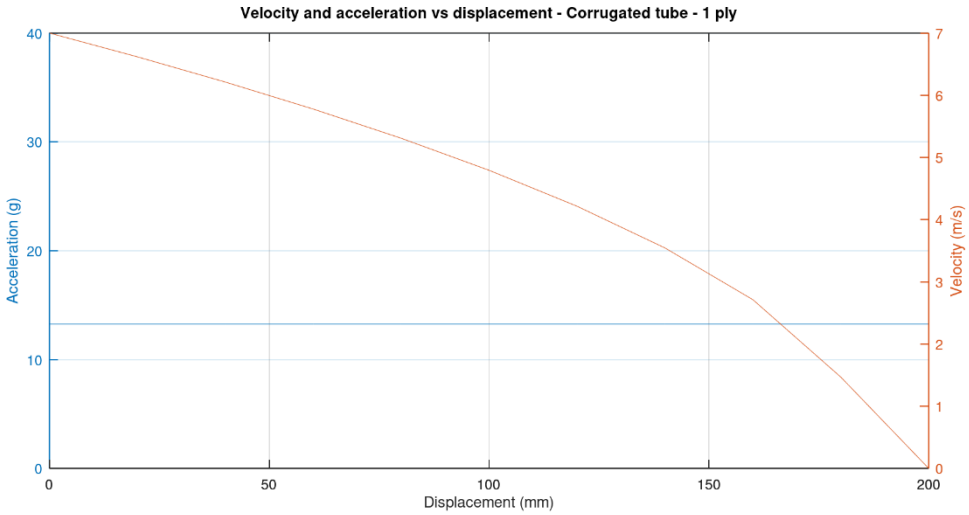

Figure 33 - Corrugated tube velocity and acceleration for 1 ply

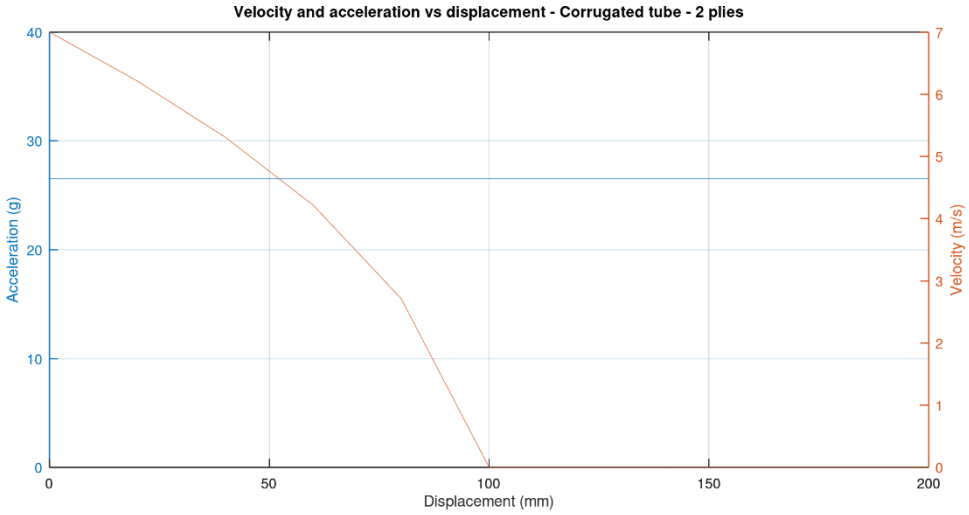

Figure 34 - Corrugated tube velocity and acceleration for 2 plies

Table 14 - Preliminary number of plies for each structure

	Round tube	Corrugated tube	Corrugated Frustum	Multi-cellular crashbox	Cone	Structural Nosecone
Preliminary number of plies	3	1	2	1	3	2

After the preliminary number of plies was calculated, the stiffness simulation could be finally conducted. The simulation was based in the Formula 1 push-off test (See Figure 35).

13.6.2 Front Impact Structure Push-Off Tests

During these tests, the nose must be mounted to the same fixture that is used for the test described in Article 13.6.3.

a. **Lateral Push-off test**

A constant transversal horizontal load of 66.7kN must then be applied to one side of the impact absorbing structure, using a pad 200mm long and 300mm high, at X_A= -750.

All loads must be applied through a ball-jointed junction at the centre of area of the pad.

The stiffness of the pad may be chosen by the team.

Rubber or foam may be used between the pad and the test structure.

The centre of area of the pad must pass through the plane mentioned above and the mid- point of the height of the structure at the relevant section. After 30 seconds of application, there must be no failure of the structure or of any attachment between the structure and the fixture.

Figure 35 - Lateral push off test requirements [7]

Despite the aim of the F1 test being to ensure that the structure does not fail, the same setup can be used to evaluate the lateral stiffness of the several different designs.

Firstly, the structures were imported into ABAQUS, and the geometry was cleaned to ensure a structured mesh. The pad was also defined having initial dimensions of 35x52 mm, determined by proportionality with the size of the pad and of the structures used in formula 1. The final mesh was defined to use elements with 2.5 mm, for a S4R shell element (See Figure 36). While the reason for the usage of S4R elements will be explained in the simulation chapter the usage of a 2.5 mm mesh was determined using a mesh sensitivity analysis. As it can be seen in Table 15 the results converge for elements with 10 mm or less, nevertheless since we are performing contact simulations, using

coarse meshes may result in convergence problems. Therefore, it was chosen to use a 2.5 mm mesh which was the finest mesh with acceptable computational times.

Table 15 - Mesh sensitivity analysis for the lateral stiffness test

Mesh size (mm)	Computational time (s)	Displacement (mm)
1	1423	12.11
2.5	131	12.11
5	30	12.11
10	25	12.11
20	23	12.02

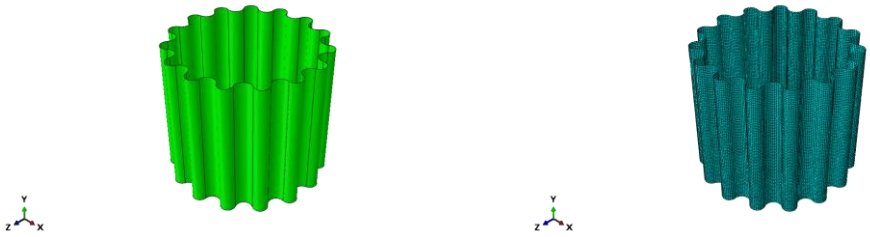

Figure 36 - Surface cleaning and meshing

After this step the composite layups were attributed to the different structures using the elastic properties of the material used on the coupon testing which is going to be the same for the final manufacturing of the structure. Since the FIA regulations do not specify the pad's material, this structure was defined as a 3 mm silicone rubber pad [125].

The pad was then loaded with a load of 30 kN, which corresponds to a proportional load to the one used in the Formula 1 test. The structure is encastred at its end.

The simulations were conducted with a 1 second static general step, which is the default, and this value does not have an influence on the final results since a static analysis is being conducted. The general contact was defined as being frictionless in the tangential direction, since the values for friction were not known and could not be tested due to time constrains, and hard in the normal direction since penetration should not be allowed. Despite the stiffness definition, a rigid body constraint was defined between a reference point and the pad to apply the concentrated load.

Initially the simulations would not converge, and several solutions were attempted. Firstly, a change in pad stiffness was tried since the rubber used has very low stiffness [125], and high deformations could be causing the simulation to not converge. To solve this problem, the pad's stiffness was increased to the carbon fibre stiffness which caused even more convergence problems and then to 10 times the stiffness of the silicon rubber, that despite working on the cylinder simulation did not work on the remaining simulations, so this parameter was changed again to the initial rubber stiffness.

Secondly, the pad was initially defined to have dimensions proportional to the dimensions required by F1 regulations. So instead of 200x300 mm, it had 35x52 mm, by applying a simple linear proportionality rule between the linear dimensions of the impact structure in F1 and its respective pad, and our structure to calculate its respective pads dimensions. The combination between this pad and also a proportional force applied to the structure resulted in the pad indenting the structure. This might be caused by the fact that since F1 structures need to endure higher impact velocities than FS structures (900 kg at 17 m/s [7] rather than 300 kg at 7 m/s [9]), they have more plies and are therefore subjected to less deformation, and do not get indented by the defined parameters. To solve this

problem the load was reduced from 66 kN to 3 kN and the pads dimensions increased to have the same height as the structure's height (See Figure 37). In the case of the F1 push off test, the objective is to ensure that the structures are securely attached to the car, but in our case the only result to be taken is the lateral displacement of the structure, therefore the applied force shouldn't be a limiting factor as long as the same force is applied to all the structures.

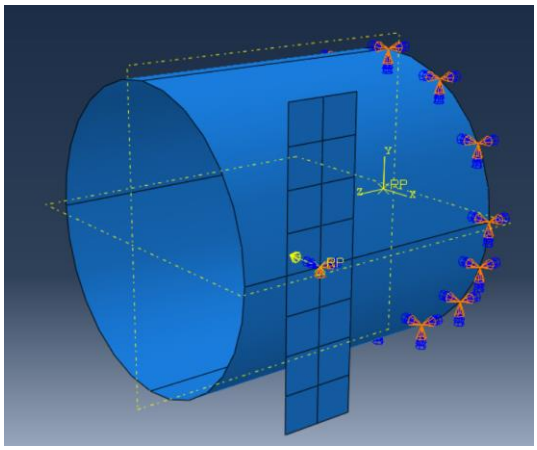

Figure 37 - Load and applied boundary conditions

Regarding the positioning of the pad, initially a rule of proportionality was also done, since by F1 regulations the pad is positioned at 65% of the structure in the longitudinal direction, that is the impact direction, and in the middle of the structure on the height direction. But this would cause several problems: in terms of convergence since the pad would not be completely in touch with the structures in the longitudinal direction which caused the simulations to not converge; in terms of the moment applied on the surface which would be different for structures of different dimensions; and in the specific case of the corrugated frustum the pad would be in the interface of the zone with and without corrugations causing again convergence problems. To solve this, this last structure served as a reference for the axial positioning of the pad, in which the pad was completely touching the structure surface, which then was the same for the remaining structures, and had a value of 145 mm from the base of the structures (See Figure 38).

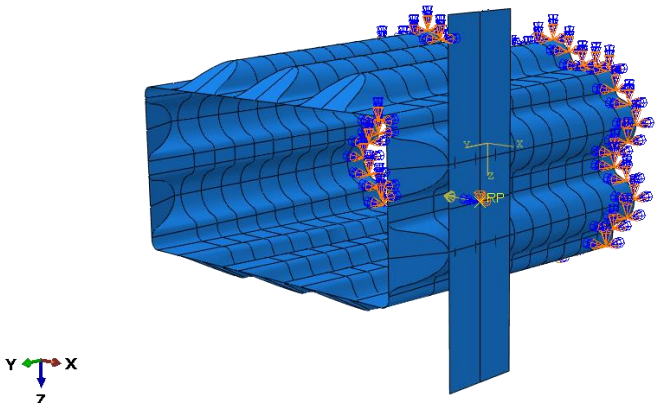

Figure 38 - Corrugated frustum pad positioning

At this point the cylinder simulation was converging but not the rest of the simulations, the problem was later found to be the excessive number of degrees of freedom in the rotation of the pad that would cause it to rotate over itself. This was caused again by following the FIA regulations which

state that the force should be applied with a ball jointed connection. This rotation would not happen in the real simulation due to the friction between the pad and the structure but in the simulation, it would rotate since the general contact was defined to be frictionless in the tangential direction. To solve this problem the rotations of the pad on the axis perpendicular to its plane and the rotation over the longitudinal axis of the impact structure were blocked. In the remaining direction, for the varying cross-section structures the pad was inclined to meet the inclination of the structure being in perfect contact with it (See Figure 39).

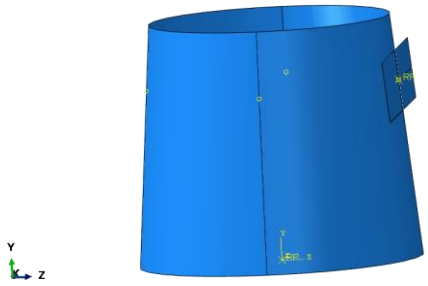

Figure 39 - Pad's starting position following the cone's inclination

Finally, it was found that in some of the simulations the pad would bounce from the surface after impact, which shouldn't happen in the real test. To solve this, the force was applied with a smooth step amplitude and in the general contact properties the pad was forced to be always in contact after the first touch.

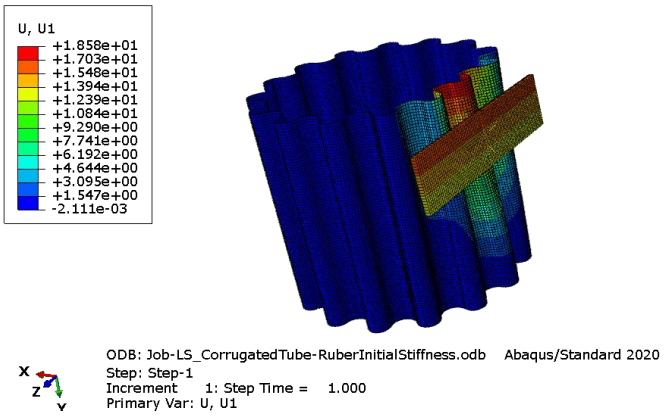

Figure 40 - Corrugated tube result

Due to problems in the simulation and time constraints, the multi-cellular crashbox lateral displacement was not able to be calculated. Nevertheless, as it can be seen in the results of the second decision matrix even classifying this structure as the worst performer in this criterion it would still be one of the structures chosen for the simulations.

The result for the corrugated tube can be seen in Figure 40. The structures were then classified by the following criteria:

- 5 points: 10 to 11.8 mm
- 4 points: 11.8 to 13.6 mm
- 3 points: 13.6 to 15.4 mm
- 2 points: 15.4 to 17.2 mm
- 1 point: 17.2 to 19 mm

The final results are presented in Table 16.

	Round tube	Corrugated tube	Corrugated Frustum	Multi-cellular crashbox	Cone
Lateral displacement (mm)	12.11	18.58	15.71	-	10.93
Score	4	1	2	-	5

Table 16 - Lateral push-off test results

4.3.5. Weight

Regarding the weight of the structure, *to* do the weight calculation, the structures were considered to have the number of plies calculated for the preliminary ply calculation, with the exception of the structural nosecone that due to its geometry, as it is going to be seen later, is going to need more plies to fulfil the requirements. For this initial calculation 8 plies were considered for this structure.

Table 17 contains the calculated weights calculated for each structure based on the density defined by the composite manufacturer [126] and a thickness per layer of 0.3 mm.

Considering, for scoring purposes, classes of 20g of difference corresponding to:

- 1300 to 1320 grams: 5 points
- 1320 to 1340 grams: 4 points
- 1340 to 1360 grams: 3 points
- 1360 to 1380 grams: 2 points
- 1380 to 1400 grams: 1 point

It results in the following scoring:

- 1 point: Curved multi-cellular crashbox; Cone; Tube
- 2 points: Corrugated frustum
- 3 points: -
- 4 points: Corrugated tube
- 5 points: -

Table 17 - Weight of the different designs

	Round tube	Corrugated tube	Corrugated Frustrum	Multi-cellular crashbox	Cone	Structural Nosecone
Weight (g)	1395.3	1329.2	1379.2	1384.5	1383.6	2185.6

4.3.6. Energy absorption efficiency

Regarding the energy absorption efficiency, mainly curvature decided the scoring. As referred before, this parameter influences greatly the structure energy absorption efficiency.

Scoring methodology:

- 1 point: Large flat sections with no corrugations
- 5 points: Highly curved main structure with corrugations

Firstly, the lower scored structure was the corrugated frustum. Despite the existence of corrugations to increase the curvature of the structure, the main geometry contains large flat sections that result in lower crush stresses and therefore lower energy absorption. It was scored with 2 points.

The corrugated tube and multi-cellular crashbox are the best scored structures, since in the first the existence of corrugations in a structure that already had curvature leads to a structure that will probably result in a greater crush stress (will not receive 5 points due to the large diameter), and in the second case the interior tubes can benefit in relation to a single tube since it allows for the existence of multiple tubes with higher curvature instead of a single one with lower curvature (will not receive 5 points due to the existence of large flat surfaces on the outside).

Then the round tube and cone were classified with 3 points since these designs have curvature (but not high curvature) but no corrugations. Since the angle of inclination of the cone is not going to be above 10 or 15 degrees, the decrease of crush stress in the cone due to the diameter enlargement is not enough to receive a lower score than the round tube.

5. Simulation and detailed design

Considering the decision matrix, and the decision already stated of simulating the nosecone, the structures that should be chosen to be simulated are the round tube, the multi-cellular crashbox and the circular cross-sectioned cone. But since, as explained in the literature review, cones surpass tubes in terms of energy efficiency and progressive crushing, the tubes are not going to be simulated.

The objective of this section is to simulate dynamically each structure and to check for rule compliance.

Firstly, the simulation modelling will be explained.

5.1. Abaqus®

To do the simulation a software had to be selected. In the literature review, three different software were found to be used for crashworthiness simulations: LS-Dyna®, PAM-Crash® and Abaqus®. Since the university only has licenses available for Abaqus® this was the software that was used.

Abaqus® is a finite element analysis software created by Dassault Systemes®. It has several features that are going to be useful for this project:

- Abaqus®/CAE: a visual interface that allows the user to model and define all of the simulation parameters.
- Abaqus®/Standard: a general-purpose finite-element analyser based on implicit integration scheme.
- Abaqus®/Explicit: a finite-element analyser based on explicit integration scheme to solve highly non-linear systems with transient loads and complex contact conditions
- Abaqus®/Viewer: a post-processing module to analyse the data obtained from the solver

It also allows for other non-mechanical analysis that will not be mentioned in this work.

5.2. Simulation concept definition

To define a finite element analysis in general or a more specific crush finite element analysis, a few concepts need to be understood. In this section a brief description of several important aspects of this kind of simulation will be presented.

5.2.1. Macro Vs Meso-modelling

As it was already explained in the literature review, two approaches are generally used for composite crushing simulation: meso-scale and macro-scale. Meso-scale modelling is able to represent interlaminar failure like delamination, through the usage of solid or stacked shell elements, but it requires the usage of several interlaminar parameters that if not well calibrated will end up giving inaccurate results. Besides that, it requires a large computational time to run the simulations.

Macro-scale modelling on the other hand is not able to represent these kinds of failure since the whole ply is simulated as a single shell. Nevertheless, it is still able to give accurate outputs in terms of load-displacement curves with low computational times which allows for faster design iterations.

Since the scope of this thesis is not to study the interlaminar failure mechanisms but to design a structure able to comply with the rules defined by the FSG, the excessive time consuming meso-scale models makes them impractical. Therefore, macro-scale modelling is going to be used which will allow for faster simulations for the different configurations and geometries without compromising the final results.

5.2.2. Explicit and implicit simulations

There are two methods of analysis for dynamic systems: implicit or explicit. The implicit method works by direct integration of the equations of motion while the explicit method uses the central-difference operator, which allows for much inexpensive analyses. The only drawback has to do with the fact that this type of analysis is only conditionally stable, and, therefore, there is a maximum time increment above which the analysis becomes unstable. It is therefore recommended that explicit analysis is only used in: systems where the response that needs to be analysed is only a few orders of magnitude higher than the stable time increment of the simulation; in very large problems with extremely discontinuous events; or in systems with complicated contact interactions and high deformations and with stress wave propagation [127].
This is the case for our system, that involves complex contact interactions at the crush front as well as large element deformations and for a very short period of time and for this reason explicit simulations will be used.

5.3. Modelling and meshing

To run the simulations, the structures had to be imported to Abaqus after being modelled in SolidWorks, partitioned, and meshed. To do this it had to go through some preparation since the complex geometries resulted in poor meshing. For the case of the structural nosecone, the structure was divided in transverse partitions distanced 20 mm from each other in the longitudinal direction. The curved sections were also separated from the flatter sections allowing for lower distortions in the mesh. This allowed for most of the structure to be meshed with quadrilateral fist-order elements, that, as already described in the literature review result in more accurate results. The frontal section of the nosecone had to be meshed with triangular elements since the complex geometry could not be meshed with quadrilateral elements, but since this section is not going to have a big contribution to the energy absorbed due to being almost parallel to the impactor, the final results should not be affected.

The final meshing is represented in Figure 41. Both the CZone plugin as well as the damage model, as it will be seen in the next sections, only allow for the utilization of shell elements, therefore S4R elements were chosen for several reasons. Firstly, as we are working with composite thin features the utilization of shell elements allows for computational time reduction with very little influence in the final results as already explained in the literature review and explained by S.Boria et al. [56]. Secondly, Abaqus/Explicit only allows for the use of first-order elements, and finally reduced-integration is recommended for applications where large strains and bending are expected, which is the case of crashworthiness applications [87]. Due to the possibility for the occurrence of hourglass effect, an enhanced hourglass control was used.

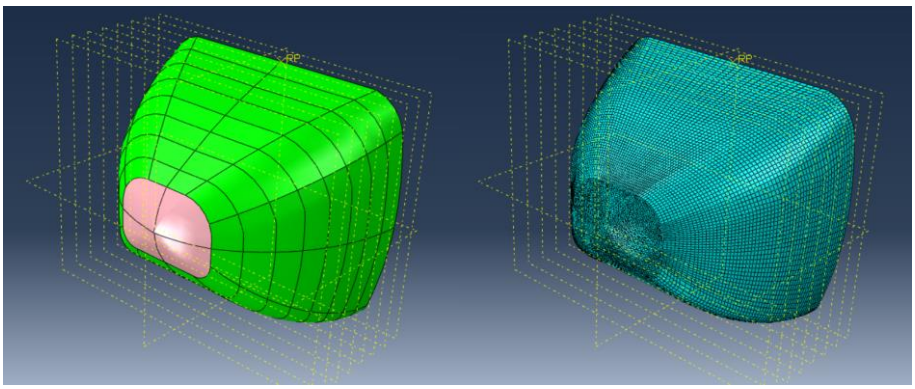

Figure 41 - Structure partitioning and meshing

The seed was defined to be 5 mm to all of the structures initially like performed by Boria et al. [59] but the mesh influence on the results will be studied in a later section through a sensitivity analysis.

Besides the structure to be simulated an impactor also had to be modelled, since the rules don't specify the size of the impactor, this structure was defined to be 600 x 500 mm to cover the entire area of the nosecone. It was modelled with R3D4 rigid elements since the rules specify that the impact attenuator testing should be conducted with a solid non-yielding impactor, and the stress results on the impactor are not necessary and would only result in unnecessary higher computational times.

5.4. Material model and layup definition

Within the Abaqus® software there is a built-in constitutive model for fabric reinforced composites, implemented as a built-in VUMAT user subroutine, that can be accessed by naming the material in a way that it begins with "ABQ_PLY_FABRIC".

The model can only be used for plane-stress elements like conventional shell (S4R and S3R), continuum shell (SC6R and SC8R) and membrane (M3D family) elements.

The model considers the fibres in the fabric orthogonal and aligned with the 1 and 2 directions, defining the local Cartesian coordinate system from where the constitutive stress-strain relations are formulated. It considers the ply as a homogeneous orthotropic elastic material which can sustain progressive stiffness degradation due to failure mechanisms like fibre failure or matrix cracking and also plastic deformation under shear loading.

The stress-strain relations accounting for damage are given by the following system:

$$\begin{pmatrix}\varepsilon_{11}\\ \varepsilon_{22}\\ \varepsilon_{33}\end{pmatrix}=\begin{bmatrix}\frac{1}{(1-d_1)E_1} & \frac{-\nu_{12}}{E_1} & 0\\ \frac{-\nu_{21}}{E_2} & \frac{1}{(1-d_2)E_2} & 0\\ 0 & 0 & \frac{1}{(1-d_{12})2G_{12}}\end{bmatrix}\begin{pmatrix}\sigma_{11}\\ \sigma_{22}\\ \sigma_{33}\end{pmatrix} \tag{5.1}$$

Where d_1 and d_2 are associated with fibre failure along the 1 and 2 directions respectively, while d_{12} is related with matrix micro-cracking due to shear deformation. Each damage variable is defined according to the loading state, assuming different forms when loaded in tension or in compression. The damage variables for tension and compression, d_{1+}/d_{2+} and d_{1-}/d_{2-}, respectively, are activated according to the following expressions:

$$d_1 = d_{1+}\frac{\langle\sigma_{11}\rangle}{|\sigma_{11}|}+d_{1-}\frac{\langle-\sigma_{11}\rangle}{|\sigma_{11}|};\ d_2 = d_{2+}\frac{\langle\sigma_{22}\rangle}{|\sigma_{22}|}+d_{2-}\frac{\langle-\sigma_{22}\rangle}{|\sigma_{22}|} \tag{5.2}$$

The values of the elastic constants E_1, E_2 and G_{12} take their tensile or compressive values according to the sign of $tr(\varepsilon)=\varepsilon_{11}+\varepsilon_{22}$.

The damage variables are assumed to be a function of the corresponding effective stress, while the effective stress is given by:

$$\tilde{\sigma}_\alpha = \left|\frac{\sigma_\alpha}{1-d_\alpha}\right| \tag{5.3}$$

Where $\alpha = 1(+/-), 2(+/-)$ depending on the sign and direction of the corresponding stresses.

The elastic domain is defined by the following activation function,

$$F_\alpha = \phi_\alpha - r_\alpha \leq 0 \qquad (5.4)$$

Where

$$\phi_\alpha = \frac{\tilde{\sigma}_\alpha}{X_\alpha} \qquad (5.5)$$

$$r_\alpha(t) = \max_{\tau \leq t} \phi_\alpha(\tau) \qquad (5.6)$$

Where ϕ_α is a stress-based criterion for fibre failure and r_α is a damage threshold initially set to one and that, through its definition, it is a non-decreasing value that ensures that the activation function never goes above zero, remains zero while $\phi_\alpha \geq 1$ and goes again below zero when $\phi_\alpha \leq 1$.

The evolution of the damage variables is a function of this damage threshold as well as the intralaminar fracture toughness under uniaxial tensile/compressive loading, G_f^α. This formulation allows for the damage variables to be monotonically increasing, ensuring that the damage is irreversible and that the correct amount of energy is dissipated, for example when under uniaxial tensile loading in the fibre 1 direction, the dissipated energy is going to be the fracture energy G_f^{1+}. The formulation is as follows,

$$d_\alpha = 1 - \frac{1}{r_\alpha}\exp\big(-A_\alpha(r_\alpha - 1)\big); \quad \dot{d}_\alpha \geq 0 \qquad (5.7)$$

Where,

$$A_\alpha = \frac{2g_0^\alpha L_C}{G_f^\alpha - g_0^\alpha L_c} \qquad (5.8)$$

Where L_c is the characteristic length of the element, and g_0^α is the elastic energy density at the damage initiation point given by,

$$g_0^\alpha = \frac{X_\alpha^2}{2E_\alpha} \qquad (5.9)$$

Regarding the shear response, it is mainly dominated by the non-linear behaviour of the matrix which includes plasticity and stiffness degradation due to microcracking.

The elastic stress-strain relation is given by

$$\tilde{\sigma} = \frac{\sigma_{12}}{1 - d_{12}} = 2G_{12}(\varepsilon_{12} - \varepsilon_{12}^{pl}) \qquad (5.10)$$

While the plastic behaviour assumes an associative flow rule and a yield function to transition from elasticity to plasticity with a hardening function as follows,

$$\tilde{\sigma}_0\left(\bar{\varepsilon}^{pl}\right) = \tilde{\sigma}_{y0} + C(\bar{\varepsilon}^{pl})^p \tag{5.11}$$

Where $\tilde{\sigma}_{y0}$ is the initial effective shear yield stress and C and p are a coefficient and a power term to define the hardening behaviour.

In terms of the damage modelling, it works in a similar way as the tension and compression loadings defined by an activation function composed by a stress-based shear damage initiation criterion and a damage threshold, as defined below,

$$F_{12} = \phi_{12} - r_{12} \leq 0 \tag{5.12}$$

$$\phi_{12} = \frac{\tilde{\sigma}_{12}}{S} \tag{5.13}$$

$$r_{12}(t) = \max_{\tau \leq t} \phi_{12}(\tau) \tag{5.14}$$

With S being shear strength of the material.

The damage variable is given by,

$$d_{12} = \min\left(\beta_{12} \ln\left(r_{12}\right), d_{12}^{max}\right) \tag{5.15}$$

Where $\beta_{12} > 0$ and $d_{12}^{max} \leq 1$ are material properties.

Finally, regarding element deletion, there are two methods available that can be activated by attributing a certain value to the flag $lDelFlag$:

- $lDelFlag = 1$, elements get deleted once d_1 or d_2 reach a maximum specified value, d_{max} or when the plastic strain due to shear deformation reaches a maximum specified value $\bar{\varepsilon}^{pl} = \bar{\varepsilon}_{max}^{pl}$
- $lDelFlag = 2$, elements get deleted once both d_1 and d_2 reach a maximum specified value, d_{max} or when the plastic strain due to shear deformation reaches a maximum specified value $\bar{\varepsilon}^{pl} = \bar{\varepsilon}_{max}^{pl}$

In this model the first setting was chosen to make the simulations more conservative by allowing failures away from the crash-front to be identified earlier.

All the parameters necessary for the model can be determined experimentally. The elastic constants and the fibre tension/compression strengths can be determined by standard tensile and compressive coupon loading of the 0/90 laminate that is going to be used. The fracture toughness can be determined via double cantilever beam tests.

For the determination of the shear response parameters namely: shear strength S, hardening coefficients C and p, and parameters β_{12} and d_{12}^{max} cyclic tensile tests on +45/-45 specimens should be done. Considering that there is no hysteric behaviour the loading cycles can be represented as in Figure 42.

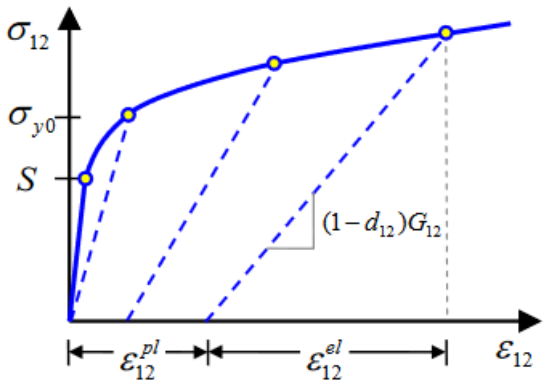

Figure 42 - Shear response to cycle tests on +45/-45 laminates [128]

Using the ratio of the unloading stiffness to the initial undamaged stiffness it is possible to calculate the damage level and for each unloading cycle to create pairs of stress-damage values (σ_{12}, d_{12}). Then this data can be used to create a d_{12} versus $\ln(\tilde{\sigma}_{12})$, where $\tilde{\sigma}_{12} = \frac{\sigma_{12}}{1-d_{12}}$. A linear fit will provide β_{12}, which is the slope of this curve, $\ln(S)$, the intersection between the curve and the x-axis and d_{12}^{max}, the values to which the damage variables tend to.

From each unloading curve the plastic strain at the onset of unloading, $\bar{\varepsilon}^{pl}$, can also be determined by the value of the residual deformation in the unloading state. A new dataset can then be generated containing pairs of stress and plastic strain at the onset of the unloading, $(\tilde{\sigma}_{12}, \varepsilon_{12}^{pl})$. By plotting these values, we can find the fitting values for the hardening equation, C and p.

Dali [14, 88] determined all of these properties for the same material that is going to be used on this work. These properties are represented in Table 18.

Table 18 – Ply-level E745 Toray CFRP prepreg material properties [14]

Material Property	Ply-level values
Density	$\rho = 1504.8\ kg/m^3$
In-plane tensile elastic moduli	$E_{11}^T = E_{22}^T = 63.6\ GPa$
In-plane compressive elastic moduli	$E_{11}^C = E_{22}^C = 61.0\ GPa$
In-plane tensile Poisson's ratio	$\nu_{12}^T = 0.03\ [-]$
In-plane compressive Poisson's ratio	$\nu_{12}^C = 0.03\ [-]$
Shear modulus	$G_{12} = 3.69\ GPa$
In-plane tensile strengths	$X_{11}^T = X_{22}^T = 1046\ MPa$
In-plane compressive strengths	$X_{11}^C = X_{22}^C = 595\ MPa$
Onset of shear matrix damage	$S_{12} = 100\ MPa$
Mode I intralaminar fracture toughness	$G_{Ic}^{1T} = G_{Ic}^{2T} = 96.2\ kJ/m^2$
Compressive intralaminar fracture toughness	$G_{Ic}^{1C} = G_{Ic}^{2C} = 32.5\ kJ/m^2$
Shear damage parameter	$\beta_{12} = 1.0\ [-]$
Maximum shear damage	$d_{12}^{max} = 0.9\ [-]$
Shear yield stress	$\tilde{\sigma}_{y0} = 80\ MPa$
Coefficient present in the hardening function	$C = 40\ MPa$
Power term present in hardening equation	$p = 0.42\ [-]$
Maximum damage	$d_{max} = 0.99\ [-]$
Element deletion	$lDelFlag = 1$
Maximum plastic strain	$\varepsilon_{max}^{pl} = 0.3229$

For the flax composite, experimental tests could not be performed therefore the elastic properties were determined from the material's datasheet [129]. The remaining properties, related to damage, that couldn't be determined were considered to be the same as the carbon fibre ones. Since this material model is only going to predict the behaviour of the structure away from the crash front, leaving the crush front behaviour to the CZone add-in, if the model predicts failure initiation away from the crash front, the structure is going to be considered as a failed structure independently of how much energy it is dissipated after damage has initiated and therefore these damage properties will not have any influence on the final results. The results that could be retrieved from the material datasheet are represented in Table 19.

Table 19 - Ply-level APX 300T IMP503Z-HT BC 44 FFRP prepreg material properties [129]

Material Property	Ply-level values
Density	$\rho = 1337.6\ kg/m^3$
In-plane longitudinal tensile elastic modulus	$E_{11}^T = 16.6\ GPa$
In-plane transverse tensile elastic modulus	$E_{22}^T = 18.5\ MPa$
In-plane longitudinal compressive elastic modulus	$E_{11}^C = 15.6\ GPa$
In-plane transverse compressive elastic modulus	$E_{22}^C = 16.6 MPa$
In-plane tensile Poisson's ratio	$\nu_{12}^T = 0.10[-]$
In-plane compressive Poisson's ratio	$\nu_{12}^C = 0.09[-]$
Shear modulus	$G_{12} = 1.99\ GPa$
In-plane longitudinal tensile strength	$X_{11}^T = 163\ MPa$
In-plane transverse tensile strength	$X_{22}^T = 185\ MPa$
In-plane longitudinal compressive strength	$X_{11}^C = 142\ MPa$
In-plane transverse compressive strength	$X_{22}^C = 142\ MPa$
Onset of shear matrix damage	$S_{12} = 45.7\ MPa$

With the material model and respective properties defined the next step was to define the composite layup. The orientation of the plies was defined as the same used by Dalli et al. [14] for the tubular coupons, $[0°/90°]_{2S}$ to reduce the error that might come from using a certain crush stress for a different layup. For the initial solution only CFRP was considered as the structure's material.

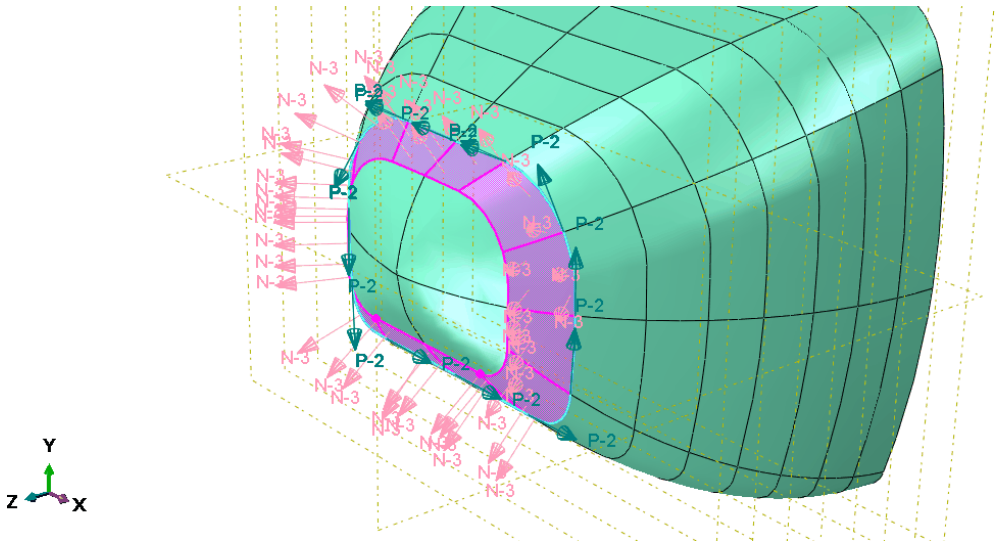

Figure 43 - Composite layup

The normal direction of the ply was defined in the normal direction of the structure while the transverse direction was defined to be tangent to the edge of each section (See Figure 43).

With the behaviour of the structure away from the crush front being already define, the behaviour at the crush front needs to be specified. This behaviour is predicted by the CZone® plugin which is going to be described in the next section.

5.4.1. CZone®

Besides the finite element analysis software itself, a plugin was used to simulate the crash behaviour at the crush front: CZone®.

CZone® is a software created by Engenuity®, that allows for crush simulations of composite structures without the need for input of non-physical parameter variables. It only relies on crush stress to predict failure on the back-up structure as well as the energy absorption at the crushing front. This technology allows for designing of impact structures with precision without the need for tweaking of mathematical coefficients [130]. Crush stress represents the combination of the several failure modes that can occur in the crush front like delamination, matrix cracking, fibre rupture, fibre pull-out and fibre buckling [91].

A CZone® plug-in is available to be integrated in Abaqus® allowing for the combination of the crushing methodology used by this software with the analysis capabilities of Abaqus®/Explicit, to determine the behaviour of the structure away from the crush front. Elements that fail during the simulation are deleted to not affect the remaining calculations [91].

The plug-in uses general contact for interactions and limits the contact pressure to the crush stress of the material. This limitation leads to significant penetration of the crushing plate into the structure, this penetration then serves as the element deletion method, with the elements being deleted whenever all the nodes penetrated the crushing plate. The crush stress only limits the contact pressure and does not have any direct influence in the constitutive calculations associated with element integration points [131].

The plugin has some limitations like only being able to work with shell elements. This will not pose a problem to our work since it is going to be simulated as a macro-scale model.

The crushing representation works by assigning several states to the nodes. Nodes can be [131]:

- Not crushable, if the node has no associated crush stress and will never be crushed
- Non-trigger node, if are not considered as trigger nodes neither previously crushing nodes
- Trigger node, when the node developed contact pressures according to the assigned contact pressure-overclosure, when adjacent nodes begin to crush or adjacent elements exhibit material failure
- Actively crushing node, if it was a trigger node that reached contact pressures equal to the crush initiation stress (crush stress by default) and the contacting surfaces' angle is greater than the crushing initiation angle (30° by default); if adjacent secondary node is actively crushing and the angle between contacting surfaces is greater than the crush continuation angle (25° by default); or if a previously crushing node resumes crushing by having surfaces' contact angle greater than the crush continuation angle and the pressures reaches the crush stress or and adjacent node is actively crushing
- Previously crushing node, when comes out of contact after being active or the angle between contacting surfaces drops below the crush continuation angle
- Failed node, when all adjacent elements are deleted due to crushing or other types of material failure

As an initial assignment, certain nodes can be attributed to a specific state. All the nodes were left on default which means that every node is considered to be in the trigger state.

The contact was defined as a hard contact with an isotropic penalty friction with a friction coefficient of 0.25 as done by Dali [88], Raponi et al. [60] or Joosten et.al [89], with the latter two having coefficients between 0.2 and 0.3, and 0.20 respectively.

The crush stress for these initial simulations was considered to be the crush stress for E745 carbon fibre flat specimens tested dynamically as determined by Dalli et al [14] with a layup of alternating 0 and 90º plies, for a total of 8 plies.

As it was referred before, the number of plies influences the crush stress and therefore, the crush stress for 8 plies may differ from the crush stress for different numbers of plies. But since an extensive database is not available at the moment this crush stress will be considered independently of the number of plies.

5.4.2. Hourglassing

Hourglassing is a problem that arises with first-order, reduced-integration elements in stress/displacement analysis. Since CZone and the material model used can only work with shell elements with these characteristics, this phenomenon can be a problem. Since these elements only have a single integration point and 4 nodes at the vertexes it is possible for the element to distort while the strains calculated at the integration point remain zero (See Figure 44). This leads to uncontrolled distortion of the mesh forming hourglass shapes throughout the elements and giving overestimated displacement values [84].

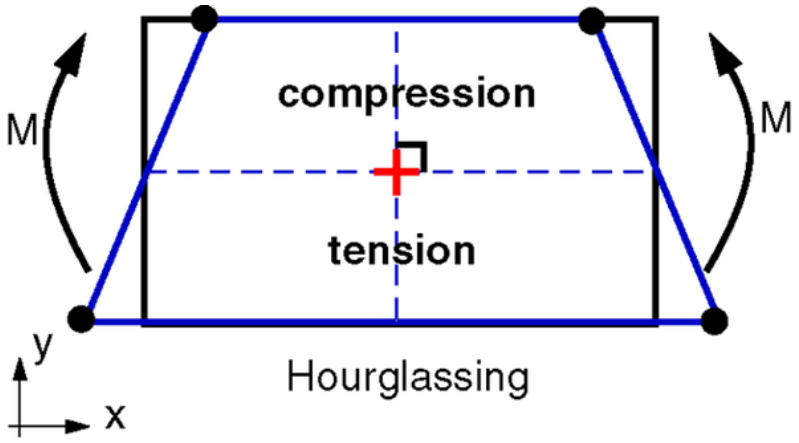

Figure 44 - Hourglassing effect [132]

This problem can be solved through the use of hourglass control, refining the mesh, or using full-integration or second-order elements. Within hourglass control there are several modes which mainly rely on increasing the stiffness of the element to the hourglass forces, resisting the distortion of the element. The enhanced hourglass control available in Abaqus gives the most accurate displacement solutions to coarse meshes and therefore, independently of the mesh used this is going to be the hourglass control used [133].

5.5. Step definition and boundary conditions

After material definition the step had to be defined. The step time was set to 0.08 s, which for a first estimate considering an average impactor velocity of 3.5 m/s, corresponding to half the initial velocity required by rules, allows for 280 mm of displacement, more than the needed for the structure with the biggest length.

After defining the step, the boundary conditions can now be defined. A reference point was defined in the impactor and a rigid body constraint between this RP and the impactor was applied in order calculate the necessary output parameters: acceleration, reaction forces, displacement, and velocity.

To attribute the properties required by the FSG rules an inertia had to be attributed to the impactor corresponding to a mass of 300 kg and an initial velocity of 7 m/s as required by the rules [9]. Besides that, the movements of this part were limited to horizontal displacement, since only frontal impact is being studied like it is required by the rules. The structures to be crushed were encastred on the back end.

5.6. Mass scaling

When talking about simulation procedures generally models where the elements undergo large deformations or rotations or quasi-static analysis with complicated contact conditions are run on an explicit dynamic analysis [134]. This is also the case for crushing simulations where elements at the crushing front undergo large deformations with complicated contact conditions. The accelerations at the beginning of each increment are calculated using element mass matrices, which are going to control the minimum stable time which in turn is going to control the time increment through:

$$\Delta t \leq min\left(L_c \sqrt{\frac{\rho}{\hat{\lambda} + 2\hat{\mu}}}\right) \tag{5.16}$$

Where L_c is the characteristic length associated with an element, ρ is the density of the material in the element, and $\hat{\lambda}$ and $\hat{\mu}$ are material constants. This means that when the density or mass of each element is increased then the time increment also increases, reducing the computational time [134].

Mass scaling does precisely that by scaling, at each increment, the mass of a certain element to ensure that the minimum increment time defined by the user is reached (There are several other methods that can be used within mass scaling options, the one described is the one which is going to be used) [135].

In the case of quasi-static simulations, since the simulation should remain quasi-static, mass scaling should be used with caution since it may increase the kinetic energy to a point that inertia is relevant for the results and the simulation becomes dynamic, and the results are not accurate. To avoid that, in this kind of simulations the ratio between kinetic energy and internal energy should not surpass 10% [134].

For the case of the dynamic simulations, which are the ones that are of most interest for the purpose of this work mass scaling can alter the overall mass of the system which in turn is going to affect the simulation accuracy. To define the adequate mass scaling, several dynamic simulations were conducted in the CFRP cone changing the mass scaling used to understand the effect of changing this parameter.

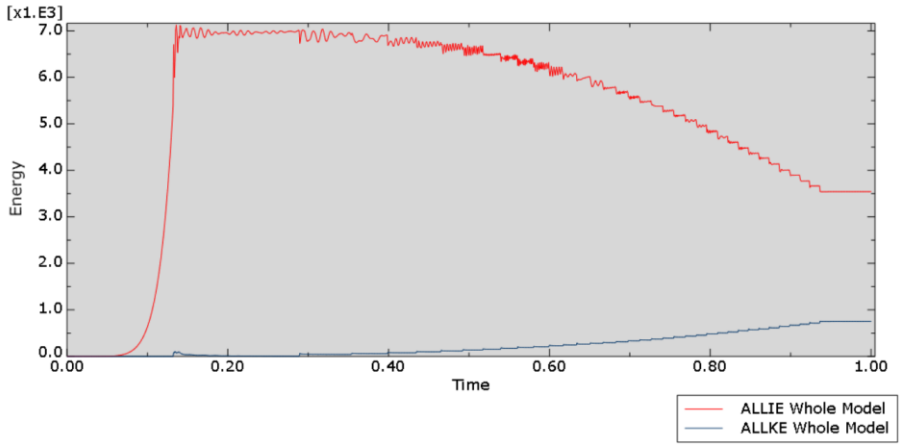

Figure 45 - Internal and Kinetic energy Vs Time for 2e-6 mass scaling

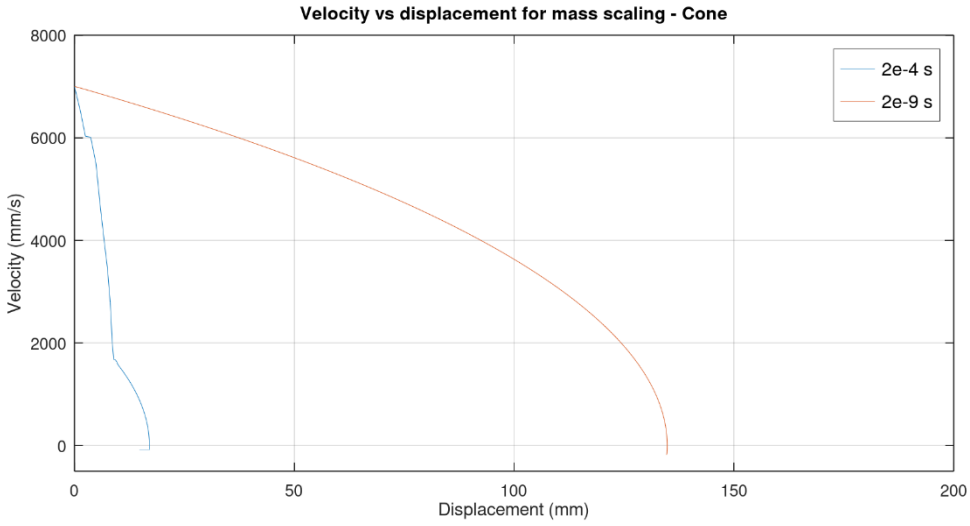

Figure 46 - Velocity Vs Displacement for 2e-4 and 2e-6 mass scaling

When we look at the results for the dynamic simulations for a mass scaling of 2e-6 and 2e-4, as can be seen in Figure 45 and Figure 46, there is a big difference in the length that is necessary to absorb the initial energy. If we compare these results with the ones obtained for the preliminary ply calculation, we can see that the value for the 2e-6 mass scaling is closer to the value obtained in this script.

The final mass scaling was defined through the maximum impactor displacement. As it can be seen by the table below, from a mass scaling of 2e-7 the results stabilize. Therefore, from this point the increase in time does not result in more accurate results. The mass scaling that is going to be used for the rest of the simulations is then going to be 2e-7s.

Table 20 - Mass scaling sensitivity analysis for 2 cpus

Mass scaling	Processing time (s)	Displacement (mm)
2e-4	7	17.0416
2e-5	61	134.553
2e-6	101	134.756
2e-7	544	134.822
2e-8	573	134.822
2e-9	794	134.822

5.7. Mesh sensitivity analysis

To understand the influence of the mesh in the crushing behaviour of the structures, several simulations were made varying the element size. The simulations were performed for the CFRP cone with the parameters already defined before for element sizes varying from 15 to 2 mm.

As it can be seen in Table 21 and Figure 47 all the mesh sizes return stable results with less than 1% change in the total displacement in relation to the finer mesh, nevertheless, since the processing time does not increase exponentially until 5 mm and the results start to vary even less after this value, this was the mesh size chosen for the rest of the simulations.

Table 21 - Mesh sensitivity analysis

Mesh Size (mm)	Processing time (s)	Displacement (mm)	Difference (%)
15	107	134.970	0.115
10	113	134.895	0.059
7	244	134.860	0.033
6	287	134.846	0.023
5	544	134.822	0.005
4	1873	134.824	0.007
3	4440	134.820	0.004
2	9915	134.815	0

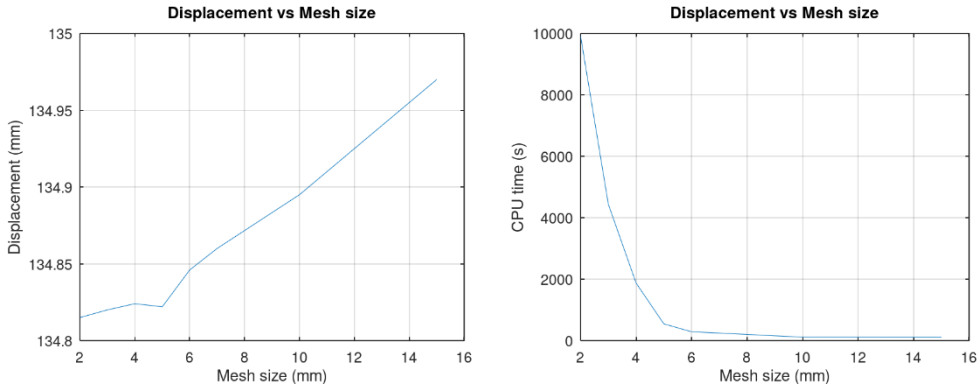

Figure 47 - Displacement and CPU time vs mesh size, respectively

5.8. Carbon fibre structures

In this chapter, a preliminary simulation of the structures made out of CFRP without accounting for curvature will be made. It will serve to determine the overall behaviour of the designed impact attenuators as well as to serve as a comparison to the later simulations when curvature effects are considered.

5.8.1. Structural nosecone

The first structure to be simulated is the structural nosecone that will then serve as a comparison to the remaining structures.

Despite the preliminary ply calculation resulting in a value of only 2 plies for the structural nosecone to fulfil the formula student requirements, by previous experience, it was expected that the structure would not progressively crush but instead it would buckle. To mitigate this problem, the first simulation was run starting with 6 plies on the first zone of the impact attenuator and then increasing one layer in each zone until a total of 14 plies was reached.

As it can be seen in Figure 48, this number of plies was still not enough since at the end of the structure, roughly 250 mm, the velocity was still 3 m/s. The fluctuations on the acceleration values are caused by full parts of the structure getting ripped instead of progressively crushing (See Figure 49).

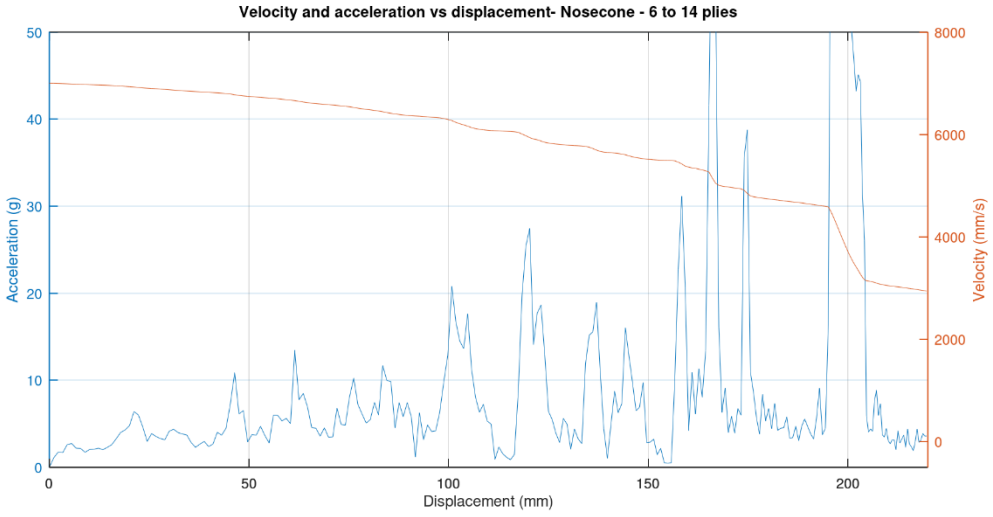

Figure 48 - Acceleration and velocity vs displacement

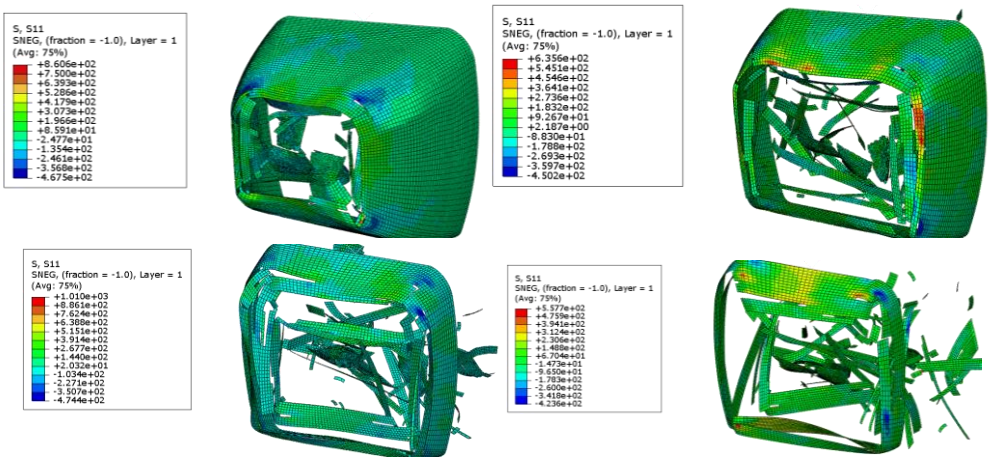

Figure 49 - Structural nosecone crushing (6 to 14 plies)

Despite existing spikes of deceleration that surpass greatly the 40 g allowed by the competition regulations, a few more simulations will be done with more plies to see if it is possible to decelerate the impactor into 0 m/s at the end of the structure.

Since the initial simulation resulted in the reduction of the velocity from 7 m/s to roughly 4m/s, a rough ply estimation would be to double the number of plies of the structure. So, the next simulation was conducted with 12 to 28 plies, with an increase of 2 plies per section, but result was not satisfactory, with the structure decelerating to 0 m/s but exceeding the acceleration requirements by large values. It was noticed that most of the energy was being absorbed in the last sections of the nosecone since those sections have lower angles and therefore will be less prone to buckling. Therefore, multiple iterations were made from the 12 to 28 plies attempt, reducing 2 plies per zone until satisfactory results were achieved, knowing that a low number of plies on the front would not be critical for the overall structure performance.

Several iterations were done until a simulation with a ply distribution going from 2 to 18 plies was able to absorb the necessary energy within the length of the nosecone (See Figure 50). The average deceleration from the unfiltered raw data was calculated to be 12.327 g but the maximum acceleration of 100.98 g exceeded the maximum acceleration of 40 g allowed by the rules. Nevertheless, rule T 3.19.6 [9] states that "If peaks above the 40 g limit are present in the data, a 100 Hz, 3rd order, low pass Butterworth (−3 dB at 100 Hz) filter may be applied". Applying this filter reduces the maximum deceleration to 34.607 g, as it can be seen in Figure 51, complying with the rules.

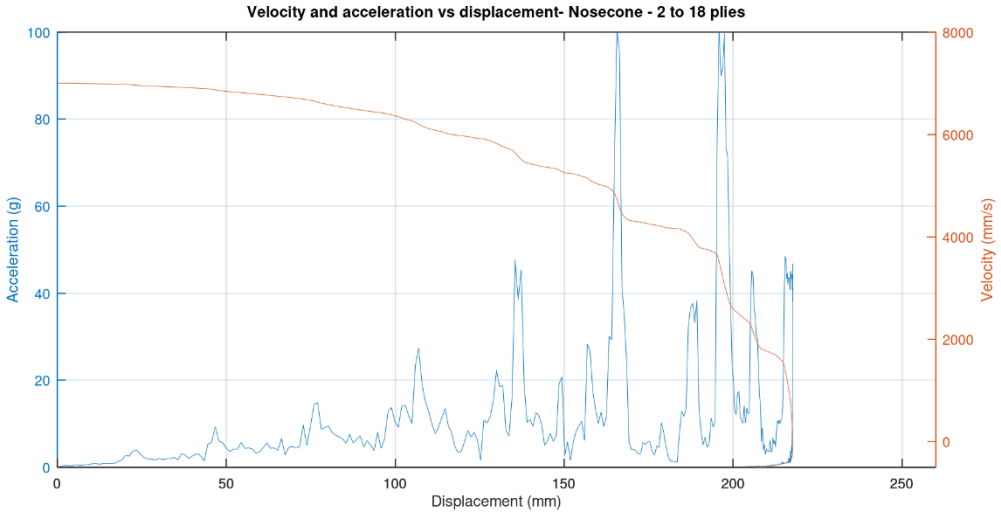

Figure 50 - Velocity and acceleration vs displacement for the structural nosecone using 2 to 8 plies

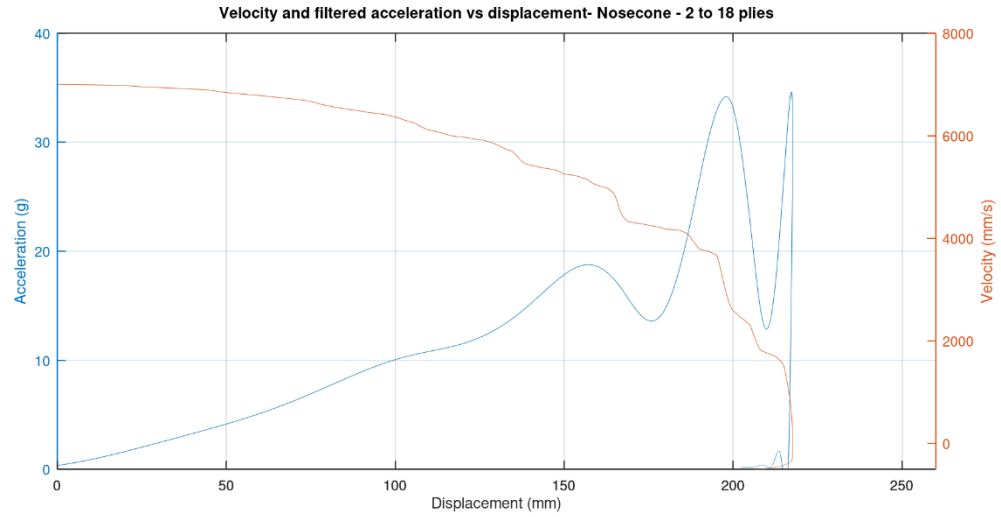

Figure 51 - Velocity and filtered acceleration vs displacement for the structural nosecone using 2 to 8 plies

These preliminary nosecone simulations allowed to predict a volatile behaviour of this structure when subjected to compressive loads. Due to the highly angled surfaces to the direction of the impactor, the structure tends to buckle which make the preliminary ply calculations obsolete.

5.8.2. Cone

For the case of the cone, the results were more positive, the structure was able to absorb the required energy, decelerating the impactor to a null velocity without surpassing the average 20 g acceleration maximum that is allowed by the FSG rules (See Figure 52).

Besides that, the cone was crushed in a progressive manner as can be seen in Figure 53. There were no parts of the cone projected, with the nodes at the crush front being erased progressively as they reached the crush stress indicated for this material.

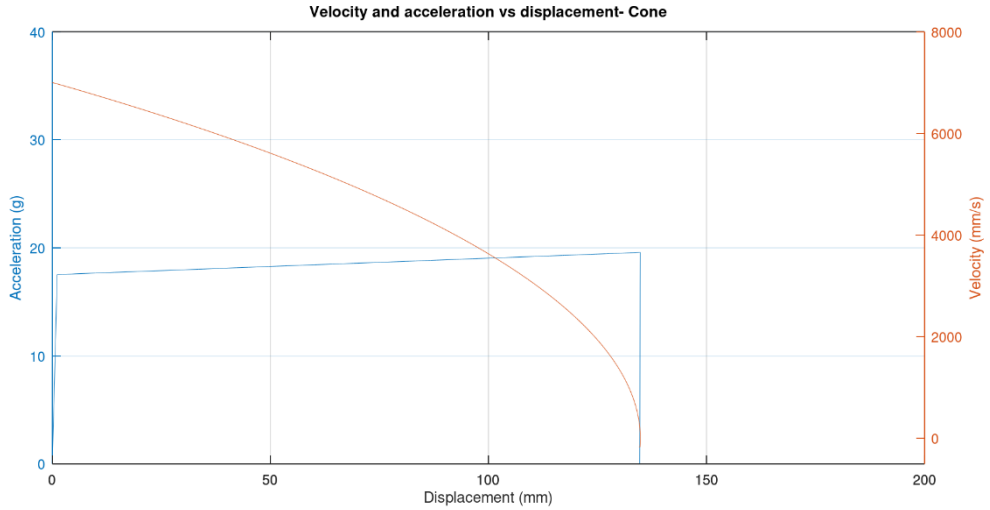

Figure 52 - Velocity and acceleration vs displacement

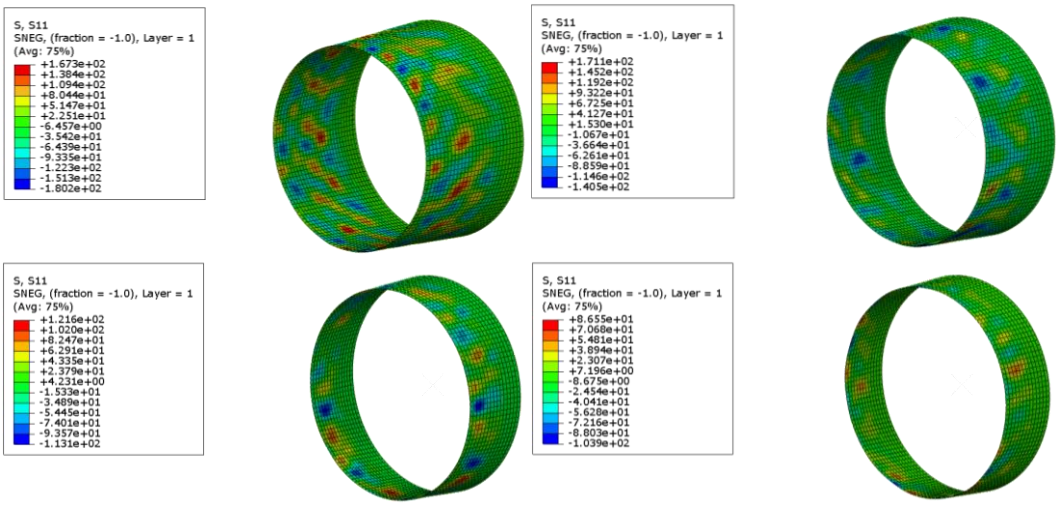

Figure 53 - Cone crushing

5.8.3. Multi-cellular crashbox

Having in mind the result for the preliminary ply calculation, the first dynamic simulation of the Multi-cellular crashbox was ran with one ply. The results can be seen in Figure 54.

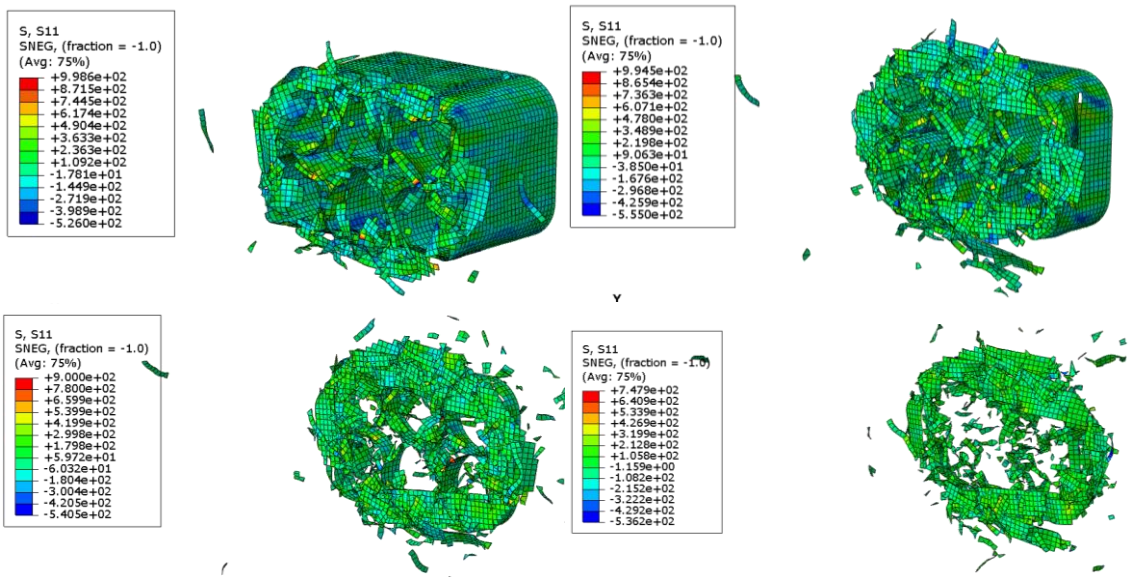

Figure 54 - Multi-cellular crashbox simulation for 1 ply

As it can be seen from the figures above, the structure does not crash in a progressive way, with big pieces of material being projected, this will result in lower energy absorbed than the expected, resulting in a non-zero velocity at the end of the crash (See Figure 55). Regarding the acceleration values, the average acceleration is below the 20 g allowed by the rules, this means that the number of plies can be increased to achieve the first requirement.

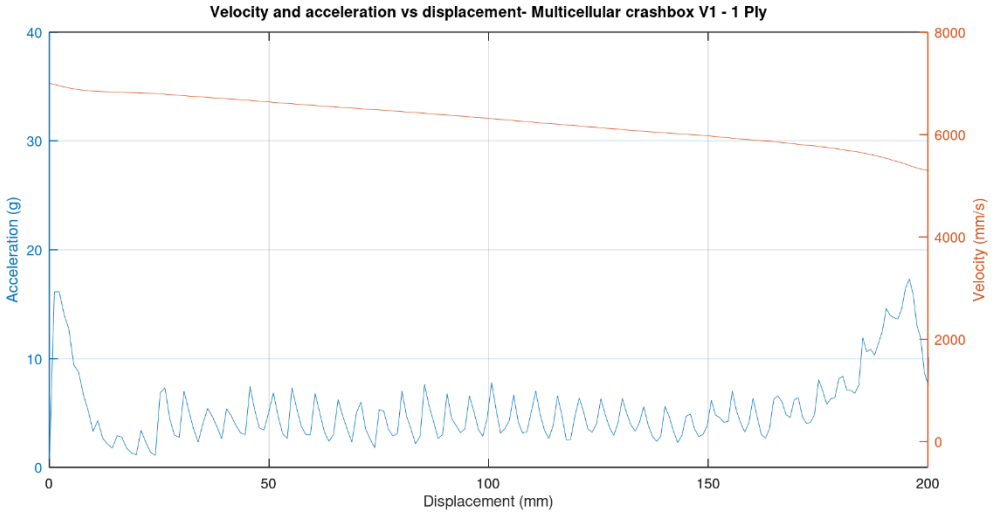

Figure 55 - Acceleration and velocity vs displacement for 1 ply

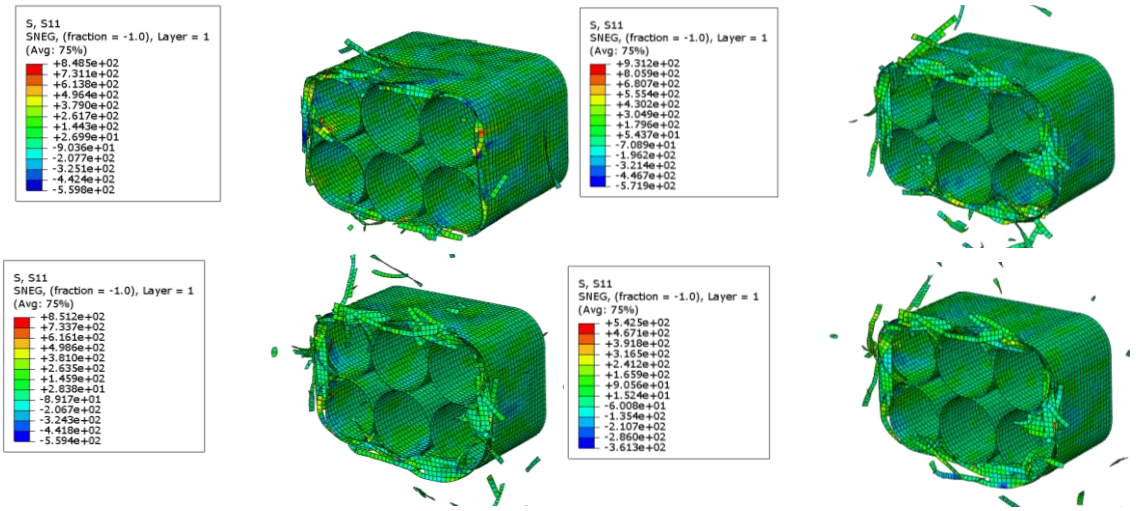

Figure 56 - Multi-cellular crashbox with 2 plies

With the increase of the number of plies, the structure was able to absorb all of the necessary energy as it can be seen in Figure 57. But it also increased the acceleration values to a point where the average acceleration does not comply with the rules anymore, surpassing the 20 g. To solve this problem, the structure was redesigned, reducing the number of tubes inside, and therefore reducing the curvature of the tubes, which, as explained in the literature review, reduces the crush stress and therefore the induced accelerations. Despite the curvature parameter not being included in this section, this change should be noted, as later in this work the curvature effects will be considered.

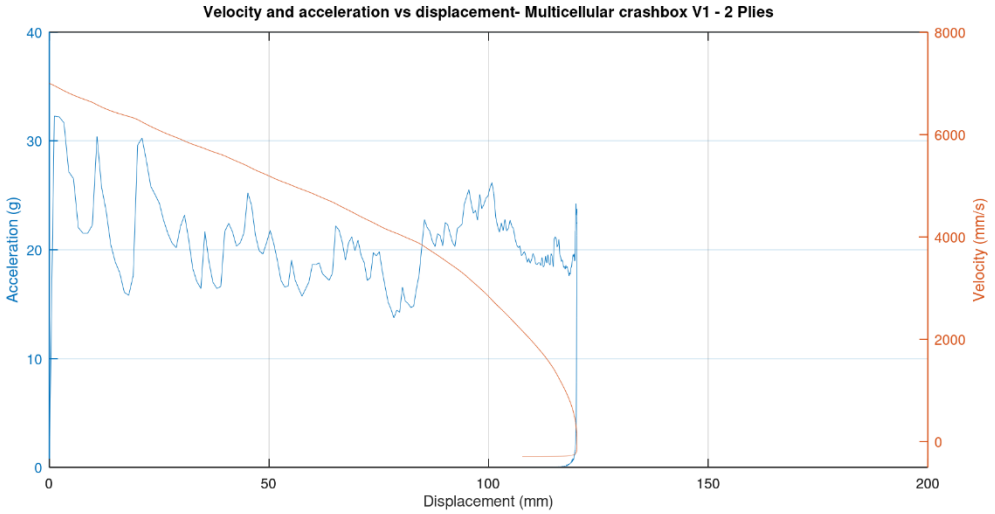

Figure 57 - Acceleration and velocity vs displacement for 2 plies

5.8.3.1. Multi-cellular crashbox V2

As it was referred in the last section, since the initial multi-cellular crashbox was not able to fulfil the FSG requirements, a redesign had to be made, for the same 2 plies. Instead of the initial 6 tubes with 70 mm of diameter, the new structure is composed of 4 tubes with 100 mm of diameter (Figure 58).

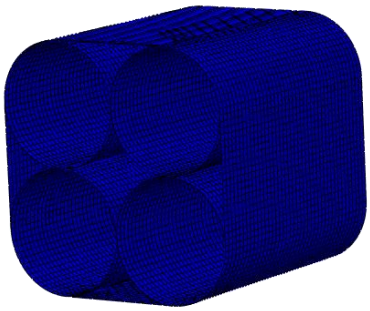

Figure 58 - Multi-cellular crashbox V2

Despite an increase in surface area from the version 1 to the version 2, the structure was able to perform better absorbing the necessary energy without surpassing the allowed values for the average and maximum accelerations, as it can be seen by Figure 60. Nevertheless, if we look to Figure 59, it can be seen that the structure does not crash progressively, which means that its whole capabilities are not being used, probably because of the large flat sections on the side that lead to premature buckling. Therefore, these results may not be valid when comparing with the real-world results since the structure may buckle and fail catastrophically.

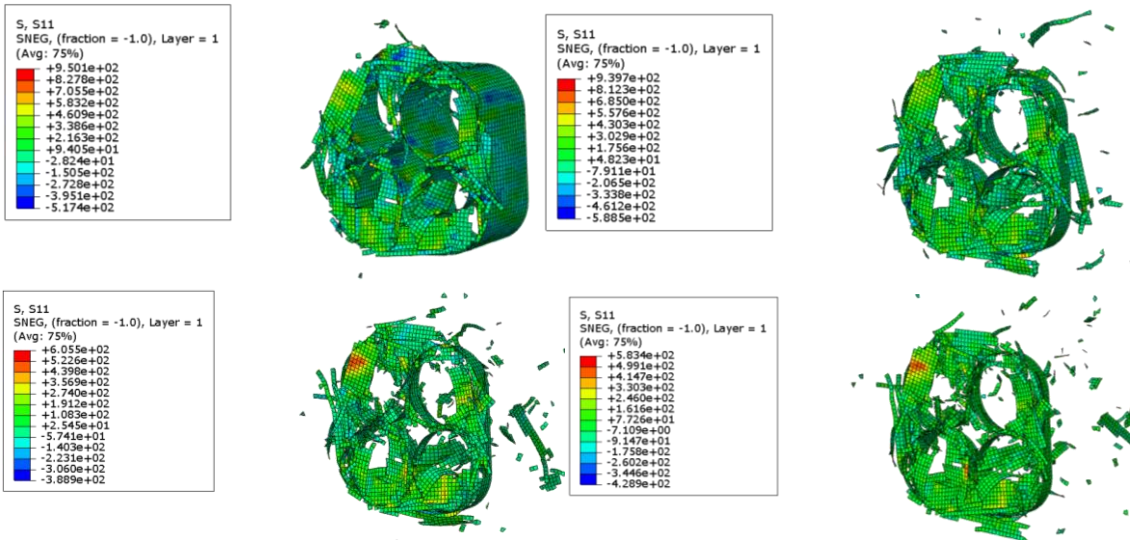

Figure 59 - Multi-cellular crashbox V2 crush

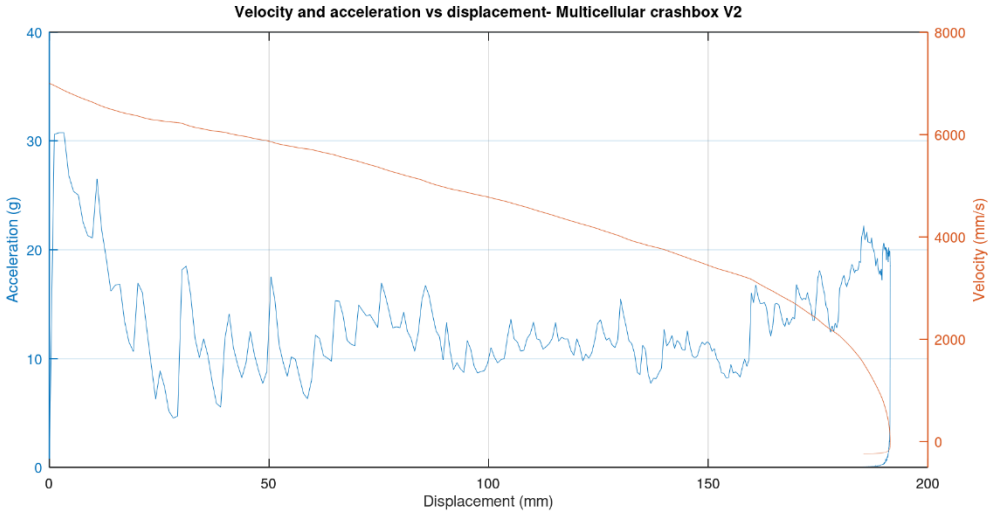

Figure 60 - Acceleration and velocity vs displacement

5.8.4. Carbon fibre results discussion

This subchapter presents the numerical results for these preliminary simulations, with the average and maximum accelerations, length crushed, and specific energy absorption calculated (SEA).

To calculate the SEA, the crushed length was obtained from the simulations, from which the mass of the crushed section was calculated based on the number of plies, surface area and material density. Having this mass calculated, to obtain the specific energy absorption is just a matter of dividing the initial kinetic energy applied to the impactor, that is 7350 J obtained from an initial velocity of 7 m/s and a mass of 300 kg, by the crushed mass.

$$SEA = \frac{EA}{Crushed\ mass} = \frac{7350}{SA * th * N * \rho} \tag{5.17}$$

With SA being the crushed surface area, t the ply thickness, N the number of plies and ρ the material density.

The results are represented in Table 22.

Table 22 - Specific energy absorption for the structures that pass the requirements

Structure	Number of plies	Length crushed (mm)	Mass of the crushed zone (g)	Average acceleration (g)	Max acceleration (g)	SEA (J/g)
Nosecone	2 to 18	217.681	1133.9	11.458	34.607*	6.48
Cone	3	134.756	121.89	18.454	19.571	60.30
Multi-cellular crashbox V1	2	120.11	212.48	20.70	32.28	34.59
Multi-cellular crashbox V2	2	191.44	340.67	12.987	30.750	21.58

As it can be seen the cone results are very promising, the SEA is 2.8 times greater than the one obtained for the second version of the multi-cellular structure, the only one that passes the requirements. The multi-cellular crashbox, despite fulfilling the requirements, due to its large flat sections ends up failing by buckling, supressing progressive failure mechanisms, and therefore needing a larger mass to absorb the same amount of energy as the cone.

Nevertheless, these results were obtained using a crush stress for flat coupons, since at the time the results for curved specimens were not available, despite the structures having curvature. In the next sections, curvature will be considered, and the results compared with the ones obtained until now.

The results for the structures that were not able to absorb the necessary energy are presented in the annexes.

5.9. Carbon fibre including curvature

As it was mentioned in the literature review, curvature has a great influence on the energy absorption of a structure. In the last section, the simulations of the structure were conducted considering a constant crush stress for all of its sections and equal to 91 MPa. This section will consider curvature dependence, based on the data presented on section 3.3, using a 1% sensitivity since for the cone example all of the sections of the cone would fall on the same category if other discretization was used. The minimum crush stress registered in this study, corresponding to the flat coupons, was equal to 81.5 MPa, considerably lower than the initial considerations, which will have influence in the comparison of the energy absorption capabilities of the structures when accounting for curvature or considering all the structure to have the crush stress of a flat coupon. The layup was also altered in the simulations since the data retrieved for the curvature dependence was obtained for a layup of $[45,0,45,0]_S$, as already mentioned in section 3.

Note that from this chapter onwards, the nosecone will not be simulated due to time constraints. Since this structure was already discarded in the first decision matrix, this will not influence the final conclusions of this thesis. Furthermore, the simulations with no curvature already proved the poor performance of this structure that would result in a heavy and expensive structure, due to the large number of plies needed for it to be rule compliant.

After having the data available, each section of the structures was assigned with the crush stress corresponding to its medium curvature in each of the partitions made.

In the case of the cone, two different sections were assigned with different crush stresses due to the change in the curvature of the cone. In the Multi-cellular crashbox also two different sections were assigned corresponding to the curved and flat sections, since the curved sections had a constant cross section. The sections average radius and respective crush stress for each partition are presented in Table 23 and Table 24.

Table 23 - Cone section average radius and crush stress

Cone section average radius (mm)	Crush stress (MPa)
100.875	90.3
102.75	90.3
104.5	90.3
105.25	90.3
106.125	90.3
109.625	90.3
111.5	90.3
113.25	88.9
114.875	88.9
116.625	88.9

Table 24 - Multi-cellular crashbox section radius and crush stress

Multi-cellular crashbox V2 section radius (mm)	Crush stress (MPa)
Flat	81.5
50 mm	99.2

In the case of the cone all of the values of crush stress for the different sections are lower than the value used on the last section, which will result in worse energy absorption capabilities while in the multi-cellular crashbox only the values for the flat section are lower while the values for the curved sections increase in relation to the simulations of the previous chapter.

As can be seen in Figure 61, this decrease in crush stress resulted in an increase in the necessary length to absorb all the necessary energy, therefore the necessary mass to absorb this energy is also increased resulting in lower SEA values (See Table 25).

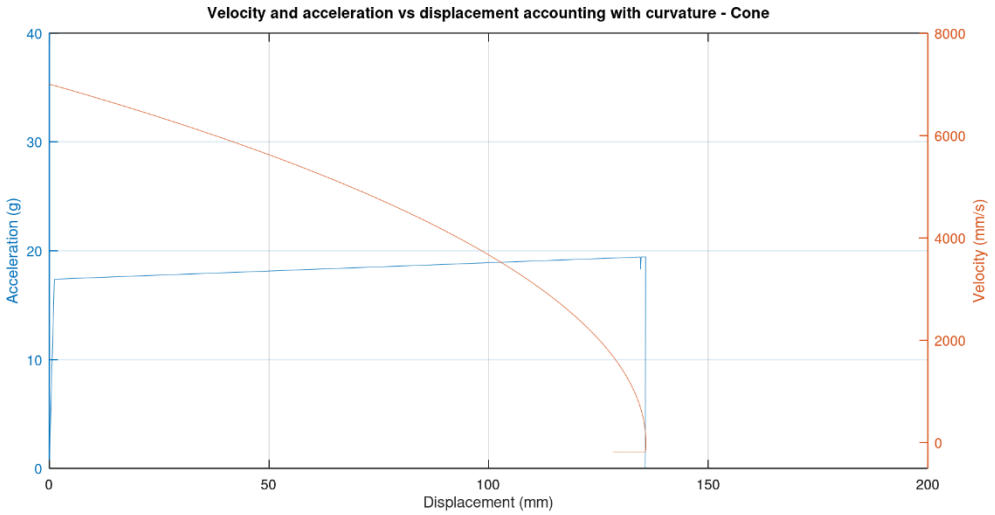

Figure 61 - Acceleration and velocity vs displacement for the CFRP cone accounting for the curvature with 3 plies

The same effect can be seen, however in a larger scale, for the multi-cellular crashbox. The SEA with curvature dependence and its variation in relation with the values calculated in the last chapter can be seen in Table 25.

As it can be seen the cone suffered a 0.4% SEA decrease in relation to the value calculated in the previous section while the multi-cellular crashbox suffered a decrease of 3.25%. This serves to demonstrate the influence of curvature in the energy absorption capabilities of a certain structure.

For the case of the multi-cellular crashbox, as shown in Table 25 and Figure 62, the structure is only able to absorb the necessary energy at almost 198 mm when the whole structure only has 200 mm, which gives little margin for error that may be present in the simulations. To look for other solutions, the same structure was again simulated with the number of plies increased to 3, but the average acceleration requirement was not met. So, the first version of the multi-cellular crashbox (V1) was again simulated with 2 plies, accounting for curvature. This structure also did not pass the average acceleration requirement. So, the solution for this problem would be to increase the length of the impact attenuator above the minimum required. Accounting for a 10% error between the simulations and the experiments, the structure should then have at least 220 mm, but the 200 mm impact attenuator is already too close to nosecone structure and therefore its length cannot be increased. The plots for these two structures can be seen in appendix D.

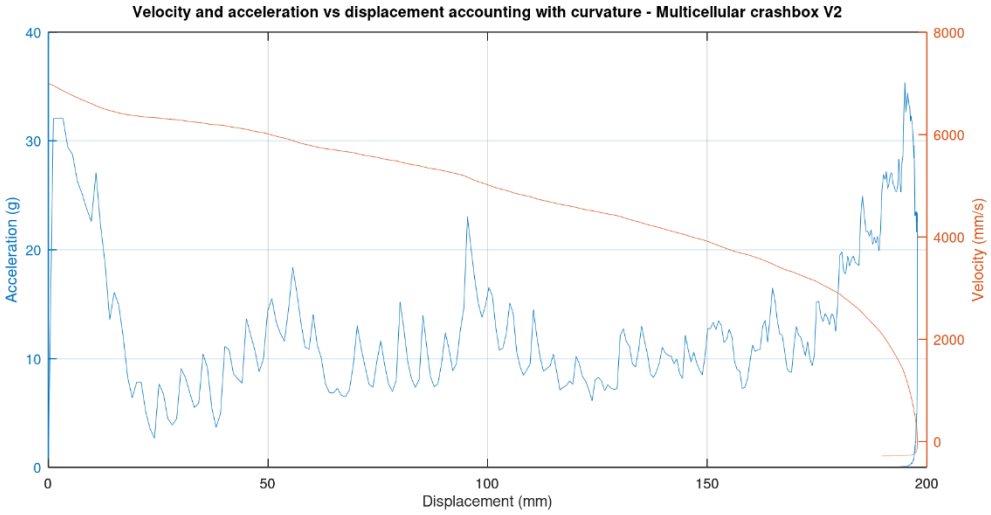

Figure 62 – Acceleration and velocity vs displacement for the Multi-cellular crashbox V2 with 2 plies accounting for curvature

Table 25 - Results for the simulations with curvature (requirements not met are represented with a red box)

Structure	Number of plies	Length crushed (mm)	Mass of the crushed zone (g)	Average acceleration (g)	Max acceleration (g)	SEA (J/g)	SEA variation (%)
Cone	3	135.81	122.32	18.323	19.442	60.09	-0.4
Multi-cellular crashbox V2	2	197.89	352.15	12.545	35.34	20.87	-3.25
Multi-cellular crashbox V2	3	70.00	186.85	35.270	48.130	39.34	-
Multi-cellular crashbox V1	2	114.89	203.24	21.579	35.343	36.16	-

5.10. Flax structures

In this section the same structures used in the last chapter are going to be simulated as being completely made out of flax.

To start the simulations, another estimation of the minimum number of plies for the structures was calculated, using this time, the crush stress for flat flax coupons. The results can be seen in Table 26.

Table 26 - Preliminary ply calculation for flax structures

Structure	Preliminary number of plies
Cone	7
Multi-cellular crashbox V1	3
Multi-cellular crashbox V2	3

For these simulations, all structures were assigned curvature dependent crush stresses. The same method used for the CFRP coupons was used with the flax coupons to discretize the crush stresses for the different bands (see Figure 63).

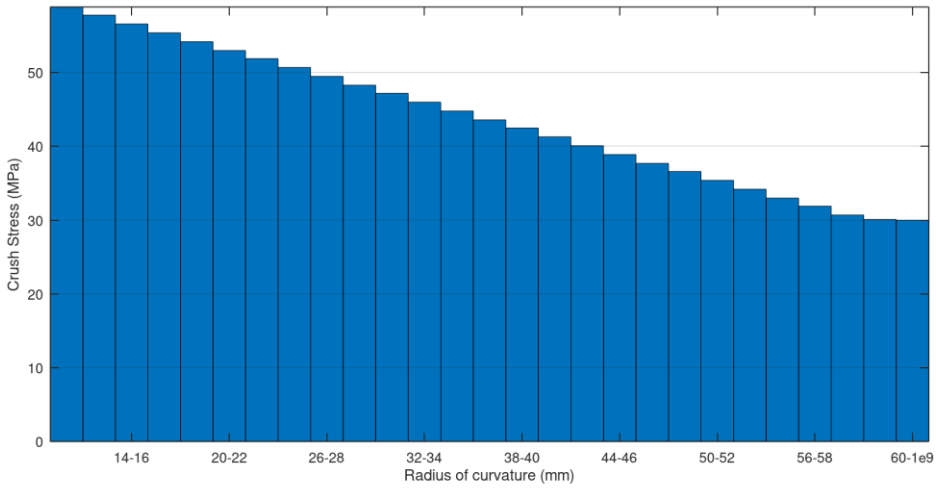

Figure 63 - FFRP crush stress curvature dependence for 1% sensitivity

The crush stress distribution for the cone and the multi-cellular crashbox V1 and V2 can be seen in Table 27, Table 28 and Table 29.

Table 27 - Cone section average radius and respective crush stresses

Cone section average radius (mm)	Crush stress (MPa)
100.875	30.0
102.75	30.0
104.5	30.0
105.25	30.0
106.125	30.0
109.625	30.0
111.5	30.0
113.25	30.0
114.875	30.0
116.625	30.0

Table 28 – Multi-cellular crashbox V1 section average radius and respective crush stresses

Multi-cellular crashbox V1 section radius (mm)	Crush stress (MPa)
Flat	30
35 mm	44.8

Table 29 - Multi-cellular crashbox V2 section average radius and respective crush stresses

Multi-cellular crashbox V2 section radius (mm)	Crush stress (MPa)
Flat	30
50 mm	35.4

Table 30 represents the results for the simulations that were able to absorb the necessary energy. Nevertheless, the first version of the multi-cellular crashbox with three plies was not able to pass the average acceleration requirement with an average 26 g acceleration.

Table 30 - Flax simulations results (failed requirements presented in red)

Structure	Number of plies	Length crushed (mm)	Mass of the crushed zone (g)	Average acceleration (g)	Max acceleration (g)	SEA (J/g)
Cone	7	131.48	328.45	18.907	20.035	22.38
Multi-cellular crashbox V1	3	95.07	299.00	26.077	29.628	24.58
Multi-cellular crashbox V2	3	155.05	490.49	16.036	23.056	14.98
Multi-cellular crashbox V1	2	186.896	392.83	13.321	19.421	18.76

The SEA results are considerably lower than the obtained for the CFRP structures, which was expected to the reduced crush stresses for flax. The cone suffered a 63% decrease in the specific energy absorption induced by the increased mass.

To try to mitigate this mass increase and find a compromise between the mass of the structure and its carbon footprint, the next chapter will focus on hybrid structures.

5.11. Hybrid structures

After obtaining the results for the structures completely made out of flax, now the possibility of using hybridisation to obtain a compromise between weight saving and bio-mass content in the crash structure remains to be studied.

The acquisition of the crush stress for hybrid structures is complex due to the large number of combinations that are possible besides the multiple orientations of each ply and all the other already mentioned properties that influence this value. Since there is not an extensive database of coupon testing for these kinds of structures, a simplification will be made. The crush stress will be considered for each individual ply of material instead of attributing a crush stress to each curvature that corresponds to a hybrid of a certain number of carbon and flax plies. Despite this approximation not being accurate, it is the best that can be achieved with the data available at the moment.

To facilitate this crush stress attribution, several materials were defined corresponding to a certain material and curvature, as it can be seen in Table 31.

Table 31 - Material fabrics definition

Fabric designation	Material	Thickness (mm)	Radius of Curvature (mm)	Crush Stress (MPa)
ABQ_PLY_FABRIC_1	CFRP	0.3	34 to 37	105.4
ABQ_PLY_FABRIC_2	CFRP	0.3	48 to 53	99.2
ABQ_PLY_FABRIC_3	CFRP	0.3	97 to 113	90.3
ABQ_PLY_FABRIC_4	CFRP	0.3	113 to 135	88.9
ABQ_PLY_FABRIC_5	CFRP	0.3	1000 to flat	81.5
ABQ_PLY_FABRIC_6	FLAX	0.4	34 to 36	44.8
ABQ_PLY_FABRIC_7	FLAX	0.4	50 to 52	35.4
ABQ_PLY_FABRIC_8	FLAX	0.4	60 to flat	30

To determine which layups to simulate, a preliminary ply calculation was performed (see Table 32). This preliminary ply calculation follows the same method that will be used in the simulations with each ply having its respective crush stress, therefore, the preliminary ply calculation is only able to estimate the necessary number of plies of each material.

Table 32 - Hybrid preliminary ply calculation

Structure	Preliminary number of CFRP plies	Preliminary number of FLAX plies
Cone (Near the limit)	1	2
Cone	1	3
Cone	2	1
Multi-cellular crashbox V1	----------	----------
Multi-cellular crashbox V2	1	1

As it can be seen in the table above, the first configuration to pass the requirements in preliminary ply calculation was a cone with 1 carbon fibre ply and 2 flax plies, nevertheless it was only able to absorb the necessary energy near the 200 mm of the structure. So, a second hypothesis with one more flax ply was immediately considered. As it will be seen later, the first configuration was not able to achieve the necessary requirements in the finite element's simulation.

According to this calculation, the first version of the multi-cellular crashbox was not able to meet the necessary requirements for a hybrid with one ply of each material due to excessive acceleration and therefore this design did not allow for hybridization. Nevertheless, the preliminary ply calculation considers a progressive crush of the structure, which, as it was seen in the CFRP and flax simulations, does not happen for this design, so a simulation with one ply of each material for this structure will be conducted.

All of the hybrid structures were considered to be symmetric whenever possible, this ensures that there is no extension-bending, that is, the structure does not generate bending loads due to axial loading. This property decreases the probability of the structure bending. For the case of the structures that cannot be symmetric a study was conducted with two simulations for the multi-cellular crashbox V1, a structure that is expected to not crush progressively and tends to buckle to see which configuration gave the best results. The structure behaviour was the best when the carbon fibre layer was on the outside of the structure, with the structure absorbing more energy. Having in mind that generally simulations tend to overestimate the energy absorbed, the structure that absorbs the most energy should be considered, so this will be the configuration used for the other structures.

The layup and respective crush stresses as well as the plots for the velocity and acceleration for the several simulations are presented in the annexes.

Table 33 present the results for the structures that were able to absorb the necessary energy. From this point forward the layers of the respective structures will be referenced with the letters "C" for carbon and "F" for flax presented by the stacking order, e.g., "FFFC" represents a layup where the first 3 plies to be laid are flax and the last one is carbon, which with male moulds means that in this case the carbon fibre ply is facing the outside of the structure.

Table 33 - Hybrids simulation results (failed requirements presented in red)

Structure	Stacking	Length crushed (mm)	Mass of the crushed zone (g)	Average acceleration (g)	Max acceleration (g)	SEA (J/g)
Cone	CFC	165.072	173.27	15.081	15.985	42.42
Cone	FFFC	172.427	260.31	14.437	15.422	28.24
Multi-cellular crashbox V1	CF	158.716	306.78	15.658	27.290	23.96
Multi-cellular crashbox V1	FC	138.15	267.03	17.957	30.715	27.53
Multi-cellular crashbox V2	CFC	113.896	322.76	21.780	37.406	22.77
Multi-cellular crashbox V2	FCF	154.725	463.96	16.084	29.631	15.84
Multi-cellular crashbox V2	FFFC	127.543	810.614	19.444	36.923	14.22

Despite the Multi-cellular structure V2 with 3 layers of flax passing the requirements, this solution is clearly worse than the FCF solution since we are just increasing the mass of it for a structure that already passed the requirements with enough margin. Due to this fact, this solution is not going to be considered in the final decision matrix.

Despite both the CF and FC configurations of the Multi-cellular crashbox passing the requirements, only the FC configuration will be considered for the rest of the decision matrices, due to having a higher specific energy absorption than the other configuration for the same geometry.

As it can be seen, the hybridization allowed for weight reduction in relation to the fully flax structures without completely discarding the utilization of the more sustainable flax material.

In the next section all the results will be compared to choose a final design for the impact attenuator.

5.12. Overall results discussion

Since the main objective of this thesis is the development of a sustainable impact attenuator for a formula student car, two indicators will be used to assess the sustainability of the simulated structures:

- Bio-based mass: The mass percentage of bio-based materials in the structure.
- Carbon footprint: Which assesses the amount of greenhouse gases produced by the whole life cycle of a product.

These indicators in conjunction with some of the criteria already defined in the previous decision matrices will help to determine a final design.

For the bio-based mass calculation, since the matrix of the flax prepreg is not bio-based, only the fibres mass was considered. Considering a 44% resin weight content as specified in the flax prepreg datasheet [129] the bio-based mass percentage was calculated.

The carbon footprint was based on the GRANTA EduPack software [112] which contains a tool for the carbon footprint and energy consumption calculation based on the whole life cycle of the product.

The software takes as inputs the product material, the mass, the production process, the transportation, its utilization, and its end of cycle.

The CFRP was introduced as a woven prepreg with a biaxial layup composed of an epoxy matrix and high strength carbon fibres, while the FFRP, since the software didn't have the prepreg available in the database was introduced as flax fibres, that go through a weaving process, and epoxy resin joined

by a impregnation process whose carbon footprint is 3,84E-03 kg CO2 eq [136]. For the final structures a process of autoclave moulding, available within the software, was added. By selecting the material, the software relies on its database to obtain the carbon footprint for the materials that was retrieved from several sources that account for the whole life cycle of these materials.

For the transportation section, the software asks for information on the distance travelled by the feedstock, in our case the prepregs or the aluminium honeycomb itself. The CFRP prepregs come from Toray based on the United Kingdom and the flax prepregs from the Angeloni Group based in Italy. The exact address of both factories were used to calculate the distances travelled by plane and truck to FEUP, resulting in distances of 1575 and 1759 km respectively. For the case of aluminium honeycomb impact attenuator, the solution that is currently on the FSFEUP 2023 car, it was bought from plascore in the United States of America, and the distance was calculated to be 6160 km. The distance travelled by the feedstock used to produce these prepregs is already included in the carbon footprint of the materials.

The software then asks for an input if the structure is used statically or dynamically (in the case of being used in a vehicle). Since this product is going to be used in a racing car with a very limited life cycle (calculated to be around 500 km divided by 25 km sessions), the use of this parameter would not be correct. A racing car travels more distance being transported than actually racing and therefore a transportation analysis would be extremely more complex. Since this carbon footprint determination serves only as a comparison method and all of the structures are going to be used in the same way, this parameter was discarded.

For the end of life, all of the composite structures were considered to be destined to landfill, which is the most common disposal method for composites at the current state of the art. For the case of the aluminium honeycomb, it was considered to be completely recycled.

These parameters are presented in Table 34 and Table 35.

Table 34 - Flax input parameters

	Input	Additional Input 1	Additional Input 2	Additional Input 3
Material	Flax Fibre	Weaving process	Mass	Landfill end of life
Material	Toughened epoxy resin	Impregnation	Mass	Landfill end of life
Manufacturing	Autoclave curing			
Transportation	Short distance airplane	1759 km		

Table 35 - CFRP input parameters

	Input	Additional Input 1	Additional Input 2
Material	CFRP prepreg: woven, biaxial layup	Mass	Landfill end of life
Manufacturing	Autoclave Moulding		
Transportation	Short distance airplane	1575 km	

The software then returns a report with the carbon footprint and energy consumption of each step of the product lifecycle and a bar plot with a summary of results (see Figure 64).

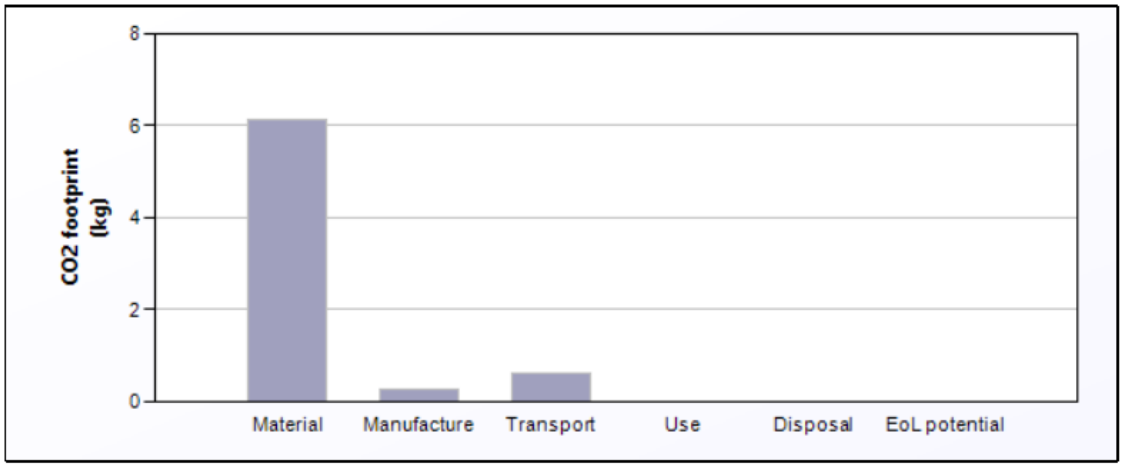

Figure 64 - CFC carbon footprint summary plot

A summary of the results obtained for all the structures are presented in Table 36. As it can be seen the full flax structure with the highest carbon footprint still has a carbon footprint 1.4 times lower than the best performing structure that includes carbon. This can be explained by the high energy consumption and carbon footprint carbonization processes that are used in the production of carbon fibres. The reduction of the carbon footprint comes with the downside of the increased mass with the best performing structure in terms of carbon footprint having a 226% weight increase in relation to the lightest carbon structure.

In terms of bio-based mass, the value is going to be proportional to the number of layers of flax until an upper limit of 56% which corresponds to the maximum fibre content in terms of mass in the FFRP prepreg.

The SEA was not included in this table since for this specific application this value ends up not having any practical advantages. Despite higher SEA meaning a higher energy absorption with lower mass, due to the minimum dimensions specified by the rules a structure that is rule compliant and with higher SEA may end up being heavier than another rule compliant structure with a lower SEA. For this reason, in the comparison table only the whole structure mass was considered.

In relation to the currently used aluminium honeycomb impact attenuator, without considering the recycling process, the FCF version of the multi-cellular crashbox V2 and the fully carbon version of this same structure perform worst in terms of carbon footprint. Considering the recycling of this product the scenario gets worse, with only one composite structure being able to outperform it in terms of carbon footprint, the 100% flax Multi-cellular crashbox V1. Nevertheless, several structures are able to outperform the aluminium honeycomb IA in terms of weight which is the main reason why composites are used over metallic structures in motorsports applications.

Table 36 - Mass, bio-based mass and carbon footprint results for the structures that passed the FSG requirements

Structure	Layup	Total mass (g)	Bio-based mass (%)	Carbon Footprint (kg)	Safe Margin (%)
Cone	CCC	185.8	0	9.47	8.4
	FFFFFFF	513.8	56	2.8	5.5
	CFC	197.2	20.8	7.04	17.5
	FFFC	282.1	43.7	4.78	13.8
Multi-cellular crashbox V1	FF	419.3	56	2.28	6.6
	FC	386.58	30.4	10.8	10.2
Multi-cellular crashbox V2	CC	355.9	0	18	1.1
	FFF	632.7	56	3.43	19.8
	FCF	599.72	39.4	12.3	19.6
Al Honeycomb IA	-	430	0	12.1 (2.5)	100

Besides the parameters already presented above, another parameter referred as safe margin was added. This parameter represents the lower percentual difference between three different safety margins that are represented by the equations below.

$$S_{a\,max}\ (\%) = \left(1 - \frac{a_{max}}{a_{\max Al.}}\right) * 100 \tag{5.18}$$

$$S_{a\,avg}\ (\%) = \left(1 - \frac{a_{avg}}{a_{\mathrm{avg}\,Al.}}\right) * 100 \tag{5.19}$$

$$S_{length}\ (\%) = \left(1 - \frac{l_{cr}}{l_{t}}\right) * 100 \tag{5.20}$$

$$Safe\ Margin\ (\%) = Min(S_{a\,max}, S_{a\,avg}, S_{length}) \tag{5.21}$$

$S_{a\,max}$ represents the safe margin corresponding to the ratio between the maximum acceleration obtained in the simulations, a_{max}, and the maximum acceleration allowed by the rules, $a_{\max Al.}$.

For the average acceleration, the safe margin is calculated in the same way, with a_{avg} being the simulated average acceleration and $a_{\mathrm{avg}\,Al.}$, the average acceleration allowed by the rules.

In the case of the length margin, l_{cr} represents the crushed length while l_t represents the total length of the impact attenuator. Despite the length of the impact attenuator being able to be increased according to the rules, all of the structures are already in the limit of not fitting inside the structural nosecone and therefore this length cannot be changed.

To do the final decision matrix, the criteria had to be defined. Initially the same criteria used in the structures design decision matrix were considered.

The cost of the structures was recalculated, including the material cost. The prices were roughly 150 and 35 euros per square meter, for the carbon fibre and the flax prepregs, respectively. These prices were the ones provided by the prepreg manufacturers. The prices for each structure were calculated adding the mould price plus the material price that can be calculated by multiplying the surface area times the number of plies and the respective price per square meter. Table 37 contains the calculated prices for the structures to be compared.

Table 37 - Prices and respective scoring for the final structures

Structure	Cone CCC	Cone 7F	Cone CFC	Cone FFFC	Multi-cellular V1 FF	Multi-cellular V1 FC	Multi-cellular V2 CC	Multi-cellular V2 FFF	Multi-cellular V2 FCF	Aluminium honeycomb
Price (€)	120.23	92.11	104.46	93.51	72.03	117.10	117.52	84.89	131.32	60
Scoring	2	3	3	3	5	2	2	4	1	5

The cost scoring was done according to the following system:

- 60 to 76 euros: 5 points
- 76 to 92 euros: 4 points
- 92 to 108 euros: 3 points
- 108 to 124 euros: 2 points
- 124 to 140 euros: 1 point

The manufacturability scorings were maintained from this last matrix since, despite the flax manufacturability requiring more care due to the more flexible nature of the fibres, the manufacturing process and mould materials used remain the same.

The oblique crushing stability scoring also remains the same since the structure geometry does not change.

The overall structure stiffness was not included in this final table since this parameter was used to predict premature failure due to buckling when crushing, and since the structures to be compared were already simulated, its buckling behaviour is known and included in the crush related results.

For the structure mass criteria, the mass was recalculated for each of the structures, with the same criteria weight of 1 used before, and the mass scoring system redefined for these specific masses, as follows:

- 150 to 250 grams: 5 points
- 250 to 350 grams: 4 points
- 350 to 450 grams: 3 points
- 450 to 550 grams: 2 points
- 550 to 650 grams: 1 point

In spite of having considered the bio-based mass in the sustainability analysis performed before, this parameter ends up being less important than the carbon footprint, since the amount of bio-based mass in a certain structure may not result in less energy consumption and carbon emissions. For that reason, only the carbon footprint is included as a criterion.

- 2 to 5.4 kg: 5 points
- 5.4 to 8.8 kg: 4 points
- 8.8 to 12.2 kg: 3 points
- 12.2 to 15.6 kg: 2 points
- 15.6 to 19 kg: 1 point

Since sustainability is the main focus of this project, this criterion will be weighted with 5 points out of 5.

Finally, for the safety margin, 20% was defined as being the threshold for what can be considered to be a safe structure as this was the maximum value of deviation between numerical and experimental results found by Bisagni [8] for maximum and average loads and specific energy absorption, which in our case is related with the length margin. The scoring system was defined as follows:

- 0 to 5%: 1 point
- 5 to 10%: 2 points
- 10 to 15%: 3 points
- 15 to 20%: 4 points
- 20 to 100%: 5 points

As this thesis considers the development of this structure in the context of the current conditions of the FSFEUP team, where reliability is one of the main concerns, this criterion was weighted with 5 out of 5 points, to ensure that, more importantly than any performance indexes, the structure would be able to fulfil all of the requirements.

Table 38 represents the results of the final decision matrix. As it can be seen, the aluminium honeycomb impact attenuator, according to these criteria still outperforms the composite structures studied. This is due to the context where these studies are being considered, and that were already mentioned before when the several weights were attributed to the different criteria. On one hand, the FSFEUP is still a very young team with restricted budgets, low experience on composite manufacturing and focusing the design on reliability instead of weight reduction. On the other hand, in the context of this thesis, the budget is limited and the timeframe tight. All of these factors result in a high weight of the cost, manufacturability, and safety margin criteria, which make the aluminium honeycomb still the best option to choose.

Nevertheless, if the context is shifted in the direction of the context of a more advanced team: with composite sponsors that eliminate cost constraints; with manufacturability being in the opposite extreme where the added structure complexity is a mean to acquire knowledge and the team has enough experience to make it easier; with the main focus on weight reduction and therefore increased risk, weight and carbon footprint would be the main criteria within this scope.

Table 39 and Table 40 represent this second scenario where the criteria referred before were alleviated or eliminated in the case of the cost where the sponsor can provide the whole structure for free. As it can be seen, now the best performing structure is a composite structure, the hybrid cone with 2 layers of carbon and one of flax, followed by a hybrid cone with 3 layers of flax and 1 of carbon which were able to decrease the mass by 54% and 34% in relation to the aluminium honeycomb. Nevertheless, this weight decrease resulted in 181,6% and 91.6% increase in the carbon footprint.

Table 38 - Final decision matrix current conditions ("Co." stands for cone, "M.Cr." for Multi-cellular crashbox and "A.H." for aluminium honeycomb)

	Weights	Co. CCC	Co. 7F	Co. CFC	Co. FFFC	M.Cr. V1 FF	M.Cr. V1 FC	M.Cr. V2 CC	M.Cr. V2 FFF	M.Cr. V2 FCF	A.H.
Cost	4	2	3	3	3	5	2	2	4	1	5
Manufacturability	4	4	4	4	4	4	4	4	4	4	5
Oblique crushing stability	3	5	5	5	5	1	1	1	1	1	5
Weight	1	5	2	5	4	3	3	3	1	1	3
Carbon footprint	5	3	5	4	5	5	3	1	5	2	5
Safe margin to minimum requirements	5	2	2	4	3	2	3	1	4	4	5
Sum		21	22	25	24	20	16	12	19	14	28
Weighted Sum		69	84	88	87	77	60	40	81	58	108

Table 39 - Final decision matrix future team ("Co." stands for cone, "M.Cr." for Multi-cellular crashbox and "A.H." for aluminium honeycomb)

	Weights	Co. CCC	Co. 7F	Co. CFC	Co. FFFC	M.Cr. V1 FF	M.Cr. V1 FC	M.Cr. V2 CC	M.Cr. V2 FFF	M.Cr. V2 FCF	A.H.
Cost	0	2	3	3	3	5	2	2	4	1	5
Manufacturability	1	4	4	4	4	4	4	4	4	4	5
Oblique crushing stability	3	5	5	5	5	1	1	1	1	1	5
Weight	5	5	2	5	4	3	3	3	1	1	3
Carbon footprint	5	3	5	4	5	5	3	1	5	2	5
Safe margin to minimum requirements	1	2	2	4	3	2	3	1	4	4	5
Sum		21	22	25	24	20	16	12	19	14	28
Weighted Sum		61	56	68	67	49	40	28	41	26	65

Table 40 - Results and relative differences for the second scenario

	Mass	Carbon footprint (kg)	Scoring	% Mass	% Carbon Footprint
Cone CFC	197.2	7.04	68	-54.1	181.6
Cone FFFC	282.3	4.78	67	-34.3	91.2
M.C. V1 FF	419.3	2.28	49	-2.5	-8.8
A.H	430	2.5	65	0	0

To finalize this scenario, there is a structure, composed completely out of flax, that was able to not only decrease the weight of the structure in 2.5%, as to also decrease the carbon

footprint in 8.8%, showing the potential for this kind of material. It ended up scoring less points due to its weak behaviour in oblique crushing stability and lower safety margin when compared to the structures that scored the most.

Current formula 1 vehicles use structures entirely made out of carbon fibre, so to finalize this analysis it is worth comparing some hybrid structures that stand out in terms of weight and carbon footprint with the lighter carbon fibre structure.

Table 41 represents two hybrid cones composed of 2 carbon fibre and one flax ply and 1 carbon fibre ply and 3 flax fibre plies, respectively. As it can be seen, a weight increase as low as 6% can result in a carbon footprint reduction of 25.7%. Increasing the mass 52% can generate a 49.4% carbon footprint reduction. These results show that, with proper design, flax/carbon hybrids can result in far more sustainable structures with low compromise on weight.

Table 41 - Second case results comparison

	Mass (g)	Carbon footprint (kg)	Scoring	% Mass	% Carbon Footprint
Cone CFC	197.2	7.04	68	6	-25.7
Cone FFFC	282.3	4.78	67	52	-49.4
Cone CCC	185.8	9.47	61	0	0.0

6. Conclusions and future work

In this thesis, the possibility of designing a sustainable hybrid or pure flax impact attenuator for a formula student car was studied. In this chapter, the main conclusions of this study, its design choices and simulations will be presented. Furthermore, based on the work developed and the conclusions drawn, future activities that would complement this work are proposed.

6.1. Conclusions

The automotive and motorsports industry is constantly pushing for the construction of lighter cars to reduce fuel-consumption and to allow for faster and more competitive cars. In this context, the use of composite crash structures has been gaining popularity due to their increased specific energy absorption capabilities. This led to several studies being conducted on coupon testing, numerical analysis and approaches and the manufacture and testing of larger structures to assess fibre-reinforced polymers energy absorption.

Formula student is no exception in terms of the objective of lightweight design and fierce competition. It was found in the literature that the majority of the teams have made the move from the old-fashioned heavy and high-volume foam impact attenuators to the lighter and smaller aluminium honeycomb structures. Nevertheless, the need to further reduce the weight of the car has led to a large number of studies being conducted on the possibility for the introduction of composite impact attenuators in formula student.

Nevertheless, due to the environmental issues that the world has been facing, the scientific community and the automotive and motorsports industries have been trying to find more sustainable options to the most common carbon/epoxy composites. These composites reveal several problems, from the high-temperature transformation processes to the oil-based nature of the raw materials and the low recyclability due to the thermoset matrix. The introduction of natural fibre composites appears to be a promising way to mitigate these problems with lower levels of embodied energy and lower carbon footprint. The hybridization between these natural fibres with the conventional fibres also appears as a way to mitigate sustainability problems with reduced impact on performance.

The geometry influence on the energy absorption capabilities of composites has also been highlighted in several studies. It was found that tulip and saw-tooth triggers are able to increase the specific-energy absorption of coupons through the reduction of peak force and supressing of catastrophic failure. The inclusion of a small 5-degree slope has also been found to contribute for a more stable and progressive crushing. Finally, it has also been found that for both CFRP (carbon fibre reinforced polymers) as well as FFRP (flax fibre reinforced polymers) an increase in radius of curvature leads to lower crush stresses and therefore lower specific energy absorption for tubular coupons.

Due to the high cost involved in composite manufacturing and testing, mainly caused by the expensive materials and manufacturing labour, numerical simulations play a huge role in the crashworthiness industry. This led to several studies being conducted on different numerical approaches to this subject. Meso-scale modelling has been found to be able to reproduce accurately the interlaminar behaviour of composite crushing. Nevertheless, their high computational time combined with the extensive amount of material data obtained through experiments as well as a time-consuming calibration process, makes it unsuitable for industry. The macro-scale modelling approach on the other hand has been proving to obtain accurate simulation results in a more cost-effective way, although it still requires extensive testing to determine the crush stress of coupons which is dependent on geometry, layup, and the material itself.

In this thesis, initially, several CFRP and FFRP tubular coupons were manufactured and tested. The manufacture posed several problems inherent to the pre-preg layup process which led to external geometric effects and demoulding difficulties. Despite these effects apparently not having effects on the crushing behaviour, the quantitative results might be affected. A more extensive coupon testing was conducted by another student in a parallel thesis [105] which allowed to prove a curvature dependence on the crush stress, which reduces with the increase of radius of curvature, which was used to feed the numerical simulations.

An in-depth analysis of several designs, based on criteria defined within the context of the formula student FEUP team and this thesis, led to the choice of internal impact structures instead of a nosecone as the impact structure. Initially based on a decision-matrix, the structural nosecone option was found to be more expensive and harder to manufacture due its dimensions, less stiff because of the large flat inclined surfaces that would result in premature buckling, and that are fixed due to the aerodynamic constraints, as well as heavier. The option of introducing reinforcement ribs in this structure to mitigate the stiffness problem was also discarded, since it would increase even more the price of the structure and the manufacturing difficulty.

A second decision matrix with a more detailed cost and overall structure stiffness analysis resulted in the choice of a circular cross-sectioned cone and a multicellular structure to be simulated with a finite element analysis. The structural nosecone was also simulated to be used as a term of comparison. A detailed study of several mould materials, according to their weight and mechanical capabilities, allowed for the determination of the most adequate manufacturing process for each structure, which was then used to calculate the mould price associated with each structure. The aluminium moulds were found to be the most adequate for the smaller structures with a simple geometry while the epoxy moulds were chosen for the remaining more complex structures. A lateral push-off test, numerically simulated using a static-general contact simulation within a finite element analysis on Abaqus®, allowed for the determination of the lateral displacement of each structure when subjected to the same loading condition, allowing for a rough comparative value of the overall stiffness of the structure. The lateral displacement for one of the structures was not determined due to simulation problems and time constraints, but it was found that the final design choice was independent of the value found on the overall structure stiffness of that specific structure.

The numerical analysis confirmed the poor energy absorption capabilities of the structural nosecone that revealed several acceleration spikes caused by buckling. Nevertheless, a solution was found where this structure would pass the FSG requirements but with a weight of over 1 kg and a low value of specific energy absorption around 6.5 J/g. The cone was able to crush progressively while the multicellular crashbox had several buckling occurrences but was still able to absorb the necessary energy. For carbon fibre, two kinds of simulations were conducted with the difference being that on the first type the simulation did not account for curvature and considered the structures to have the crush stress of a flat plate. The use of an overestimated flat plate crush stress, due to the lack of data for the dynamic crush tests performed in a parallel thesis [105], at the time of the initial simulations, actually resulted in a worst performance of the structures when the curvature was considered, nevertheless if the simulations were to be repeated with the more recent values the inclusion of curvature would result in higher specific energy absorptions.

Several structures were able to pass the competition requirements, from CFRP and FFRP structures to hybrids. The structures were compared in terms of several criteria including their carbon footprint. Nevertheless, due to the context of the current FSFEUP team, the aluminium honeycomb structure was found to be the most suitable, with the best scoring in the final decision matrix, mainly due to the high cost, manufacturing complexity, safety margins applied, and the low importance given to weight reduction. However, if the context was one of a more advanced team, with access to more

resources and with weight reduction playing a more important role, two cone hybrid structures would have a greater scoring.

Nevertheless, it was found that it is possible to reduce the weight and carbon footprint of the current aluminium honeycomb impact attenuator by 2.5% and 8.8% respectively, using a multicellular crashbox with two layers of flax. It was also found that by including flax fibres to form a hybrid cone composed of 2 layers of carbon and one of flax it is possible to reduce the carbon footprint of a carbon fibre composite structure by 25.7% with a mass increase as low as 6%.

Overall, the conclusions reached in this study proved the possibility of designing a composite structure to serve as a Formula Student impact attenuator. Furthermore, it was able to design a hybrid structure able to reduce the weight and carbon footprint in relation to the aluminium honeycomb impact attenuator currently used by the team.

6.2. Future work

Despite being able to fulfil the main purpose of the thesis to design a more sustainable composite crash structure to serve as an impact attenuator in a formula student car, there are several points that remain to study and should be addressed in the future.

Firstly, to validate the results obtained from the simulations, the structures with the best overall performance should be manufactured and tested, which did not happen in this thesis due to the time constraints.

Regarding the overall design of the structure, the analysis performed does not represent the exact configuration that would happen in a formula student car crash. In this work, the structure was represented as being encastred in one of its ends and being hit by a rigid impactor. While this is enough to assert the energy absorption capabilities of the structure, it does not comply completely with the test required by the competition. In this test, the impact attenuator should be mounted on the anti-intrusion plate by a desired method, which will be replicated in the car, which in turn will be mounted in a structure with a stiffness similar to that of the chassis. Besides the acceleration requirements, in the test, the anti-intrusion plate should also not permanently deflect more than 25 mm from the initial position, which was not part of the conducted simulations. Therefore, it is recommended that an attachment method is chosen and the whole assembly simulated.

In this work, the oblique crushing stability of the several designs was purely classified based on the structures slope. However, the off-axis energy absorption of the structure not being required by the rules for the impact attenuator, it is of extreme importance in terms of safety. It is therefore recommended that the structures that were able to pass the initial acceleration requirements should be tested for several impacting angles to determine its oblique crushing capabilities.

Due to the lack of experimental data on CFRP and FFRP coupons, the crush stress used was the crush stress obtained for tubes with 8 plies and a layup of $[45,0,45,0]_S$ for carbon and $[0]_8$ for flax, independently of the number of plies used in the structures studied. However, the layup sequence being maintained in the CFRP coupons, the number of layers varied, which, as mentioned in the literature review, should influence the crush stress. Besides that, since hybrid coupons were not tested, there was no crush stress data for a hybrid configuration, so the crush stress was attributed for each ply instead, so the carbon fibre plies would have the CFRP crush stress while the flax ones would have the FFRP crush stress. In a literature analysis it is possible to verify that when hybrids are tested, the crush stress is higher than the arithmetic mean of the crush stresses of both fibres and due to the different fibre diameters, there is also a decrease in density, which means that the hybrid results should show better results in terms of SEA from what was obtained. To mitigate this problem,

hybrid coupons with different hybrid ratios and diameters should be tested to provide the model with more accurate results.

As also stated in the literature review, the crush stress is also dependent on the slope of the structure. In these simulations, the curvature was not accounted for since the data for crush stress dependence on slope was not available. To improve the simulation results, cones should be tested with different inclinations.

Finally, as also stated in the literature review, the crush stress is dependent on the strain-rate of the test, which means that quasi-static crush stresses are going to be different from dynamic crush stresses. Despite our simulation being dynamic, after the impactor has been decelerated due to the forces generated by the crushing of the impact attenuator, its velocity reduces to limits that might be considered as a quasi-static simulation, and this was not considered. To mitigate this problem, besides all the coupon testing already mentioned before, coupons should be tested for different strain-rates, to have a way to determine the crush stress variation with strain-rate.

Bibliography

1. European Parliament, *Reducing carbon emissions: EU targets and policies*. 2018 [12/07/2023]; Available from: https://www.europarl.europa.eu/news/en/headlines/society/20180305STO99003/reducing-carbon-emissions-eu-targets-and-policies?&at_campaign=20234-Green&at_medium=Google_Ads&at_platform=Search&at_creation=RSA&at_goal=TR_G&at_audience=carbon%20emissions&at_topic=Carbon_Emission&at_location=PT&gclid=Cj0KCQjwnrmlBhDHARIsADJ5b_n8i2-yoYa8k_45Lv1Ky9VgOAsiyJ-URELRY0a22CoRup4LXRGmZOIaAoELEALw_wcB.
2. Composites Construction UK, *Is Carbon Fibre a Sustainable Material for Strengthening Buildings and Structures?* 2022 [12/07/2023]; Available from: https://www.fibrwrap-ccuk.com/carbon-fibre-strengthening/is-carbon-fibre-a-sustainable-material-for-strengthening-buildings-and-structures/.
3. Sharma, S., et al., *Recent Progress of Composite Materials in various Novel Engineering Applications*. Materials Today: Proceedings, 2018. **5**(14, Part 2): p. 28195-28202.
4. lshai;, I.M.D.O., Engineering mechanics of composite materials. 2 ed. 2006, 198 Madison Avenue, New York, New York 10016: Oxford University Press, Inc.
5. Mackenzie, I., *Carbon fibre's journey from racetrack to hatchback*, in *BBC News*. 2011, BBC.
6. Savage, G., *Development of penetration resistance in the survival cell of a Formula 1 racing car*. Engineering Failure Analysis - Eng. Fail. Analysis, 2010. **17**: p. 116-127.
7. l'Automobile, F.I.d., *2023 Formula 1 technical regulations*, in *5*, WMSC, Editor. 2023.
8. Bisagni, C., et al., *Progressive crushing of fibre-reinforced composite structural components of a Formula One racing car*. Composite Structures, 2005. **68**(4): p. 491-503.
9. FSG, *Formula Student Rules 2023*. 2023.
10. Case, D. *History of Formula SAE*. 2010 [cited 25/07/2023]; Available from: https://www.fsaeonline.com/page.aspx?pageid=c4c5195a-60c0-46aa-acbf-2958ef545b72.
11. Formula Student Germany, *Chronicle*. 2022 [cited 25/07/2023]; Available from: https://www.formulastudent.de/about/chronicle/.
12. Mohitzadeh, S.S. and S.H. Hashemi, *Experimental and Numerical Evaluation of Momentum Variations Effect of Striker on Fracture Energy in Charpy Impact Testing of API X65 Steel*. mdrsjrns, 2020. **20**(9): p. 2275-2287.
13. Xu, J., et al., *Crashworthiness of carbon fibre hybrid composite tubes molded by filament winding*. Composite Structures, 2016. **139**: p. 130-140.
14. Dalli, D., et al., *Assessing the current modelling approach for predicting the crashworthiness of Formula One composite structures*. Composites Part B: Engineering, 2020. **201**: p. 108242.
15. Feraboli, P., *Development of a Modified Flat-plate Test Specimen and Fixture for Composite Materials Crush Energy Absorption*. Journal of Composite Materials - J COMPOS MATER, 2009. **43**: p. 1967-1990.
16. Yan, L., *Crashworthiness characteristics of flax fibre reinforced epoxy tubes for energy absorption application*. Materials and Design, 2013. **51**: p. 629-640.
17. Vettorello, A., et al., *Numerical-Experimental Correlation of Dynamic Test of a Honeycomb Impact Attenuator for a Formula SAE Vehicle*. Metals, 2020. **10**: p. 652.
18. Mamalis, A.G., et al., *Crashworthy capability of composite material structures*. Composite Structures, 1997. **37**(2): p. 109-134.
19. Hull, D., *A unified approach to progressive crushing of fibre-reinforced composite tubes*. Composites Science and Technology, 1991. **40**(4): p. 377-421.
20. Özbek, Ö., Ö. Bozkurt, and A. Erklig, *Crashworthiness of basalt fibre reinforced composite pipes subjected to quasi-static lateral compression* 2019.
21. Boria, S., et al., *Crashworthiness and lightweight design of an innovative microcar*. International Journal of Automotive Composites, 2015. **1**: p. 313-332.
22. Huang, X., G. Lu, and T.X. Yu, *Energy absorption in splitting square metal tubes*. Thin-Walled Structures, 2002. **40**(2): p. 153-165.
23. Santos, A.M.A., *Dynamic analysis and design of impact attenuator structures for a Formula Student prototype*, in *Mechanical Engineering Department*. 2017, Instituto Superior Técnico.

24. Cui, L., S. Kiernan, and M.D. Gilchrist, *Designing the energy absorption capacity of functionally graded foam materials.* Materials Science and Engineering: A, 2009. **507**(1): p. 215-225.
25. Paul, T., *Design of chassis, impact attenuator, suspension and aerodynamic systems of a formula SAE car*, in *Faculty of the Department of Engineering Technology*. 2019, University of Houston.
26. Schormans, J.M.J., *The design of a formula student front impact attenuator* in *Department of Mechanical Engineering* 2010, Eindhoven University of Technology.
27. Shaaban, A. and A.M. Elsabbagh, *Crashworthiness Optimization of Impact Attenuators Constructed of Polyurethane Foam.* International Journal of Automotive Technology, 2022. **23**(2): p. 389-401.
28. Goyal, S., et al., *Crashworthiness analysis of foam filled star shape polygon of thin-walled structure.* Thin-Walled Structures, 2019. **144**: p. 106312.
29. Dixit, A. and H.S. Mali, *Modeling techniques for predicting the mechanical properties of woven-fabric textile composites: a Review.* Mechanics of Composite Materials, 2013. **49**(1): p. 1-20.
30. Farley, G.L., R.K. Bird, and J.T. Modlin, *The role of fibre and matrix in crash energy absorption of composite materials.* Journal of The American Helicopter Society, 1989. **34**: p. 52-58.
31. Farley, G.L., *Effect of Specimen Geometry on the Energy Absorption Capability of Composite Materials.* Journal of Composite Materials, 1986. **20**(4): p. 390-400.
32. Jacob, G.C., et al., *Energy Absorption in Polymer Composites for Automotive Crashworthiness.* Journal of Composite Materials, 2002. **36**(7): p. 813-850.
33. Ramachandran, K., C.L. Gnanasagaran, and A. Vekariya, *Life cycle assessment of carbon fibre and bio-fibre composites prepared via vacuum bagging technique.* Journal of Manufacturing Processes, 2023. **89**: p. 124-131.
34. Isaac, C.W. and C. Ezekwem, *A review of the crashworthiness performance of energy absorbing composite structure within the context of materials, manufacturing and maintenance for sustainability.* Composite Structures, 2021. **257**: p. 113081.
35. Yan, L., N. Chouw, and K. Jayaraman, *Flax fibre and its composites – A review.* Composites Part B: Engineering, 2014. **56**: p. 296-317.
36. Feng, N.L., S.D. Malingam, and S. Irulappasamy, *4 - Bolted joint behavior of hybrid composites*, in *Failure Analysis in Biocomposites, Fibre-Reinforced Composites and Hybrid Composites*, M. Jawaid, M. Thariq, and N. Saba, Editors. 2019, Woodhead Publishing. p. 79-95.
37. Strohrmann, K., et al., *Crashworthiness Characteristics of Carbon-Flax Composite Tubes for Aerospace Applications*, in *ECCM18 - 18th European Conference on Composite Materials*. 2018: Athens, Greece.
38. Schrank, M., P. Gong, and Y. Pan, *Simulation of Crushing Behavior for Automotive Composites Structures.* 2014.
39. Lobão, V.M., *Development and testing of hybrid composite coupons for crush applications*, in *Departamento de Engenharia Mecânica (DEMec)*. 2022, Universidade do Porto - Faculdade de Engenharia: Porto. p. 114.
40. Oshinibosi, A., *Chassis and impact attenuator design for formula student race car*, in *School of Mechanical Engineering.* 2012, University of Leeds.
41. Rahman, A., et al., *Design and Analysis of Impact Attenuator for a Formula Student Car: A Study between Singular and Bi-tubular Tubes of Varying Geometries.* IOP Conference Series: Materials Science and Engineering, 2018. **429**(1): p. 012049.
42. Assan, N.A., et al., *Design and Analysis of Impact Attenuator for UiTM Formula SAE Car 2016.* Journal of Mechanical Engineering, 2019. **16**(3): p. 143-153.
43. Kaya, D. and E. Özyurt, *Design and optimization of impact attenuator for a Formula SAE racing car.* Sigma Journal of Engineering and Natural Sciences, 2022. **40**(2): p. 390-401.
44. Albahash, Z.F. *Enhancement of Impact Attenuator for Automotive Application*. in *2020 3rd International Conference on Engineering Technology and its Applications (IICETA)*. 2020.
45. Boria, S., *Crash analysis of an impact attenuator for racing car in sandwich material.* 2016.
46. Coppola, L., et al., *Impact Attenuator Optimum Design for a FSAE Racing Car by Numerical and Experimental Crash Analysis.* International Journal of Automotive Technology, 2020. **21**(6): p. 1339-1348.
47. Malik, P., *Analysis of impact Attenuator of the student formula*, in *Faculty of Mechanical Engineering and Design*. 2019, Kaunas University of Technology.

48. Tripathi, H.V., et al., *Design and Fabrication of Impact Attenuator for Formula SAE car.* International Journal of Engineering Research & Technology (IJERT), 2018. **7**(05).
49. Sardar, P., et al., *Cost Effective Impact Attenuator for a Formula Student Car.* International Journal of Applied Engineering Research, 2018. **13**(8): p. 5881-5888.
50. Marques, R.H.S.C., *Estabelecimento de parâmetros geométricos de um absorsor de impacto de fibra de carbono para um automóvel de competição, e sua optimização*, in *Departamento de engenharia mecânica*. 2022, Faculdade de Engenharia da Universidade do Porto.
51. Fellows, N., *Experimental Modeling of a Formula Student Carbon Composite Nose Cone.* Materials, 2017. **10**: p. 620.
52. Floreani, C., *Design and Manufacturing of Carbon-Fibre Composite Nose Cone Assembly and Impact Attenuator for Formula Students Competition*. 2017.
53. Cunningham, A., et al., *Carbon Fibre Monocoque Development for a Formula SAE Racecar.* 2015.
54. Hagan, M., J. Rappolt, and J. Waldrop, *Formula SAE Hybrid Carbon Fibre Monocoque / Steel Tube Frame Chassis*, in *Mechanical Engineering Department*. 2014, California Polytechnic State University - San Luis Obispo.
55. Rappolt, J.T., *Analysis of a carbon fibre reinforced polymer impact attenuator for a formula SAE vehicle using finite element analysis*, in *Mechanical engineering department*. 2015, Faculty of California Polytechnic State University, San Luis Obispo.
56. Boria, S. and G. Belingardi. *Composite impact attenuator with shell and solid modeling. In: 11th World congress on computational mechanics (WCC M XI)*. 2014. p. 2237-2245
57. Feraboli, P., C. Norris, and D. McLarty, *Design and certification of a composite thin-walled structure for energy absorption.* Int. J. Vehicle Design, 2007. **44**.
58. Boria, S., G. Belingardi, and A. Scattina, *Thermosetting and thermoplastic impact attenuator under axial loading.* Multiscale and Multidisciplinary Modeling, Experiments and Design, 2019. **2**(2): p. 129-139.
59. Boria, S., J. Obradovic, and G. Belingardi, *Experimental and numerical investigations of the impact behaviour of composite frontal crash structures.* Composites Part B: Engineering, 2015. **79**: p. 20-27.
60. Raponi, E., et al., *Methodology for parameter identification on a thermoplastic composite crash absorber by the Sequential Response Surface Method and Efficient Global Optimization.* Composite Structures, 2021. **278**: p. 114646.
61. Obradovic, J., S. Boria, and G. Belingardi, *Lightweight design and crash analysis of composite frontal impact energy absorbing structures.* Composite Structures, 2012. **94**(2): p. 423-430.
62. Wang, J., et al., *Design and experimental verification of composite impact attenuator for racing vehicles.* Composite Structures, 2016. **141**: p. 39-49.
63. Savage, G., I. Bomphray, and M. Oxley, *Exploiting the fracture properties of carbon fibre composites to design lightweight energy absorbing structures.* Engineering Failure Analysis, 2004. **11**(5): p. 677-694.
64. Heimbs, S., et al., *Crash Simulation of an F1 Racing Car Front Impact Structure*. *7th European LS-DYNA conference*. 2009. p. 1-8
65. Boria, S., A. Scattina, and G. Belingardi, *Axial energy absorption of CFRP truncated cones.* Composite Structures, 2015. **130**: p. 18-28.
66. Zhu, G., et al., *Energy-absorbing mechanisms and crashworthiness design of CFRP multi-cell structures.* Composite Structures, 2020. **233**: p. 111631.
67. Boria, S., et al., *Experimental crushing analysis of thermoplastic and hybrid composites.* Composite Structures, 2019. **226**: p. 111241.
68. Zarei, H. and M. Kröger, *Optimum honeycomb filled crash absorber design.* Materials & Design, 2008. **29**(1): p. 193-204.
69. Cauchi Savona, S. and P.J. Hogg, *Effect of fracture toughness properties on the crushing of flat composite plates.* Composites Science and Technology, 2006. **66**(13): p. 2317-2328.
70. Ogin, S.L., P. Brøndsted, and J. Zangenberg, *1 - Composite materials: constituents, architecture, and generic damage*, in *Modeling Damage, Fatigue and Failure of Composite Materials*, R. Talreja and J. Varna, Editors. 2016, Woodhead Publishing. p. 3-23.
71. Safri, S., M. Jawaid, and M.T. Hameed Sultan, *Damage analysis of glass fibre reinforced composites*. 2018. p. 133-147.

72. Pinho, S.T., et al., *7 - Fibre-dominated compressive failure in polymer matrix composites*, in *Failure Mechanisms in Polymer Matrix Composites*, P. Robinson, E. Greenhalgh, and S. Pinho, Editors. 2012, Woodhead Publishing. p. 183-223.
73. Broughton, W., *6 - Testing the mechanical, thermal and chemical properties of adhesives for marine environments*, in *Adhesives in Marine Engineering*, J.R. Weitzenböck, Editor. 2012, Woodhead Publishing. p. 99-154.
74. Hussein, R.D., D. Ruan, and G. Lu, *An analytical model of square CFRP tubes subjected to axial compression.* Composites Science and Technology, 2018. **168**: p. 170-178.
75. Mamalis, A.G., et al., *Energy absorption capability of fibreglass composite square frusta subjected to static and dynamic axial collapse.* Thin-Walled Structures, 1996. **25**(4): p. 269-295.
76. Solaimurugan, S. and R. Velmurugan, *Influence of fibre orientation and stacking sequence on petalling of glass/polyester composite cylindrical shells under axial compression.* International Journal of Solids and Structures, 2007. **44**(21): p. 6999-7020.
77. Khan, R.A. and E. Mahdi, *Effect of trigger mechanisms on the quasi-static axial crushing behavior of glass epoxy/polyvinyl chloride hybrid composite tubes.* Thin-Walled Structures, 2023. **182**: p. 110306.
78. Palanivelu, S., et al., *Crushing and energy absorption performance of different geometrical shapes of small-scale glass/polyester composite tubes under quasi-static loading conditions.* Composite Structures, 2011. **93**(2): p. 992-1007.
79. Chiu, L.N.S., et al., *Finite element modelling of composite structures under crushing load.* Composite Structures, 2015. **131**: p. 215-228.
80. Chiu, L.N.S., et al., *Validation of a 3D damage model for predicting the response of composite structures under crushing loads.* Composite Structures, 2016. **147**: p. 65-73.
81. Tan, W., et al., *The role of material characterisation in the crush modelling of thermoplastic composite structures.* Composite Structures, 2016. **153**: p. 914-927.
82. Feraboli, P., et al., *Predictive modeling of an energy-absorbing sandwich structural concept using the building block approach.* Composites Part A: Applied Science and Manufacturing, 2010. **41**(6): p. 774-786.
83. Feraboli, P., et al., *LS-DYNA MAT54 modeling of the axial crushing of a composite tape sinusoidal specimen.* Composites Part A: Applied Science and Manufacturing, 2011. **42**(11): p. 1809-1825.
84. ABAQUS. *22.1.1 Solid (continuum) elements.* [01/09/2023]; Available from: https://classes.engineering.wustl.edu/2009/spring/mase5513/abaqus/docs/v6.6/books/usb/default.htm?startat=pt06ch22s01alm01.html.
85. ABAQUS. *3.2.1 Solid element overview.* Available from: https://classes.engineering.wustl.edu/2009/spring/mase5513/abaqus/docs/v6.6/books/stm/default.htm?startat=ch03s02ath59.html.
86. ABAQUS. *3.2.4 Solid isoparametric quadrilaterals and hexahedra.* [01/09/2023]; Available from: https://classes.engineering.wustl.edu/2009/spring/mase5513/abaqus/docs/v6.6/books/stm/default.htm?startat=ch03s02ath62.html.
87. ABAQUS. *23.6.2 Choosing a shell element.* [01/09/2023]; Available from: https://classes.engineering.wustl.edu/2009/spring/mase5513/abaqus/docs/v6.6/books/usb/default.htm?startat=pt06ch21s01abo21.html#usb-elm-egeneral.
88. Dalli, D., *Experimental and numerical developments in predicting the crashworthiness of Formula One composite structures*, in *School of Mechanical and Aerospace Engineering*. 2020, Queen's University Belfast.
89. Joosten, M.W., et al., *Experimental and numerical investigation of the crushing response of an open section composite energy absorbing element.* Composite Structures, 2011. **93**(2): p. 682-689.
90. Waimer, M., M.H. Siemann, and T. Feser, *Simulation of CFRP components subjected to dynamic crash loads.* International Journal of Impact Engineering, 2017. **101**: p. 115-131.
91. Melo, D.R.B.d., *Composite structures impact simulation behavior*, in *Aerospace Engineering department*. 2014, Instituto Superior Técnico Lisboa.
92. Siromani, D., J. Awerbuch, and T.-M. Tan, *Finite element modeling of the crushing behavior of thin-walled CFRP tubes under axial compression.* Composites Part B: Engineering, 2014. **64**: p. 50-58.
93. Mamalis, A.G., et al., *The static and dynamic axial collapse of CFRP square tubes: Finite element modelling.* Composite Structures, 2006. **74**(2): p. 213-225.
94. Xiao, X., et al., *Progress in braided composite tube crush simulation.* International Journal of Impact Engineering, 2009. **36**(5): p. 711-719.

95. Fleming, D.C., *Modelling composite crushing initiation using a cohesive element formulation.* International Journal of Crashworthiness, 2011. **16**(5): p. 475-485.
96. David, M. and A.F. Johnson, *Effect of strain rate on the failure mechanisms and energy absorption in polymer composite elements under axial loading.* Composite Structures, 2015. **122**: p. 430-439.
97. ABAQUS. *19.3.1 Damage and failure for fibre-reinforced composites: overview.* [12/09/2023]; Available from: https://classes.engineering.wustl.edu/2009/spring/mase5513/abaqus/docs/v6.6/books/usb/default.htm?startat=pt05ch19s03abm40.html.
98. Konica, S. and T. Sain, *Phase-field fracture modelling for unidirectional fibre-reinforced polymer composites.* European Journal of Mechanics - A/Solids, 2023. **100**: p. 105035.
99. Hamilton, L., et al., *Production of a Composite Monocoque Frame for a Formula SAE Racecar.* 2013.
100. Carline, A., *Design of a Carbon Fibre Composite Monocoque Chassis for a Formula-Style Vehicle*, in *Mechanical and Aerospace Engineering.* 2020, Western Michigan University.
101. Karbhari, K.N. and Y.M. Bhinderwala, *Optimizing the manufacturing of the nose cone of a race car.* IJRET: International Journal of Research in Engineering and Technology, 2016. **05**(03): p. 4.
102. Shi, L. and K. Rice, *Carbon fibre composite monocoque chassis for a formula student race car.* 2019, Monash University.
103. Mitchell, S., *Oxford Brookes Racing 2021 chassis design*, in *Racecar engineering.* 2021.
104. Feraboli, P. and A. Masini, *Development of carbon/epoxy structural components for a high performance vehicle.* Composites Part B: Engineering, 2004. **35**(4): p. 323-330.
105. Moreira, D., *Development of hybrid composite coupons and experimental set-ups for dynamic crash testing*, in *Faculdade de Engenharia.* 2024, University of Porto.
106. Toray, *Toray AmberTool HX42*, Toray, Editor. 2022.
107. Kaufman, J.G., *Properties and Characteristics of Aluminum and Aluminum Alloys*, in *Fire Resistance of Aluminum and Aluminum Alloys and Measuring the Effects of Fire Exposure on the Properties of Aluminum Alloys.* 2016, ASM International.
108. Composites, E., *High temperature epoxy tooling board*, E. Composites, Editor. 2019.
109. AEM, T., *Ultra high temperature epoxy tooling board*, Trelleborg, Editor.
110. Easy Composites, *XT135/S 250g 3k Tooling Prepreg Carbon (1250mm).* 2022 [26/02/2023]; Available from: https://www.easycomposites.eu/xt135-250g-carbon-fibre-tooling-prepreg-surface.
111. Easy Composites, *EMP160 High Temp Epoxy Moulding Paste.* 2022 [26/02/2023]; Available from: https://www.easycomposites.eu/emp160-high-temperature-epoxy-moulding-paste.
112. Ansys, *GRANTA EduPack.* 2022.
113. American Iron and Steel Institute, *High-temperature characteristics of stainless steels*, in *A designers' handbook series. Nickel development institute.*
114. Leroy Merlin, *Placa de MDF 2440x1220x3mm.* 2022 [26/02/2023]; Available from: https://www.leroymerlin.pt/produtos/madeiras-e-acrilicos/paineis-para-construcao/mdf/placa-de-mdf-2440x1220x3mm-11190914.html?gclid=Cj0KCQiArsefBhCbARIsAP98hXT8vvsIlfWhjTYdon3O02K_r1WoPp5RZAUYymTAVpdAhPUih9oMq1gaAuV4EALw_wcB.
115. Base materials, *BE368 Everyday epoxy tooling board.* 2023 [30/04/2023]; Available from: https://www.base-materials.com/latest-innovations/be368-epoxy-tooling-board/.
116. Curbell Plastics, *High Density Urethane (PBLT) Board, Closed-Cell Rigid Polyurethane for Signage, Low Temperature, 15 lbs/ft3, (0.500 in x 48 in x 96 in), Precision Board Plus™.* 2022 [26/02/2023]; Available from: https://www.curbellplastics.com/Shop-Materials/Specialty-Product/High-Density-Urethane-(HDU)-Boards/W10-00021/High-Density-Urethane-(PBLT)-Board-Closed-Cell-Rigid-Polyurethane-for-Signage-Low-Temperature-15-lbs-ft3-(0-500-in-x-48-in-x-96-in)-Precision-Board-Plus.
117. Easy Composites, *XT135/B 415 g 12k Tooling Prepreg Carbon (1250mm).* 2023 [26/02/2023]; Available from: https://www.easycomposites.eu/xt135-416g-carbon-fibre-tooling-prepreg-backing.
118. Easy Composites, *Mirka P800 Wet and Dry Abrasive Paper.* 2022 [30/04/2023]; Available from: https://www.easycomposites.eu/p800-wet-and-dry-abrasive-paper.

119. Easy Composites, *S120 Advanced Board & Mould Sealer*. 2022 [30/04/2023]; Available from: https://www.easycomposites.eu/s120-advanced-board-sealer.
120. Easy Composites, *Spray Nozzle for 50ml and 250ml Bottle*. 2022 [30/04/2023]; Available from: https://www.easycomposites.eu/trigger-spray-nozzle-for-50ml-and-250ml-bottles.
121. Easy Composites, *CR1 Easy-Lease Chemical Release Agent*. 2022 [30/04/2023]; Available from: https://www.easycomposites.eu/easylease-chemical-release-agent.
122. Easy Composites, *EA700 Epoxy Tooling Board Adhesive 491g Kit*. 2022 [30/04/2023]; Available from: https://www.easycomposites.eu/EA700-epoxy-tooling-board-adhesive.
123. Kiwi tooling, *Epoxy Tooling Board Machining Parameters*. [27/07/2023]; Available from: https://static1.squarespace.com/static/5dc3df1bc25b0b21001f705f/t/603eb4f957d1675023652f95/1614722298629/Feed+Speeds+Epoxy+Board.pdf.
124. ASM Handbook committee., *Machining of Aluminum and AlumJnum Alloys*, A. Handbook, Editor. 1989. p. 761-804.
125. Azo materials, *Silicon Rubber*. 2023 [07/07/2023]; Available from: https://www.azom.com/properties.aspx?ArticleID=920.
126. Toray. *Toray E745*. 2020 16-04-2020 [21/05/2023]; Available from: https://www.toraytac.com/media/0aca2295-3458-437f-b756-729525495674/OIWeow/TAC/Documents/Data_sheets/Thermoset/UD%20tapes%20and%20prepregs/E745_Epoxy_PDS.pdf.
127. Abaqus. *Dynamic analysis procedures: overview*. Abaqus Documentation [12/08/2023]; Available from: https://classes.engineering.wustl.edu/2009/spring/mase5513/abaqus/docs/v6.6/books/usb/default.htm?startat=pt03ch06s03at07.html.
128. Simulia. *VUMAT for Fabric Reinforced Composites*. [08/09/2023]; Available from: https://ww3.cad.de/foren/ubb/uploads/Bierotta/VUMATforFabricReinforcedComposites.pdf.
129. *APX 300T IMP503Z-HT BC 44*, A. Group, Editor. 2022.
130. Engenuity. *CZone*. 2023 [11/08/2023]; Available from: https://engenuity.net/techniques/equipment-software/czone/.
131. *CZone analysis*. [08/09/2023]; Available from: https://docs.software.vt.edu/abaqusv2022/English/SIMACAEANLRefMap/simaanl-c-czoneanalysis.htm.
132. Webster, B. *Hourglassing and Shear Locking - What Are They And Why Does It Matter?* 2021 01/09/2023]; Available from: https://www.fidelisfea.com/post/hourglassing-and-shear-locking-what-is-it-and-why-does-it-matter.
133. ABAQUS, *21.1.4 Section controls*. 2023.
134. ABAQUS. *Explicit dynamic analysis*. ABAQUS Analysis User's Manual [28/07/2023]; Available from: https://classes.engineering.wustl.edu/2009/spring/mase5513/abaqus/docs/v6.6/books/usb/default.htm?startat=pt03ch06s03at07.html.
135. ABAQUS. *Mass scaling*. ABAQUS Analysis User's Manual [28/07/2023]; Available from: https://classes.engineering.wustl.edu/2009/spring/mase5513/abaqus/docs/v6.6/books/usb/default.htm?startat=pt04ch11s07aus63.html.
136. Postacchini, L., et al., *Environmental assessment of an automated impregnation process of carbon fibre tows*. Procedia CIRP, 2020. **88**: p. 445-450.

Appendices

A. Cost and weight for square structures

This appendix contains the cost and mould weight for the square structures that were disregarded due to their reduced performance when compared to curved specimens.

Table 42 – Square complex structures cost and mould weight for different mould materials

	Square Frustum			Corrugated tube		
Mould material	**Epoxy Blocks**	**Aluminium 6082**	**Tooling prepreg**	**Epoxy Blocks**	**Aluminium 6082**	**Tooling prepreg**
Cost (€)	515.13	70.07	230.77	515.13	56.70	324.22
Mould Weight (kg)	5.56	21.67	0.24	5.27	20.57	0.32
Maximum mould temperature (°C)	120	200	135	120	200	135

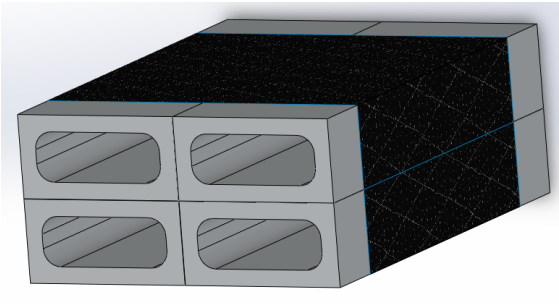

Figure 65 - Considered mould for the square multi-cellular crashbox

Table 43 – Simple square structures cost and mould weight for different mould materials

	Square Tube		Multi-cellular Crashbox	
	Epoxy Blocks	**Aluminium 6082**	**Epoxy Blocks**	**Aluminium 6082**
Cost (€)	455.91	65.12	455.91	35.65
Mould Weight (kg)	1.65	6.42	2.11	8.22
Maximum mould temperature (°C)	120	200	120	200

B. Preliminary ply calculation

This section contains the results of the preliminary ply calculation for the remaining structures that were not represented in the main text.

For the corrugated frustum, 2 plies were enough to fulfil the requirement, nevertheless another run was tried for 3 plies that resulted in an average deceleration too close to the maximum allowed, and it would introduce unnecessary mass to the impact attenuator.

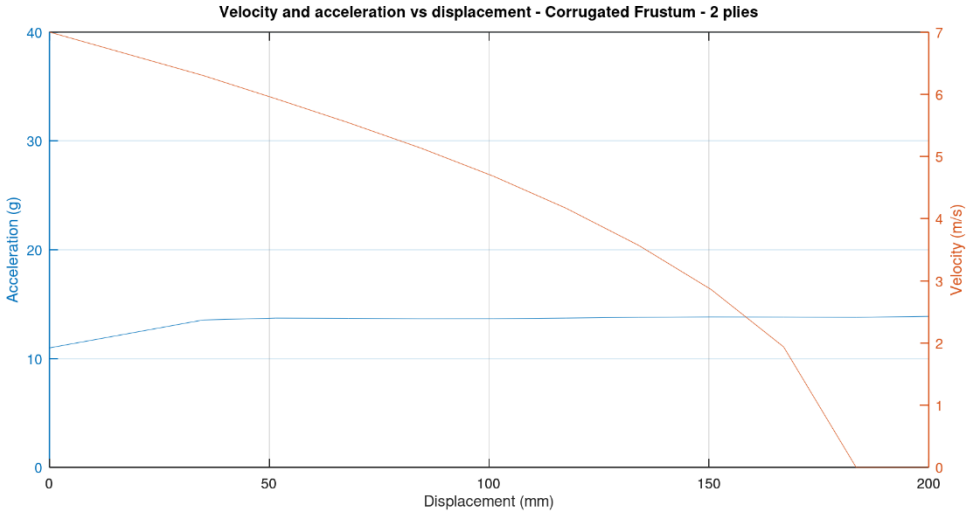

Figure 66 - Corrugated frustum results for 2 plies

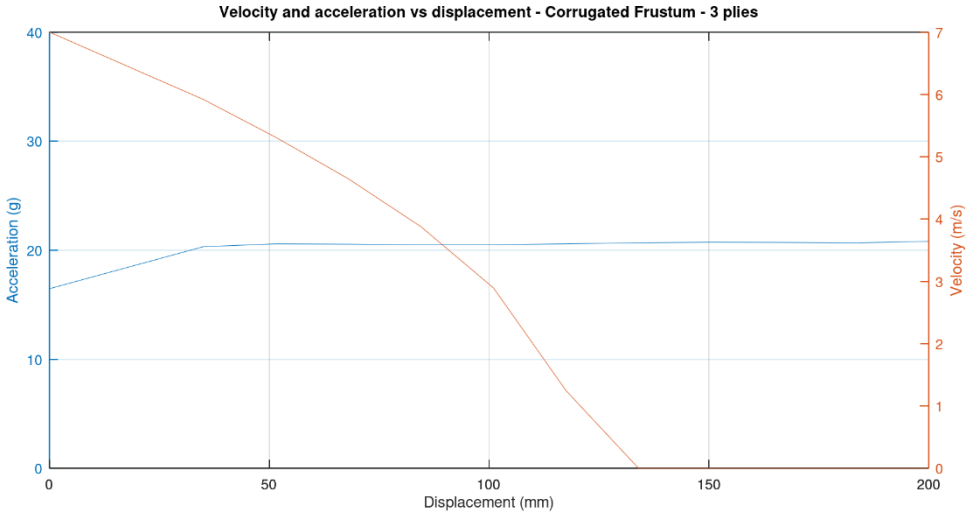

Figure 67 - Corrugated frustum results for 3 plies

The Multi-cellular crashbox fulfilled the requirements with only 1 ply.

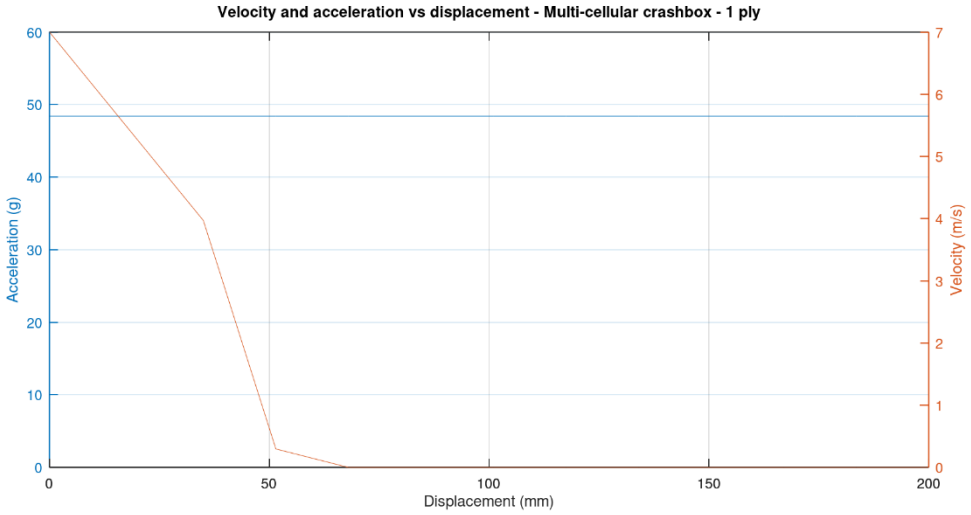

Figure 68 - Velocity and deceleration vs displacement for the multi-cellular crashbox

The cone preliminary ply calculation resulted in 3 layers.

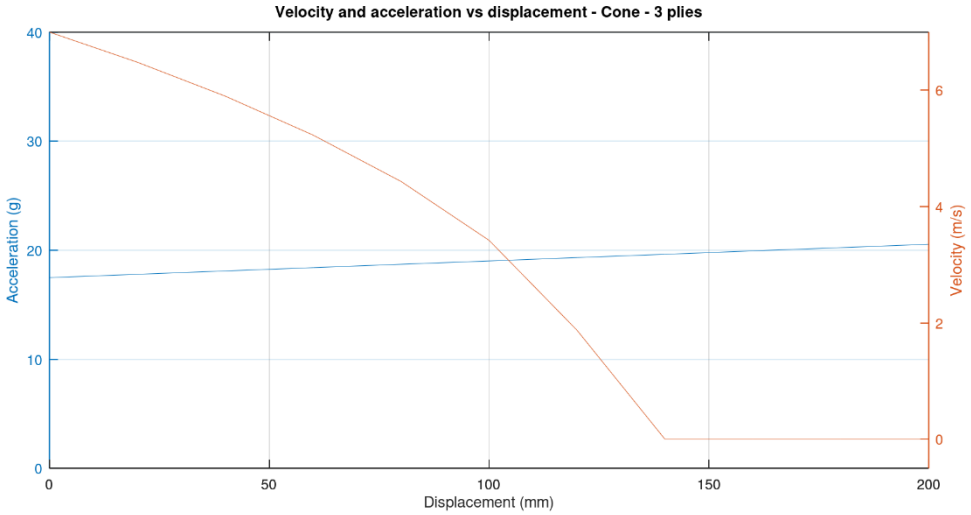

Figure 69 - Results for the cylindrical cone for 3 plies

The tube fulfils the requirements with 3 plies.

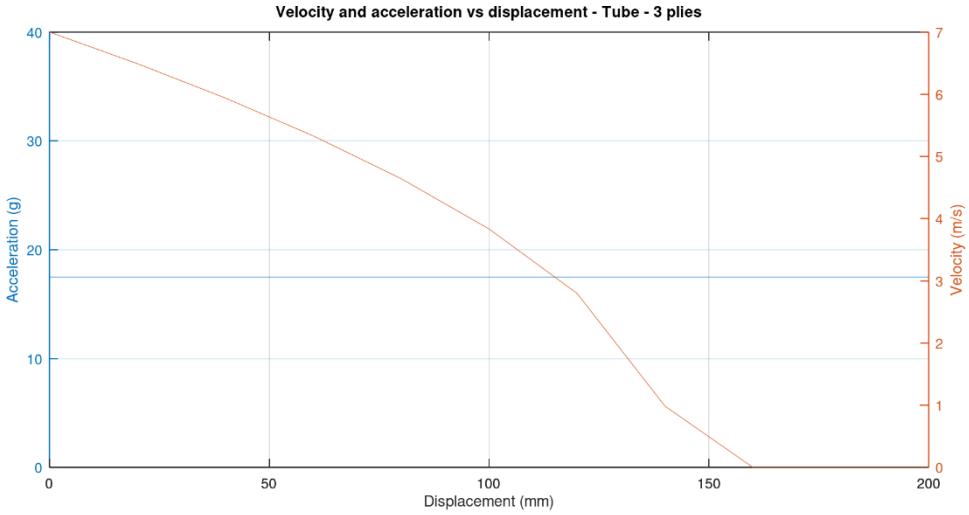

Figure 70 - Preliminary ply calculation results for the tube

C. Lateral stiffness results

This appendix section shows the results for the lateral stiffness simulation for all the remaining structures.

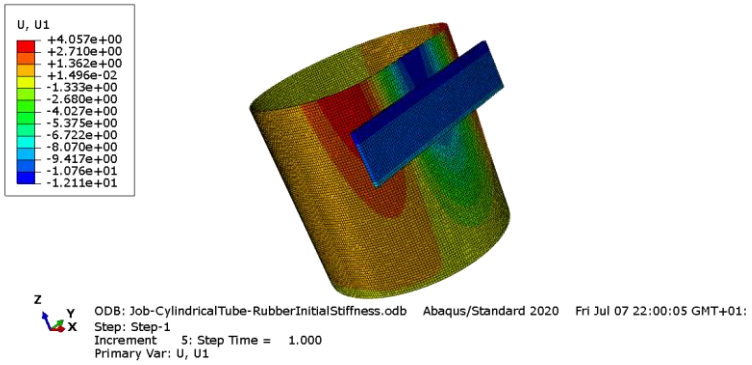

Figure 71 - Tube lateral stiffness simulation results

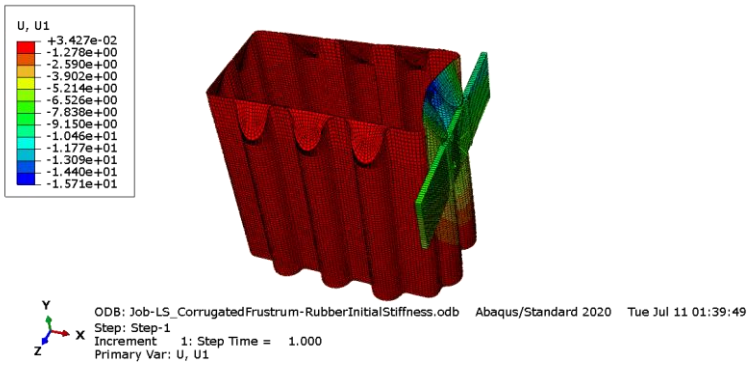

Figure 72 - Corrugated frustum lateral stiffness simulation results

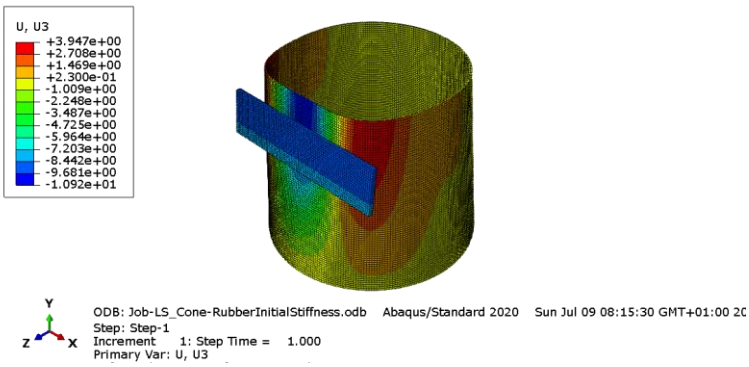

Figure 73 - Cone lateral stiffness simulation results

D. Crushing simulations

This section presents the acceleration and velocity plots obtained for every structure, including those that were not able to absorb the necessary energy.

Starting by the carbon fibre structures, Figure 74 and Figure 75 represent the plots for multi-cellular crashbox V2 with 3 plies and the multi-cellular crashbox V1 with 2 plies, respectively. Table 44 represents the multi-cellular crashbox V1 section average radius as well as the crush stress used for that section.

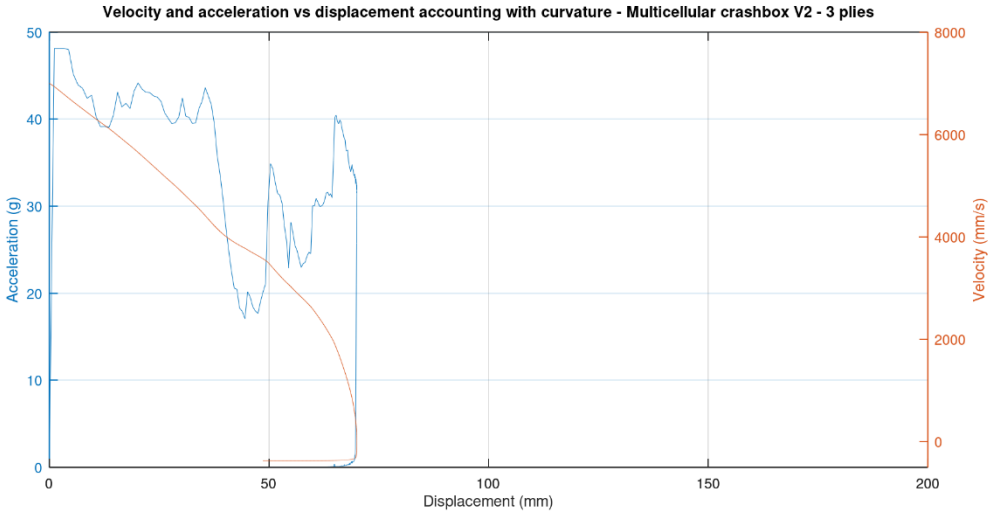

Figure 74 - Acceleration versus displacement for a carbon fibre multicellular crashbox V2 with 3 plies

Table 44 - Multi-cellular crashbox V1 section radius and respective crush stress

Multi-cellular crashbox V1 section radius (mm)	Crush stress (MPa)
Flat	81.5
35 mm	105.4

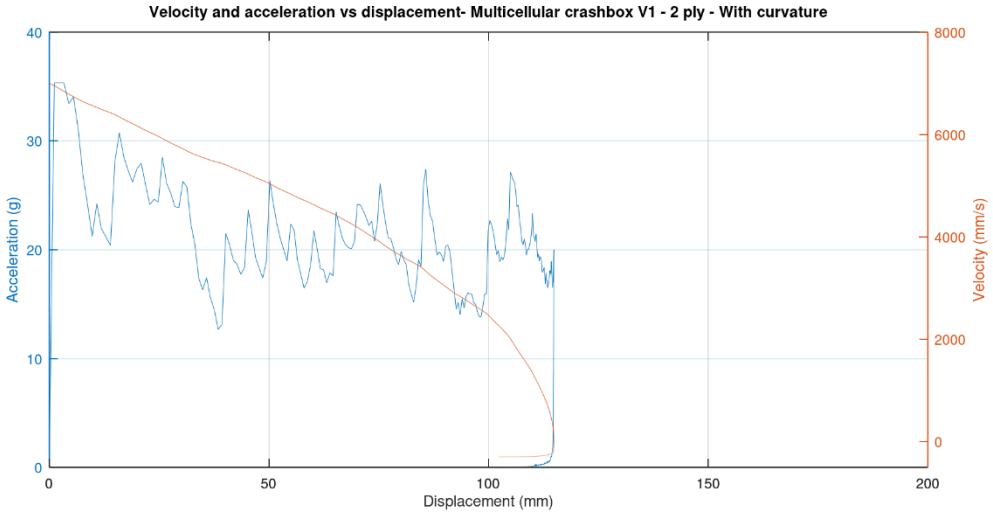

Figure 75 - Acceleration and velocity versus displacement for a multicellular crashbox V1 accounting for curvature

Secondly, the plots for the flax structures are presented. Figure 76 represents the plot for the multi-cellular crashbox V2 with 2 plies which was not able to absorb the necessary energy. Figure 77 to Figure 80 represent the plots for the remaining flax structures which were already presented in the text.

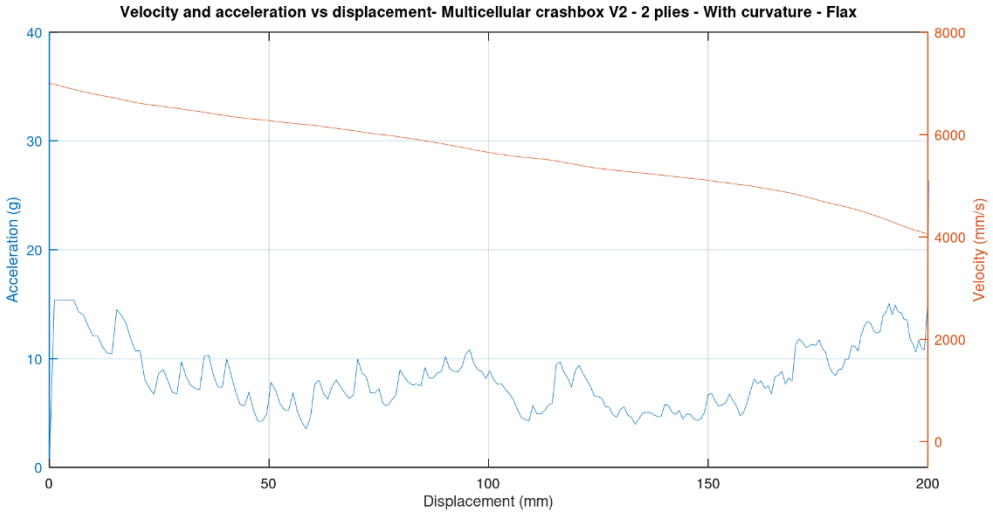

Figure 76 - Acceleration and velocity versus displacement plot for the flax multi-cellular crashbox V2 with 2 plies

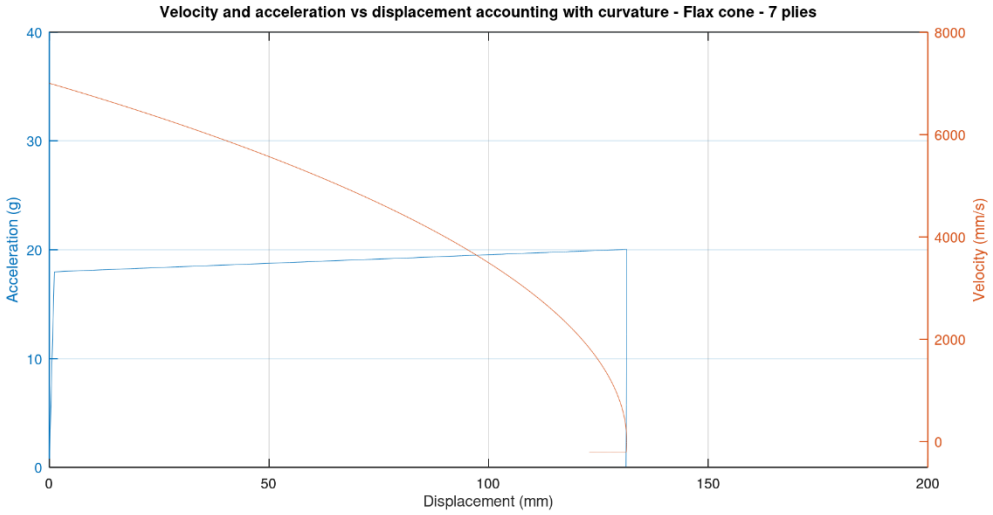

Figure 77 - Acceleration and velocity versus displacement plot for the flax cone with 7 plies

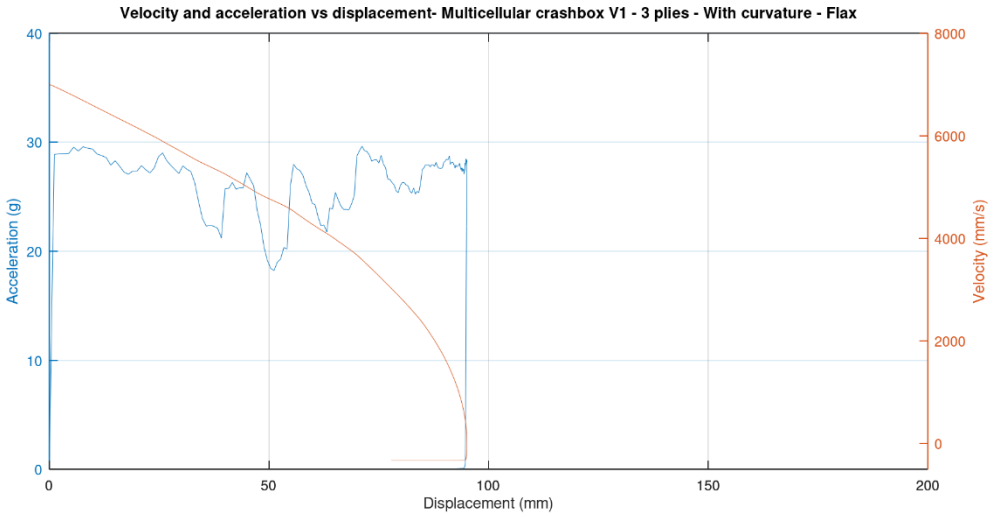

Figure 78 - Acceleration and velocity versus displacement plot for the flax multi-cellular crashbox V1 with 3 plies

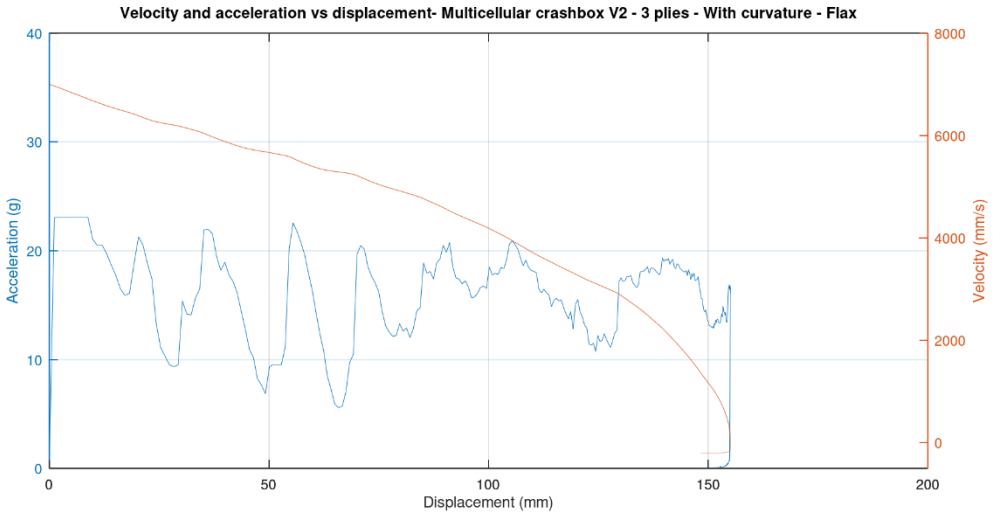

Figure 79 - Acceleration and velocity versus displacement plot for the flax multi-cellular crashbox V2 with 3 plies

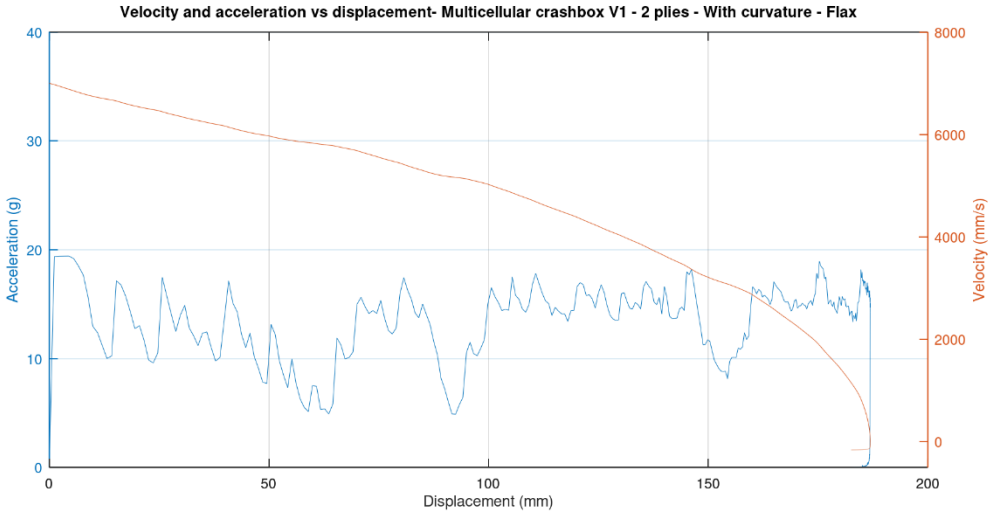

Figure 80 - Acceleration and velocity versus displacement plot for the flax multi-cellular crashbox V1 with 2 plies

Finally, the hybrids acceleration and velocity plots as well as the material plies and composite layups definition will be presented.

Table 45 to Table 47 represent the configuration for each composite layup for several structures and the attributed nomenclature. For the structures that are not represented, the same process was used.

Table 45 - CFC cone configuration

Cone C/F/C section radius (mm)	Material fabrics	Composite Layups
100.875	3/8/3	Composite Layup-1
102.75	3/8/3	
104.5	3/8/3	
105.25	3/8/3	
106.125	3/8/3	
109.625	3/8/3	
111.5	3/8/3	
113.25	4/8/4	Composite Layup-2
114.875	4/8/4	
116.625	4/8/4	

Table 46 - FCF cone configuration

Cone F/C/F section radius (mm)	Material fabrics	Composite Layups
100.875	8/3/8	Composite-Layup-3
102.75	8/3/8	
104.5	8/3/8	
105.25	8/3/8	
106.125	8/3/8	
109.625	8/3/8	
111.5	8/3/8	
113.25	8/4/8	Composite-Layup-4
114.875	8/4/8	
116.625	8/4/8	

Table 47 - CF Multi-cellular crashbox V2 configuration

Multi-cellular crashbox V2 F/C section radius (mm)	Material fabrics	Composite Layups
Flat	8/5	Composite-Layup-5
50 mm	7/2	Composite-Layup-6 Composite-Layup-7

Table 48 - CF Multi-cellular crashbox V1 configuration

Multi-cellular crashbox V1 C/F section radius (mm)	Material fabrics	Composite Layups
Flat	5/8	Composite-Layup-5
35 mm	1/6	Composite-Layup-9 Composite-Layup-10

Figure 81 and Figure 82 represent the results plot for the cone with FCF configuration and the multi-cellular crashbox V2 with FC configuration. These structures were not able to absorb the necessary energy.

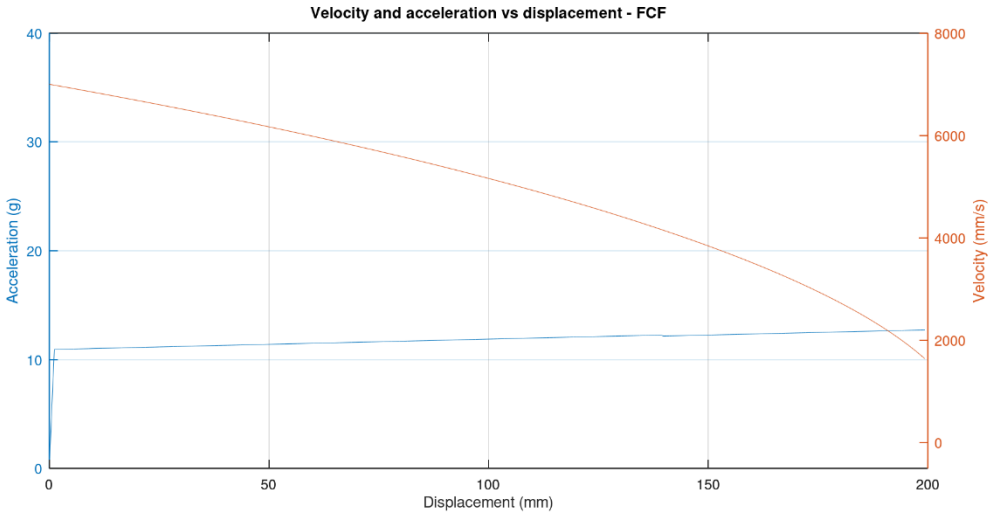

Figure 81 - Acceleration and velocity plot for the FCF cone

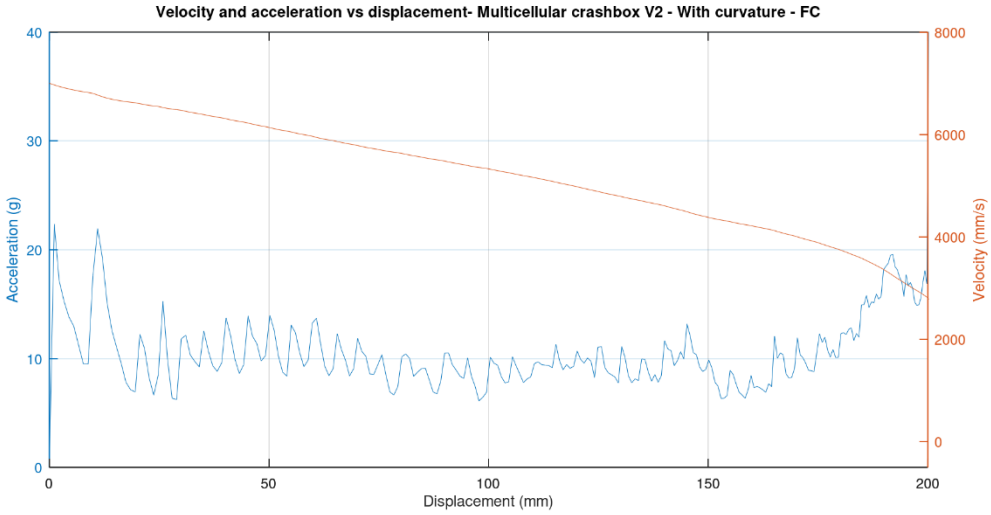

Figure 82 - Acceleration and velocity plot for the FC multi-cellular crashbox V2

Figure 83 to Figure 89 present the plots for the remaining structures already presented in the main text.

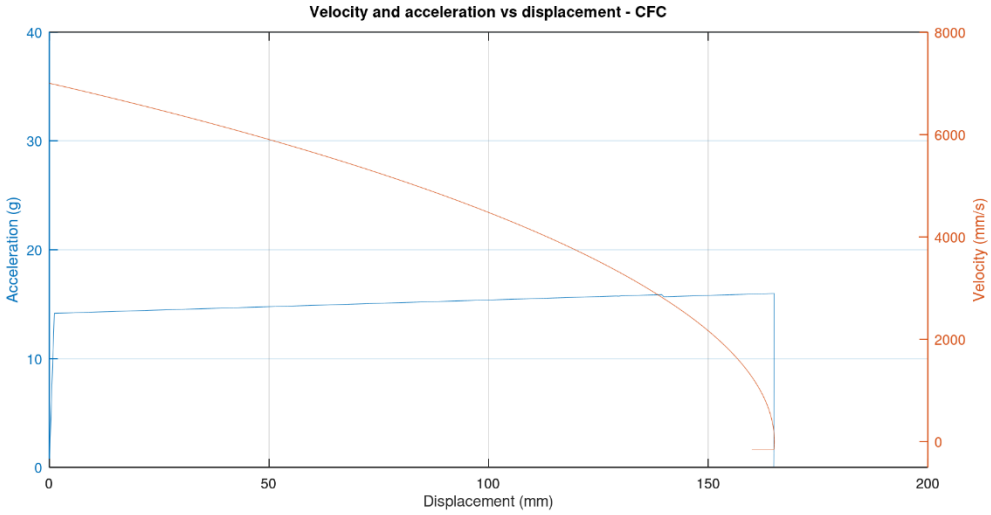

Figure 83 - Acceleration and velocity plot for the CFC cone

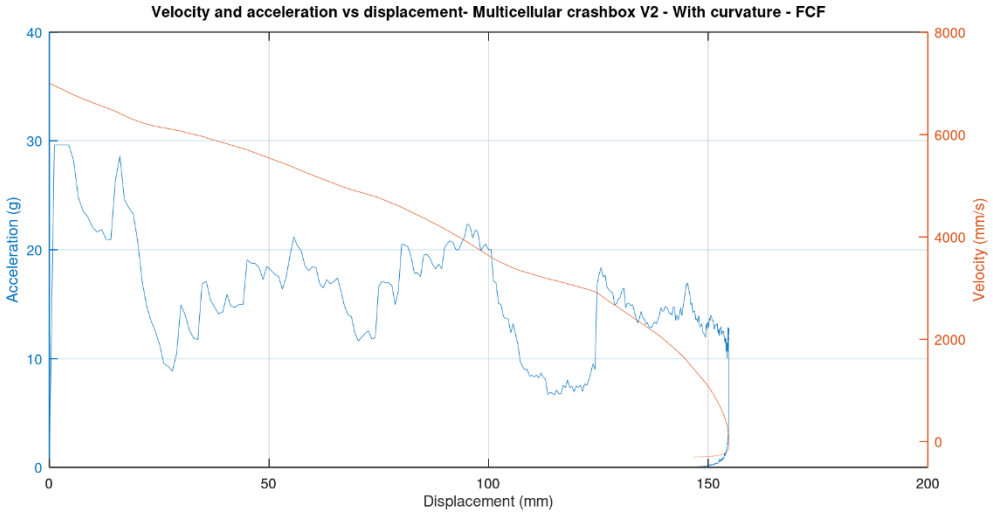

Figure 84 - Acceleration and velocity plot for the FCF multi-cellular crashbox V2

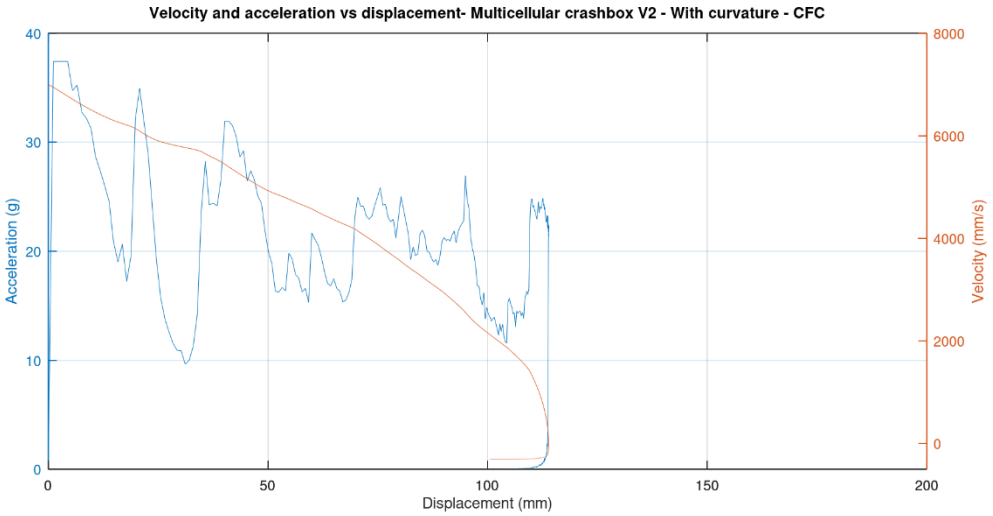

Figure 85 - Acceleration and velocity plot for the CFC multi-cellular crashbox V2

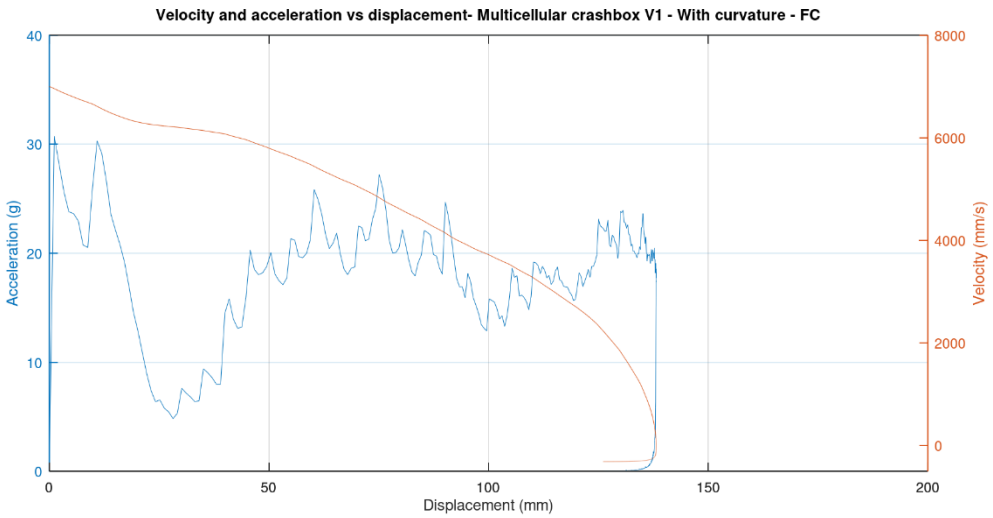

Figure 86 - Acceleration and velocity plot for the FC multi-cellular crashbox V1

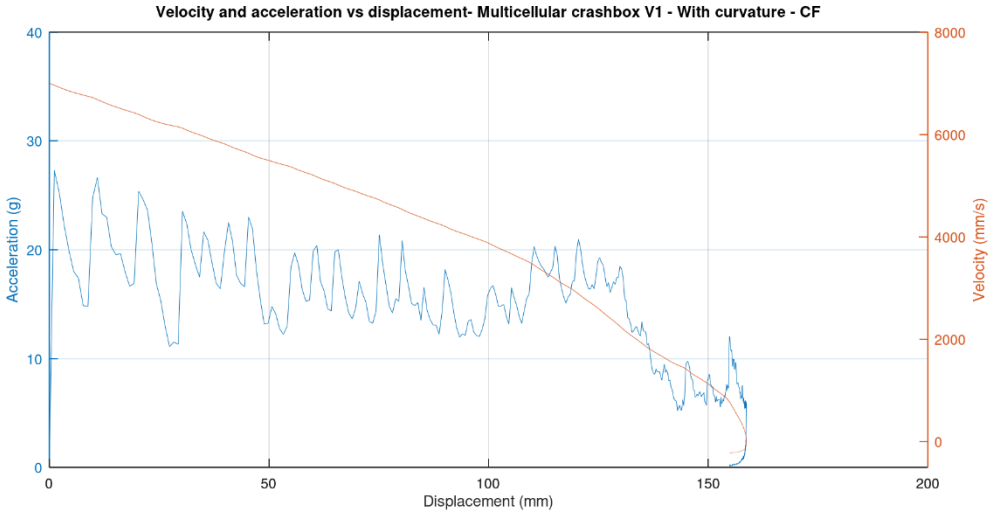

Figure 87 - Acceleration and velocity plot for the CF multi-cellular crashbox V1

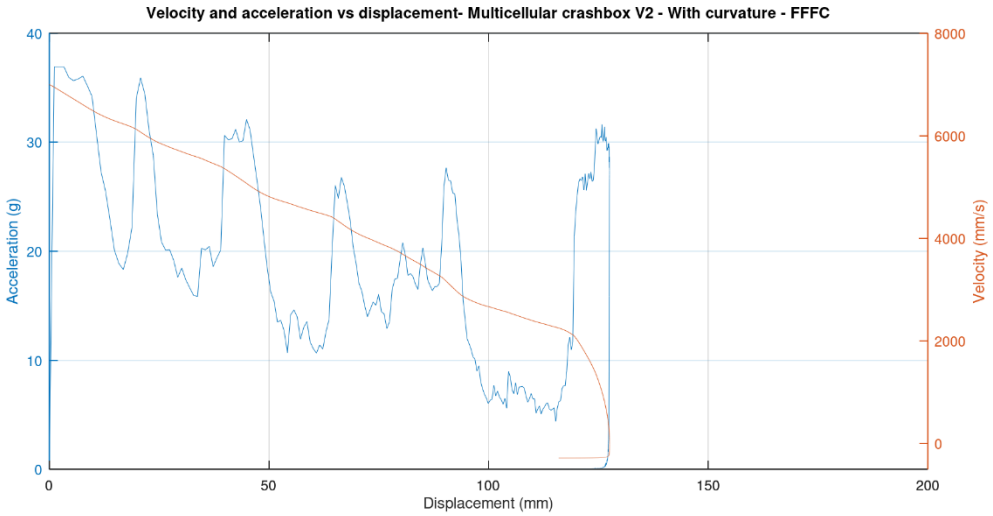

Figure 88 - Acceleration and velocity plot for the FFFC multi-cellular crashbox V2

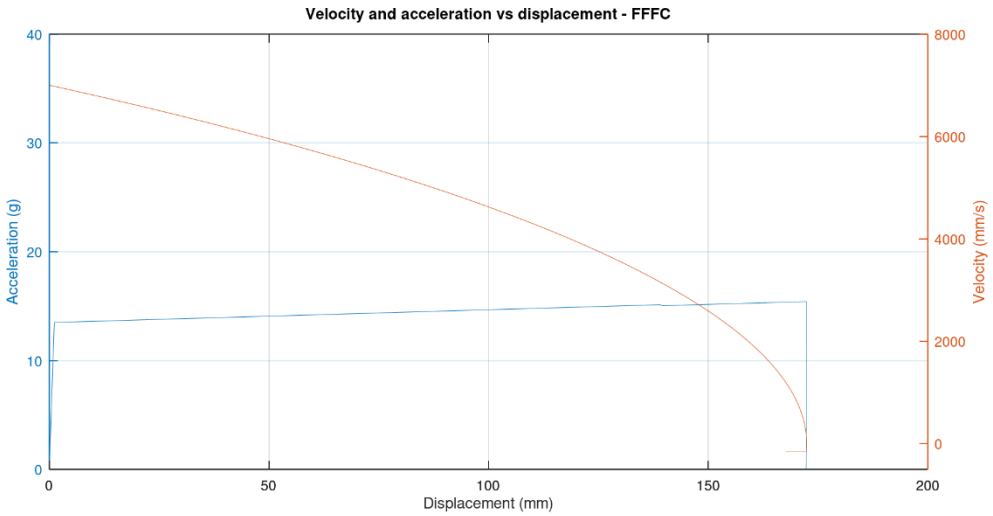

Figure 89 - Acceleration and velocity plot for the FFFC cone